Data Driven Modeling and Scheduling of Hybrid Wireless Power Transfer Charging Systems to Serve Electric Vehicles

A Dissertation

Presented to

the faculty of the School of Engineering and Applied Science

University of Virginia

in partial fulfillment

of the requirements for the degree

Doctor of Philosophy

by

Li Yan

December

2019

APPROVAL SHEET

The dissertation is submitted in partial fulfillment of the requirements for the degree of Doctor of Philosophy

Li Yan Li Yan

The dissertation has been read and approved by the examining committee:

Haiying Shen, Advisor

John A. Stankovic, Committee chair

Madhav Marathe

John Lach

Brian Smith

Joachim Taiber

Accepted for the School of Engineering and Applied Science:

Craig H. Benson, Dean, School of Engineering and Applied Science

December
2019

Abstract

Intelligent Transportation System is a major application field for Cyber-Physical Systems (CPS). Future public transportation system will be featured by Electric Vehicles (EVs). However, due to battery capacity limit, the driving range of an EV is limited. To fulfill metropolitan transit demands, public transportation EVs are expected to be continuously operable without recharging downtime. Although there have been many previous mature works on plug-in cable charging systems, EVs must stop and get plugged in the charging points of the charging stations to get recharged, which wastes time and becomes an obstacle for the continuous operability of public transportation EVs.

Wireless Power Transfer (WPT) techniques that charge an EV when it is temporarily parked (stationary wireless charger) and in motion (dynamic wireless charger) is a solution. The key contribution of this dissertation is building a hybrid WPT charging system composed of stationary and dynamic wireless chargers to support the charging demands of a metropolitan-scale group of public transportation EVs. The designed methodologies for building the hybrid WPT charging system consists of (1) a stationary wireless charger deployment approach that utilizes spatial and temporal analysis of passenger appearance and a generic traffic model to both maximize the taxicabs' opportunity of picking up passengers at the chargers and support the taxicabs' continuous operability on roads with the minimal deployment cost. (2) a dynamic wireless charger deployment approach that utilizes categorization and clustering of traffic flow attributes and a generic traffic model to support the continuous operability of electric vehicles on roads with the minimal deployment cost; and (3) a taxicab dispatching and charging approach that utilizes customized selection and training of suitable historical passenger demand data and charging optimization to minimize the taxicab's number of missed potential passengers due to charging. By

saying suitable historical data, we mean the data that are under the influence of random factors (e.g., weather, holiday) similar to current passenger demand.

Through simulation based on a metropolitan-scale mobility dataset of public transportation vehicles, we demonstrate that our proposed methodologies for developing the hybrid WPT charging system can better serve public transportation EVs in terms of continuous operability, electricity utilization efficiency, and service efficiency.

To my family...

Contents

List of Figures

List of Tables

Acknowledgements

I would like to thank many people who have helped and supported me through this long Ph.D. journey.

First, I thank my advisor, Professor Haiying Shen, whose encouragement, guidance and support from the initial to the final level of my Ph.D. study enabled me to develop an understanding of the subject. Apart from research expertise, I also learn a lot from her about organizing and managing research activities such as project/grant proposals and international conferences. I am especially thankful for her guidance and valuable suggestions at every step of my career and life.

I acknowledge my committee members, Professor John A. Stankovic, Professor Madhav Marathe, Professor John Lach, Professor Brian Smith and Professor Joachim Taiber for providing me valuable comments and suggestions in writing this dissertation.

I am grateful to my collaborators for sharing their time, ideas and enthusiasm. I had been fortunate to collaborate with each one of them at Clemson University, University of Virginia, and etc.

I am proud of knowing many colleagues and friends in Pervasive Communications Laboratory. I am thankful to all of you for supporting my research and providing me suggestions. Thank you for the laughs and happy days in the office.

All my friends and family have been a source of inspiration in my life. I thank my family for their love and support at all times. None of my achievements would have

been possible without their infinite support, and steely determination to give me the best possible education.

To my parents, Zhixin Yan and Ping Jiang, thank you for your love and all your advices through the years. I want to express my deepest gratitude to you for your financial support, raising me up, and encouraging me to complete this doctoral degree when I was depressed.

Chapter 1

Introduction

Developing Intelligent Transportation Systems, which is a major application field for Cyber-Physical Systems (CPS), to tackle various urban issues (e.g., traffic congestion, energy consumption) is increasingly needed [13, 86, 124, 127, 133, 138, 139]. Among them, charging of public transportation Electric Vehicles (EVs) in a metropolitan-scale road network is with great importance since EVs are foreseen to be the major carrier of future public transportation systems, which generally consist of taxicabs, buses and customized transit vehicles [43, 62, 136, 138]. To fulfill metropolitan transit demands, public transportation EVs are expected to be continuously operable without recharging downtime [23]. By operable, we mean that an EV's residual energy measured by State of Charge (SoC) (i.e., percentage of stored energy) is non-zero. However, due to the limit of battery capacity, the driving range of most EVs is still limited (e.g., 100 miles) [116]. Hence, EVs must be recharged frequently during driving time. Although there have been many previous mature works on plug-in cable charging systems [5, 26, 58, 93, 108, 119, 137], EVs must stop and get plugged in the charging points of the charging stations to get recharged, which wastes time and becomes an obstacle for the continuous operability of public transportation EVs.

Recently, Wireless Power Transfer (WPT) techniques for EV charging are emerg-

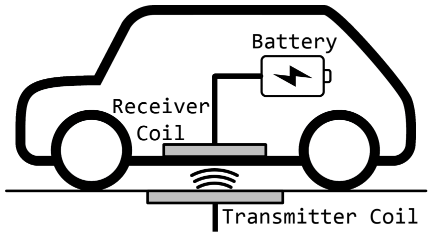

Figure 1.1: Stationary wireless charger for EVs.

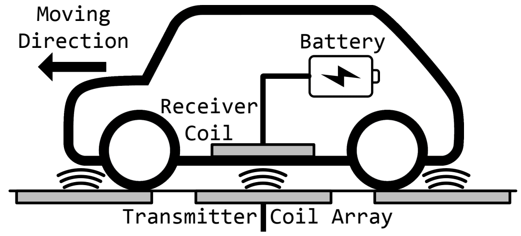

Figure 1.2: Dynamic wireless charger for EVs.

ing as a solution to keeping the EVs continuously operable [48, 53]. There have been multiple existing WPT charger products for sale in market [11, 25, 28, 40, 82, 88, 90]. Based on charging approach, WPT chargers can be grouped into two categories: stationary wireless charger (Figure 1.1) and dynamic wireless charger (Figure 1.2). As illustrated in Figure 1.1, a stationary wireless charger consists of a transmitter coil on ground and a receiver coil on EV. Whenever an EV is parked over a stationary wireless charger, electric energy is transferred from the transmitter coil to the receiver coil via electromagnetic field. Such a charger allows EVs to get charged when they are temporarily parked at somewhere (e.g., traffic lights, roadside parking lots) without plugging in a cable, which is called *opportunistic charging* [30]. As illustrated in Figure 1.2, a dynamic wireless charger consists of an array of transmitter coils on ground and a receiver coil on EV. The array of transmitter coils is embedded in a road segment, which is called a wireless charging lane. Similar to a stationary wireless charger, whenever an EV drives through a wireless charging lane, electric energy is transferred from the transmitter coil array to the receiver coil via electromagnetic field [48, 50].

1.1 Research Questions

A stationary wireless charger is potentially beneficial to charge electrified taxicabs in a public transportation system, of which idle time spent on cruising for passengers, seeking chargers, and charging should be maximally saved to increase profit and passenger service efficiency. This is because taxicab drivers usually prefer to wait at certain places (e.g., airports, malls) in order to pick up the next passenger with reduced idle miles in cruising for passengers [122, 123]. So taxicabs have relatively fixed parking patterns determined by the appearance of passengers, but random driving routes. Then, if the taxicabs can be offered sufficient opportunities of charging during parking from a proper deployment of stationary wireless chargers, it can enable charging and waiting for passengers to occur simultaneously before picking up the next passenger, which will greatly reduce the taxicabs' idle time. Therefore, we need a set of methods to extract suitable parking locations with many and frequent appearance of passengers.

Moreover, to keep the flow of all public transportation EVs operable at any position in the road network, we need to ensure that the EVs have a certain level of SoC when they arrive at any position. This SoC level enables an EV to move to its nearest wireless charger before battery exhaustion. Therefore, we need to infer the EVs' traffic (i.e., the probability of reaching each position in the road network) in order to estimate the expectation of the EVs' SoC when they arrive at each position given deployed wireless chargers. However, it is challenging to model the EVs' traffic without fine-grained analysis of their mobility characteristics. In summary, a major research question is: *How to measure the likelihood of passenger appearance at each position and establish a generic EV traffic model for selecting the positions for deploying stationary wireless chargers?*

Deploying stationary wireless chargers alone cannot completely suffice the charging demands of electrified buses and customized transit vehicles, which have relatively more determined driving routes and are expected to be continuously running (i.e., no long-time parking) on road during working hours [48, 50]. This makes the supplementary utilization of dynamic wireless chargers necessary. Different from a stationary wireless charger, when an EV drives through a dynamic wireless charger, the amount of electricity energy transferred to the EV depends on the EV's passing velocity and the length of the wireless charging lane. Slower velocity or longer charging lane leads to more received energy and vice versa, while a longer wireless charging lane costs more to deploy. Thus, locations with slower EV passing velocity are better options for deploying charging lanes in order to reduce the deployment cost. Moreover, to ensure that the deployed dynamic wireless chargers can serve as many EVs as possible, the locations with higher EV visiting frequency should have higher priority to deploy chargers. Therefore, another research question we need to handle is: *How to measure the suitability of each position based on its traffic flow attributes (e.g., driving velocity, vehicle visiting frequency) and establish a generic EV traffic model for selecting the positions for deploying dynamic wireless chargers?*

On the one hand, unlike buses, which have determined driving routes and can receive repeated charging once dynamic wireless chargers are deployed on their routes, the movement of taxicabs is not fixed. According to some previous studies [62, 104], the full recharge of a mainstream electric taxicab generally lasts for 0.5 to 2.5 hours. On the other hand, the profiting of taxicabs is highly dependent on efficient discovery of passengers. When dispatching an electric taxicab, if we let the taxicab follow the traditional pattern of "keep driving-SoC exhaustion-charge", such a long bulk of idle charging time may cause the taxicab to miss many potential passengers during busy hours [81]. Therefore, in addition to the proper deployment of chargers, another research question rises up: *How to design a taxicab dispatching and charging approach that minimizes the taxicab's number of missed potential passengers due to charging?* The approach should provide guidance for the taxicab on where to pick up a passenger or receive a recharge based on future passenger demand. Therefore, how to infer a future passenger demand with a sufficiently high accuracy, and utilize the inference result to optimize the charging of taxicabs becomes important. However, how to generate a highly accurate inference result is challenging because it is difficult to consider the influence of all the random factors. What's more, how to utilize the inference result to design a charging optimization strategy for an electric taxicab, which minimizes the taxicab's number of missed potential passengers during charging, is also non-trivial.

1.2 Proposed Methodologies

Considering increasingly abundant mobility dataset of public transportation EVs become available, it is practical to apply fine-grained data analysis on the movement characteristics of the EVs as dynamic flows and find solutions for above research questions. Accordingly, we propose new methodologies, which consist of

(1) a stationary wireless charger deployment approach that utilizes spatial and temporal analysis of passenger appearance and a generic traffic model to both maximize the taxicabs' opportunity of picking up passengers at the chargers and support the taxicabs' continuous operability on roads with the minimal deployment cost;

(2) a dynamic wireless charger deployment approach that utilizes categorization and clustering of traffic flow attributes and a generic traffic model to support the continuous operability of electric vehicles on roads with the minimal deployment cost;

(3) a taxicab dispatching and charging approach that utilizes customized selection and training of suitable historical passenger demand data and charging optimization to minimize the taxicab's number of missed potential passengers due to charging. By saying suitable historical data, we mean the data that are under the influence of random factors (e.g., weather, holiday) similar to current passenger demand.

Proposed methodologies will be based on the analysis of a large-scale mobility dataset of public transportation vehicles including buses, taxicabs and customized transit vehicles. In addition to transportation scenarios, the proposed fundamental traffic model and dispatching method can also be applied to other CPS related fields such as human mobility modeling and control, air traffic prediction and scheduling, traffic control in video-on-demand system, etc.

The **goal of the proposed research** is *to find solutions for effective integration of the proposed methodologies with the state-of-the-art WPT techniques toward developing a hybrid WPT charging system composed of stationary and dynamic wireless chargers*. For this purpose, we will use the mobility dataset to evaluate the proposed methodologies through comparing their performance with representative existing methods in terms of keeping the EVs continuously operable, efficient utilization of electricity, and service efficiency of a hybrid system of wireless chargers. This leads us to the following **thesis statement**:

> By exploiting our generic traffic model and methodologies based on spatial and temporal analysis of passenger appearance, entropy-based categorization and clustering of flow attributes, and customized selection and training of suitable historical taxicab passenger demand data, we can develop a hybrid WPT charging system that can better serve public transportation EVs in terms of continuous operability, electricity utilization efficiency, and charging service efficiency compared to the state of the art.

1.3 Contributions

I have done extensive and comprehensive study on the application of computer science methodologies, which is of great value for the application of computer science theories and methodologies in engineering domains, especially in transportation domain.

The primary application-specific contributions of the dissertation are summarized as follows:

(1) A novel approach for deploying stationary wireless chargers that incorporates different factors regarding passenger appearance, a Kernel Density Estimator (KDE) based traffic model and queuing theory based driver routing behavior model to develop a multi-objective optimization problem and its solution (Chapter 3). In this approach, the fundamental contributions include:

    1. A KDE based traffic model for estimating EVs' expected SoC in different regions of the road network.

    2. A queuing theory based driver routing behavior model designed for stationary wireless charging, which is used for estimating the possible impact of deployed chargers on existing traffic.

    3. Formulation and solution of an optimization problem and setting of specific constraints for obtaining the deployment plan of stationary wireless chargers.

    The application-specific contributions include:

    1. Application of Discrete Fourier Transform (DFT) [106] and AutoCorrelation Function (ACF) [106] for analyzing the frequency of passenger appearance.

    2. Trace-driven analysis and utilization of building functionality for determining the likelihood of passenger appearance.

    3. Extensive trace-driven experiments that consider multiple sources of vehicle traffic under standard parameter settings and multiple days with different scenarios.

(2) A novel approach for deploying dynamic wireless chargers that incorporates entropy-based categorization and clustering of traffic flow attributes, and a KDE based traffic model to develop an optimization problem and its solution (Chapter 4). In this approach, the fundamental contributions include:

1. An entropy minimization based traffic attribute clustering method for the selection of candidate dynamic wireless charger deployment positions.
2. A queuing theory based driver routing behavior model designed for dynamic wireless charging, which is used for estimating the possible impact of deployed chargers on existing traffic.
3. Formulation and solution of an optimization problem and setting of specific constraints for obtaining the deployment plan of dynamic wireless chargers.

The application-specific contribution is extensive trace-driven experiments on the SUMO [56] urban mobility simulator under standard parameter settings and multiple days with different scenarios.

(3) A taxicab dispatching and charging approach that utilizes customized selection and training of suitable historical passenger demand data and charging optimization to minimize the taxicab's number of missed potential passengers due to charging (Chapter 5).

In this approach, the fundamental contributions include:

1. An entropy based estimation of passenger demand randomness for the customized selection and training of suitable historical passenger demand data.
2. Formulation and solution of a multi-objective combinatorial optimization problem for minimizing the number of missed potential passengers caused

by charging, maximize the probability of picking up a passenger, and meanwhile avoid the taxicab's SoC from exhaustion in the rest time of a day..

3. A Reinforcement Learning model based taxicab dispatching and charging method that outputs the action on which region the taxicab should drive to and whether to get charged.

The application-specific contribution is extensive trace-driven experiments on the SUMO [56] urban mobility simulator under standard parameter settings and multiple days with different scenarios.

1.4 Organization

The rest of this dissertation is organized as follows. Chapter 2 first provides the introduction of the status-quo of EV wireless charging. Then it describes the dataset used for analysis and evaluation of the proposed methodologies, and simulation specifications. Finally, it presents the system model and global assumptions for this dissertation.

Chapter 3 proposes the approach for stationary wireless charger deployment that utilizes spatial and temporal analysis of passenger appearance and a generic traffic model to both maximize the taxicabs' opportunity of picking up passengers at the chargers and support the taxicabs' continuous operability on roads with the minimal deployment cost. Chapter 4 proposes the approach for dynamic wireless charger deployment that utilizes categorization and clustering of traffic flow attributes and a generic traffic model to support the continuous operability of electric vehicles on roads with the minimal deployment cost. Chapter 5 proposes the approach for taxicab dispatching and charging that utilizes customized selection and training of suitable historical passenger demand data and charging optimization to minimize the taxicab's number of missed potential passengers due to charging.

Chapter 6 provides an overview of the related work. Finally, Chapter 7 concludes this dissertation with future remarks.

Chapter 2

Background and Dataset Description

In this dissertation, we focus on fulfilling the methodologies of building a WPT charging system in EV based transportation scenarios. While we present our designs and results under the vehicle traffic based settings, they generalize to any traffic flow based CPS related fields, such as human mobility modeling and control, air traffic prediction and scheduling, traffic control in video-on-demand system, etc.

In this chapter, we first provide a brief introduction of the status-quo of EV wireless charging. Then we describe the dataset used for analysis and evaluation of the proposed methodologies, and simulator specifications. Finally, we specify the system model and global assumptions for this dissertation.

2.1 Wireless Charging

WPT charging for EVs is gaining more ground, since it enables power exchange between the EV and the power grid without cable connection and brings much convenience. Installed infrastructure can be utilized very effectively, since many vehicles use the same road segments that are facilitated with WPT charging capabilities. WPT charging can take place in a parking lot, in a bus stop during passenger disembarkation, along a highway or near traffic lights. As discussed in Chapter 1, WPT chargers can be grouped into two categories: stationary wireless charger (Figure 1.1) and dynamic wireless charger (Figure 1.2).

Recently, Telewatt project [92] introduced an approach to reuse existing public lighting infrastructures for WPT charging. A fraction of the power not consumed by the lamps at night can be used for the benefit of the charging stations. The service is accessible by a smartphone application, where clients specify to the Telewatt server their destination and their battery level and take as a response a list of available charging terminals close to the destination. Hevo [40] announced a novel dynamic charging system where manhole covers will be used as charging stations. The Hevo Powers pilot program is scheduled to be performed in New York City in 2014. Two buses that use dynamic wireless charging during travel have been put into service for the first time in the world on normal roads in the city of Gumi-Korea by the Korea Advanced Institute of Science and Technology (KAIST) [48, 50, 54]. The power is transmitted through magnetic fields embedded in the roads. Power comes from the electrical cables buried under the surface of the road, creating these magnetic fields. The length of power strips installed under the road is generally 5%-15% of the entire road. In [24], the authors present a method for Power Transfer between Electric Vehicles, where drivers "share" charge with each other using Inductive Power Transfer (IPT) of charge between vehicles at rendezvous points.

As for the charging model of WPT charging systems, according to prior works focusing on the technical details of stationary and dynamic wireless chargers [48, 50, 54], given a constant charging rate r, the amount of energy an EV receives from a wireless charger (denoted by E) is proportional to the length of time t the EV spends over the wireless charger. That is, for stationary wireless chargers, the amount of energy that the EV receives is calculated as $E = r \cdot t$. For dynamic wireless chargers, given the length of a charging lane L and the EV's passing velocity over the charging lane v, the amount of energy that the EV receives is calculated as $E = r \cdot L/v$.

2.2 Large-scale Mobility Dataset of Public Transportation Vehicles

Our mobility dataset for research is collected in Shenzhen, China. It records the status (e.g., timestamp, position, speed) of vehicles with a recording period less than 30 seconds, which include:

(1) **Taxicab data.** It is collected by the Shenzhen Transport Committee, which records the status (e.g., timestamp, position, speed) of 15,610 taxicabs. The daily size of the uploaded data is around 2GB.

(2) **Bus data.** It is also collected by the Shenzhen Transport Committee, which records the status of 14,262 buses (e.g., timestamp, GPS position).

(3) **Dada bus data.** It is provided by the Dada Bus corporation (a customized transit service similar to UberPool), which records the status (e.g., timestamp, position, speed) of 12,386 reserved service buses.

(4) **Road map data.** The road map of Shenzhen is obtained from OpenStreetMap [84]. According to the municipal information of Shenzhen [98], we use a bounding box with coordinate ($lat = 22.4450, lon = 113.7130$) as the south-west corner, and coordinate ($lat = 22.8844, lon = 114.5270$) as the north-east corner, which covers an area of around 2,926km^2, to crop the road map data.

For data management, we utilized a 34 TB Hadoop Distributed File System (HDFS) [3] on a cluster consisting of 10 nodes, each of which is equipped with 16

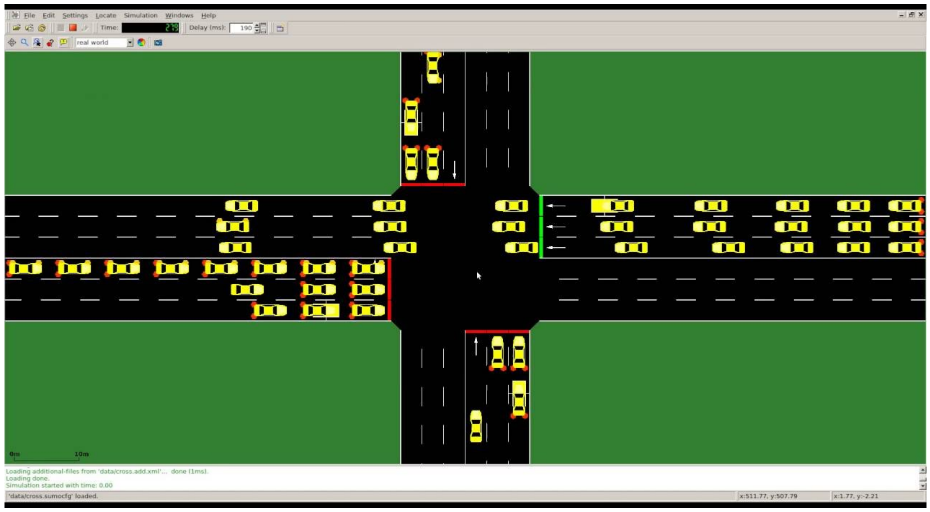

Figure 2.1: SUMO simulation platform

cores and 64 GB RAM. For data processing, we used Apache Spark [4], which is a fast in-memory cluster computing system running on Hadoop [3].

2.3 Simulator Specifications

In this dissertation, we use SUMO (Simulation of Urban MObility) [56] to implement and evaluate the proposed methodologies. SUMO is a free, open, microscopic and continuous road traffic simulation suite designed to handle large road networks. It allows modelling of intermodal traffic systems including road vehicles, public transport and pedestrians. SUMO includes a wealth of supporting tools, which handle tasks such as route finding, visualisation, network import and emission calculation. SUMO can be enhanced with custom models and provides various APIs to remotely control the simulation. The interface of SUMO is illustrated in Figure 2.1.

2.4 System Model and Assumptions

In this section, we define the system model, present the terminology and the global assumptions in this dissertation.

System Model: We consider the *road network* as a directed graph $G = (E, V)$, in which vertices V represent landmarks (i.e., intersections or turning points), and edges E represent road segments [124, 135]. For a road segment longer than 200 meters, which is the general length of a metropolitan road segment [135], we broke it into several road segments no longer than 200 meters, and set the breaking positions as new landmarks. The movement record of a taxicab is continuous, namely a sequence of GPS positions with corresponding timestamps. If a vehicle has arrived at its destination, it will usually spend a long time staying at the destination before starting its next trajectory [135]. Therefore, we suppose that a vehicle has finished its previous trajectory if its position does not change for more than 10 minutes. Such positions will cut the vehicle's movement record into multiple trajectories.

Terminologies: Based on the road network, we introduce the following definition for vehicle trajectory:

Definition 1 Vehicle Trajectory. *A vehicle's trajectory is a sequence of N^s time-ordered landmarks, $\{(p_0, t_0), \ldots, (p_j, t_j), \ldots, (p_{N^s-1}, t_{N^s-1})\}$, where each landmark is represented by a latitude and a longitude $p_j = (lat_j, lon_j)$.*

We partition the road network into multiple different regions and use them as the unit for the extraction and analysis of passenger appearance and charging demand. Specifically, we have the following definition for region:

Definition 2 Region. *The road network is partitioned into a set of $N^G = 496$ regions $G = \{g_0, g_1, \ldots, g_{N^G-1}\}$ according to administrative region planning of Shenzhen city government.*

Unless otherwise specified, the trajectories and regions in this thesis follow the above definitions.

Global Assumptions: In this dissertation, we have the following global assumptions:

(1) All buses, taxicabs and customized transit vehicles are autonomous EVs, and are fully controlled by the dispatch center (source: [42, 67]). In addition, if a vacant taxicab (i.e., no passenger onboard) encounters a hand-waving passenger on route, the taxicab can change its destination road segment to serve the encountering passenger instead (source: [122, 125]).

(2) The deployment cost of chargers mainly consists of excavation cost at the charging position, installation cost of the charger body, and the wiring cost to the chargers (source: [20, 45]). The extra cost due to policy or other regulation factors is not the focus of this dissertation. We leave the detailed analysis and optimization of economical aspects of building a WPT charging system as one of our future works.

(3) The chargers are deployed one time. We have developed a queuing theory based driver routing behavior model to take into account the possible impact of charger deployment on existing traffic distribution. When the long-term traffic flows in the city change significantly, the wireless chargers need to be re-deployed.

(4) Based on existing tests of Electreon Wireless Ltd (an Israeli company focusing on wireless charging for EVs) in Sweden and Tel Aviv [27, 46] and existing wireless charging standard SAE J2954 [95], the charging power level is currently very low (e.g., maximally 22kW). However, with the most recent research implementations (e.g., Oak Ridge National Laboratory [85]), it is expected that within a 10-year timeframe, it is possible to reach a charging rate over 100kW

for EV wireless charging. Therefore, we use 150kW as the charging rate in the performance evaluations of this thesis.

Chapter 3

Deployment of Stationary Wireless Chargers

The profiting of taxicabs is highly reliant on efficient discovery of passengers [122]. To maximize the profit of electric taxicabs, their idle time (i.e., cruising time for passengers, seeking time for chargers and charging time) must be reduced as much as possible [123]. Although many taxicab dispatching methods have been proposed to guide taxicabs to efficiently pick up passengers with reduced cruising miles [122, 123, 125, 134], the taxicabs still have to spend much time driving before picking up the passengers. Moreover, none of the previous taxicab dispatching works considers the time wasted on seeking chargers and charging. It has been reported that the daily average time wasted on seeking the nearest charging station can be almost 1 hour, and the time for charging an EV can be as long as 150 minutes [62]. Such a long idle time greatly degrades the profiting efficiency of the electric taxicabs [80]. Also, since a taxicab cannot be in service all the time due to charger seeking and charging, a metropolitan city needs to put more taxicabs on roads to satisfy taxicab demands, which increases investment cost and traffic congestion on roads.

Meanwhile, driven by the traffic flow and city-wide travel patterns of people reflected in the ubiquitous taxicab movement data, several recent works studied the problem of minimizing average seeking time for the nearest charging station of EVs from the perspective of urban facility planning [62, 89, 115, 130]. These works generally adapt the deployment of charging stations to cover the EV traffic flows so that EVs anywhere can reach the nearest charging stations with the minimal seeking time. However, no matter how well these methods place the charging stations, upon the exhaustion of a battery, the taxicabs must spend extra idle time on seeking a charger and waiting to be charged.

Previous studies have found that taxicabs have relatively fixed parking patterns determined by the appearance of passengers, but random driving routes [122, 123]. As discussed in Chapter 1, a stationary wireless charger allows EVs to get charged when they are temporarily parked at somewhere (e.g., traffic lights, roadside parking lots) without plugging in a cable, which is called opportunistic charging [30]. Then, if the taxicabs can be offered sufficient opportunities of charging during parking from a proper deployment of stationary wireless chargers, the taxicabs' processes of charging and waiting for passengers may occur simultaneously before picking up the next passenger, which will greatly reduce the taxicabs' idle time. Therefore, in this chapter, we propose *PickaChu*, a stationary wireless charger deployment scheme that enables the taxicabs to Pick up a passenger with reduced idle time and supports the taxicabs' continuous operability (i.e., always having enough energy to drive) via opportunistic Charging in an urban road network.

The remainder of this chapter is organized as follows. Section 3.1 identifies the background and challenges in the design of *PickaChu*. Section 3.2 presents our metropolitan dataset measurement results. We describe the main design of *PickaChu* in Section 3.3 and present our experiment evaluation in Section 3.4. Section 3.5 concludes this chapter with remarks on our future work.

3.1 Background

Several efforts [122, 123, 125, 134] aim to guide taxicabs to pick up the expected passengers with the shortest route to reduce the taxicabs' time wasted on cruising for passengers. Yuan *et al.* [122] introduced a method that schedules the pick-up locations with the shortest routes for taxi drivers and the waiting locations for passengers to reduce the cruising time. Zheng *et al.* [134] modeled the behavior of vacant taxicabs with a non-homogeneous Poisson process to find the optimal waiting positions for passengers. Zhang *et al.* [123] proposed a method to estimate the revenue of each route, and guide the taxicab to the route with the maximum estimated revenue. Zhang *et al.* [125] proposed *pCruise*, in which each taxicab collects the passenger requests from nearby taxicabs and accordingly cruises on the routes with the maximum probability of finding a passenger. However, these works still require the taxicabs to spend much time on driving to the suggested locations without passengers on board. Moreover, the time wasted on seeking chargers and charging is not considered in these works.

Several recent works studied the problem of minimizing average seeking time for the nearest charging station of EVs from the perspective of urban facility planning [62, 89, 115, 130]. Qin *et al.* [89] scheduled the plug-in charging stations to minimize the time on seeking and waiting in charging stations based on the estimated time and location that each EV needs to be charged. Zhang *et al.* [130] further considered the uncertainty of the EVs' arrival times at the charging stations to shorten the time on seeking chargers and charging. Li *et al.* [62] determined the locations for deploying plug-in charging stations that minimize the time on seeking chargers. Yan *et al.* [115] proposed a method on deploying dynamic wireless chargers based on the features of the positions (i.e., vehicle passing speed, vehicle visiting frequency). Although these works can support the continuous operability of the taxicabs by adapting the deployment of chargers to cover the actual traffic, the taxicabs still have to spend extra idle time on seeking chargers and charging upon the exhaustion of the battery.

To maximize the service performance of the taxicabs, we need to design a mechanism that provides opportunity of picking up passengers for the taxicabs, and meanwhile keeps the SoC of taxicabs above a threshold. Specifically, we identify two main challenges in designing such a mechanism:

(1) **Measuring likelihood of passenger appearance.** The historical average number of passengers that appeared during a unit time (e.g., per hour, per day) can be an indicator of the passenger appearance likelihood. However, using this metric alone for the likelihood measurement may not be accurate for guiding taxicab pick-ups in terms of waiting time. We hope that when a taxicab arrives at a charger and gets charged at a random time, it does not have to wait long before discovering a passenger. For example, in an area mostly consisting of residential buildings, many passengers may appear during rush hours (e.g., 08:00-09:00), resulting in a relatively high hourly average number of appeared passengers. However, this high value does not mean that passengers frequently appear at other times. Thus, the first challenge is how to design a new metric that can more accurately reflect the passenger appearance likelihood to guide taxicab pick-ups.

(2) **Supporting taxicabs' continuous operability.** Regions with higher passenger appearance likelihood should have a higher priority to be deployed with a charger in order to offer sufficient passenger pick-up opportunity at the chargers. In addition, we aim to minimize the number of chargers (i.e., deployment cost) while maintaining the taxicabs' continuous operability. Thus, the second challenge is how to optimize the deployment of stationary wireless chargers considering the above goals.

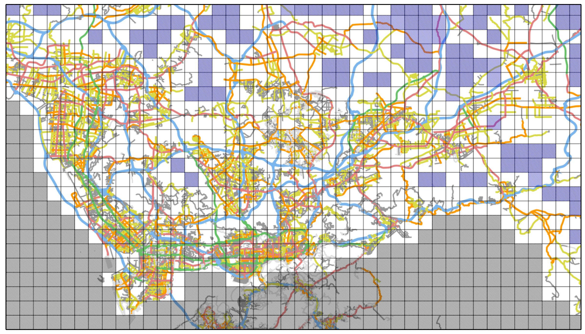

Figure 3.1: Gridded road map.

3.2 Dataset Analysis

3.2.1 Definitions

We first build a *road network*, in which vertices represent landmarks (i.e., intersections or turning points), and edges represent road segments [23, 135]. The movement record of a taxicab is continuous, namely a sequence of GPS positions with corresponding timestamps. We presume that a taxicab has finished its previous trajectory if it stops at a location for more than 10 minutes or its occupancy status changes. Thus, such stopping locations cut the movement record of a taxicab into multiple trajectories. The original GPS positions are scattered around the road segment. If we apply the optimization on all the GPS positions, we will need to ensure that the taxicabs' SoC on each position is above the threshold. This will be too complex to obtain an optimal solution for the optimization problem. To map them to a uniform road network for the reduction of optimization complexity, we normalize the original GPS positions to their respective nearest landmarks (in Euclidean distance) as in previous methods [112, 122, 125, 139]. Note we only use landmarks in the traffic estimation and optimization of the chargers. For the extraction and analysis of passenger appearance, we still rely on the original GPS positions. We introduce two definitions below.

Definition 3 Vehicle Trajectory. *A vehicle v_i's trajectory is a sequence of time-*

ordered landmarks, $Tr_i : \{(\boldsymbol{p_0}, t_0), (\boldsymbol{p_1}, t_1), \ldots, (\boldsymbol{p_r}, t_r)\}$*, where each landmark is represented by a latitude and a longitude* $\boldsymbol{p_j} = (lat_j, lon_j)$.

Definition 4 Region. *The road map is partitioned into a set of 557 regions* $G = \{\boldsymbol{g_0}, \boldsymbol{g_1}, \ldots, \boldsymbol{g_{M-1}}\}$ *with a size of 2,000 m × 2,000 m (Figure 3.1). Each region is represented by* $\boldsymbol{g_i} = \{(lat_i^0, lon_i^0), (lat_i^1, lon_i^1)\}$.

For the ease of analysis, we use a static region size to partition the road map. Some recent works have proved that partitioning the road map with dynamic region sizes can better adapt to the geographical distribution of the passenger appearance [76, 136]. We will use dynamic region size in our future work, but the region size determination does not change the fundamental methods proposed in this dissertation. The reason we choose 2,000 m × 2,000 m as the region size is to ensure that for the taxicabs within a region, they can reach any position of the region within roughly 6 minutes, which is an acceptable waiting time length for most passengers [122], at the driving speed of 40 km/h (i.e., the approximate average speed limit of Shenzhen [115]). Combining the taxicabs' trajectories with the changes of their occupancy status, we extracted the pick-up and drop-off locations of the passengers. We calculated the number of passenger pick-ups in each region per unit time (e.g., 30 minutes).

3.2.2 Building Functionality and Passenger Appearance

It was indicated that the passenger appearance in a region is closely related to its composition of buildings, and the likelihood of passenger appearance varies for different classes (i.e., functionalities) of buildings [123, 139]. In this analysis, we attempt to verify if the density and functionalities of buildings (e.g., Residential, Commercial buildings) in a city region influence the number of taxicab passengers in the region.

To study the relation between buildings and the appearance of passengers, we derived the distribution of passenger pick-up events in a part of the road map. As

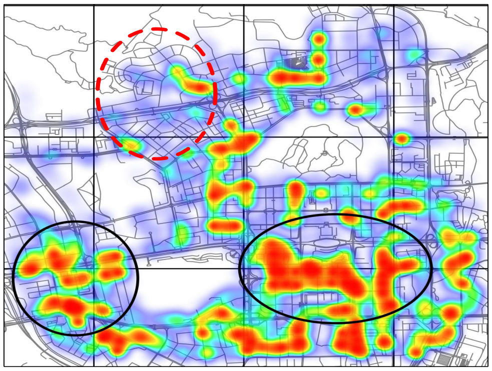

Figure 3.2: Heat map of passenger pick-ups.

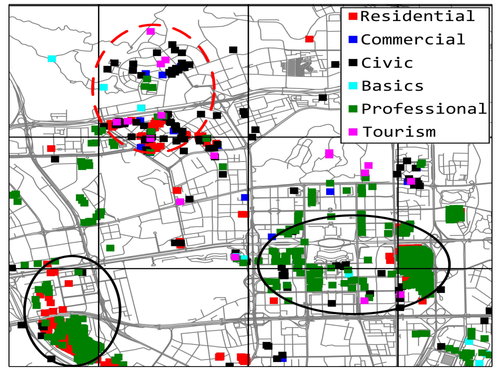

Figure 3.3: Distribution of buildings.

shown in Figure 3.2, we plot each passenger pick-up event happened in 2015 with a point and drew the heat map. The warmer color a region has, the more concentrated in a short time duration the passenger pick-up events occur. Based on [44, 120] and OpenStreetMap [84], we obtained the class and position of each building in Shenzhen. The building classes include *Residential*, *Commercial*, *Civic*, *Basics*, *Professional* and *Tourism*, as shown in Figure 3.3. The *Residential* class consists of buildings primarily for residential purposes (e.g., apartments). The *Commercial* class consists of buildings for commercial activities (e.g., supermarkets). The *Civic* class consists of buildings for municipal purposes (e.g., library). The *Basics* class consists of buildings for public service (e.g., garage). The *Professional* class consists of buildings for specific usage (e.g. train/subway stations, airports). The *Tourism* class consists of buildings for recreation (e.g., garden).

By comparing the two figures, we can see that the occurrence of passenger pick-up events generally concentrates at the regions with abundant buildings (e.g., the two regions on the bottom marked with solid circles). In the region on the top marked by red dashed circles, there are much fewer pick-up events though it has many buildings. This is because the majority are residential and civic buildings, where people often have planned travel schedules using private vehicles or public transportation. This result implies that building functionality also influences passenger appearance.

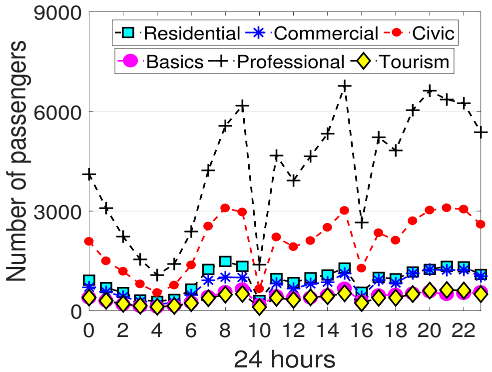

Figure 3.4: Num. of passengers for each building class.

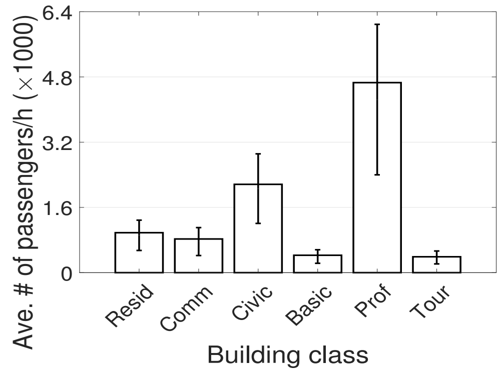

Figure 3.5: Average number of passengers per hour.

Next, we study the correlation between the building functionalities and the number of passengers. We measured the average number of passengers that appeared within 100 meters around each building in a building class during each hour of a day throughout the 365 days, as illustrated in Figure 3.4. Though we have already considered the number of passengers that appeared around each building in the measurement, additionally considering building size may further increase the precision of the measurement, which is left as our future work. We further calculated the average, 5^{th} and 95^{th} percentiles of the hourly number of passengers that appeared nearby for each building class, which are illustrated in Figure 3.5. We see that significantly more passengers appeared nearby the *Professional* buildings than the other building classes during all times. This is because the *Professional* class mostly consists of offices and business buildings that are frequently visited by many people. The *Civic* class has the second most passengers because it mostly consists of libraries and community centers with many public activities. The *Commercial* and *Residential* classes have much fewer passengers than the former two classes because these buildings are not continuously visited by people during a day. The *Basics* and *Tourism* classes have the fewest passengers because there are fewer such buildings. Therefore, the building functionality can be used as a factor to infer the likelihood of passenger appearance in the regions. As the number of pick-ups does not necessarily equal to the number

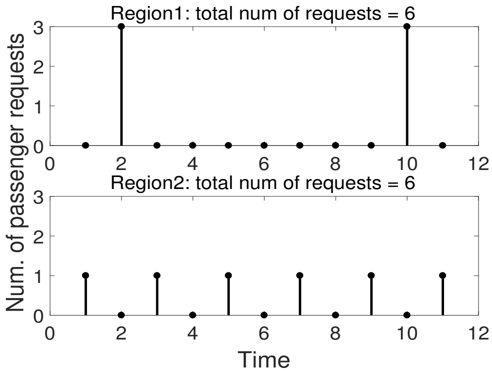

Figure 3.6: Frequency comparison of passenger requests' appearance.

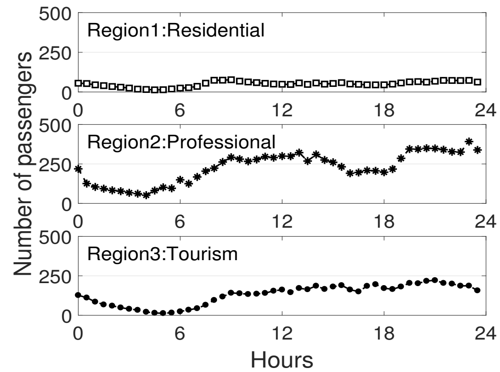

Figure 3.7: Passenger time series of regions.

of passenger requests, we need to use other additional factors to more accurately estimate the likelihood of passenger appearance.

3.2.3 Frequency of Passenger Appearance

We hope that when a taxicab arrives at a region deployed with a wireless charger, it does not need to wait long before it discovers a passenger. This means that the frequency of passenger appearance in the region must be high, namely the time interval between two consecutive passenger appearances must be short. Note that one passenger appearance means the appearance of passenger(s) at one time. In Figure 3.6, in Region1, three passengers appearing at one time is considered as one passenger appearance, and in Region2, one passenger appearing at one time is also considered as one passenger appearance. Then, the frequency of passenger appearance for Region1 is 1/8, and that for Region2 is 1/2. However, the average number of passengers per unit time (i.e., a day) cannot reflect this frequency. For example, Region1 has 3 passengers in every 8 time units, while Region2 has 1 passenger in every 2 time units. Though both regions have 6 passengers in every 12 time units, Region2 has a higher passenger appearance frequency (1/2) compared with Region1 (1/8), which makes a taxicab wait for a shorter time before it discovers a passenger. As a result, we need to develop a new method to determine the frequency of passenger appearance in a region.

To find the frequency, we draw passenger appearance time series. For each region, we calculated the number of passengers that appeared in every 30 minutes (i.e., a sample) in each day for the 365 days in the dataset. Among the regions mostly consisting of (i.e., more than 50%) *Residential*, *Professional* and *Tourism* buildings, we randomly chose one region respectively, and denote them as *Region1:Residential*, *Region2:Professional* and *Region3:Tourism*. Figure 3.7 shows the number of passengers that appeared per unit time (i.e., 30 minutes) in the first day of the three regions, respectively. We define a pattern as the periodic occurrence of a certain number of passengers in a certain time period, and its frequency as the number of such occurrences per unit time. If the time series of every region has only one pattern, identifying its frequency is easy. However, the time series may have multiple patterns, which makes it hard to measure the passenger appearance frequency in the region. In the signal processing field, the time series curve in Figure 3.7 can be considered as a composition of multiple patterns with different frequencies. To find out the frequencies of the patterns, we can decompose the time series to a group of time series with different frequencies using a signal processing technique. Specifically, we applied the Discrete Fourier Transform (DFT) on the passenger time series and got their periodogram [106], as shown in Figure 3.8. In the figure, the X-axis is the possible frequencies of the patterns in the time series, and the Y-axis reflects the number of passengers in a pattern with a frequency (e.g., 3 and 1 in the above example). We notice that the periodogram of Region2 has relatively more patterns with high frequencies than Region1 and Region3, although the numbers of passengers in the high-frequency patterns are much smaller than that of the low-frequency patterns. This is because the *Professional* buildings are frequently visited by many people, which results in more frequent passenger appearances than the *Residential* and *Tourism* buildings. Compared with Region3, Region1 has more patterns with

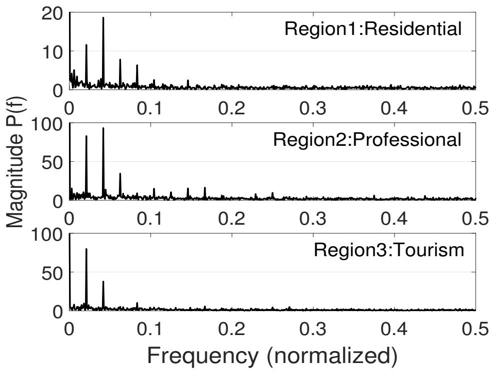

Figure 3.8: Periodogram of the passenger time series.

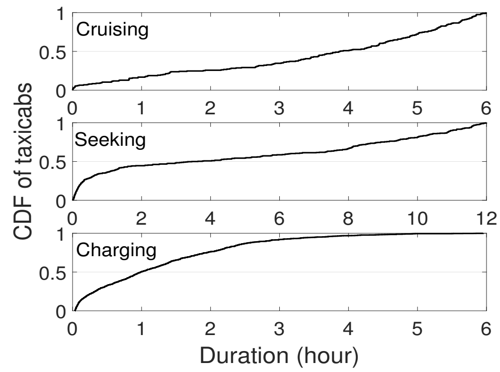

Figure 3.9: Distribution of duration of idle trips.

higher frequencies. This is because people's visiting patterns at the *Tourism* buildings is more likely to follow certain routine (e.g., open and close times) than the *Residential* buildings, which is more randomly visited by people.

Thus far, we have verified that the time series of the passenger appearance of a region can be decomposed to a group of time series with different frequencies. Then, we design a method to combine these frequencies to measure how frequently passengers appear in a region, which will be introduced in Section 4.3.3.2. As a result, the region with a higher final frequency metric should have a higher priority to deploy chargers.

3.2.4 Idle Trip Time & Taxicab Traffic

As discussed before, taxicabs may waste much time on cruising for passengers, seeking chargers and getting charged. We then analyzed the Shenzhen dataset to see how much time is spent on these idle operations. We first introduce the definitions for the operations of the taxicabs. We define the cruising time as the time interval between the taxicab dropping off a passenger and picking up the next passenger. From the Shenzhen Transport Committee, we obtained the locations of all the existing plug-in charging stations in Shenzhen. If a taxicab's movement record shows that it has stayed at a charging station for more than 5 minutes, we consider that it was being

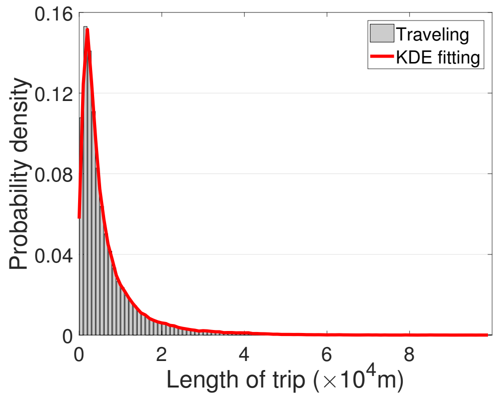

Figure 3.10: Traveling trip lengths & KDE estimation.

charged at the station at that time. Therefore, we define the time for seeking a charger as the time interval between the taxicab dropping off its last passenger and entering a charging station to charge. We define the charging time of a taxicab at a charging station as the time duration that the taxicab stayed at the charging station. For each vehicle, we calculated the duration of each idle operation in each day throughout the 365 days, and then calculated the average duration per day. We show the Cumulative Distribution Function (CDF) of the taxicabs in terms of the daily average duration of each operation in Figure 3.9. We can see that about 50% of the taxicabs spent more than 4.17 hours on cruising per day in average, about 50% of the taxicabs spent more than 2.78 hours on seeking chargers per day in average, and about 50% of the taxicabs spent more than 0.83 hours on charging per day in average. The analytical results indicate that we should try to avoid or reduce the time duration in these idle operation phases when determining the locations to deploy chargers. We can choose the locations where many passengers appear with high frequency, so that when a taxicab is being charged, it has a high probability to quickly pick up a passenger.

We should also make sure that the deployed chargers can support the continuous operability of the taxicabs considering the taxicabs' traffic flows in the city. Because the taxicabs' trajectories reflect their traffic flows between different locations [120], and the trajectory length generally determines energy consumption of a taxicab, we calculated the lengths of the taxicabs' trajectories to determine the taxicab traffic that the deployed chargers need to support. Figure 3.10 shows the Probability Density Function (PDF) of the trajectory lengths. If we can describe the taxicabs' trajectory lengths with a certain distribution, we can further determine the deployment of chargers to support these trajectory trips so that the expected SoC of a taxicab at a landmark is always above a certain threshold that allows it to reach its nearest charger. Obviously, the distribution of the trajectory lengths cannot be modeled using a parametric distribution (e.g., Gaussian). Since KDE is a non-parametric method to estimate the PDF of a random variable, we input the trajectory lengths to the KDE model to output a taxicab's probability of reaching each landmark in the road network. The red curve in Figure 3.10 represents the fitting result from the KDE. We will present more details of this model in Section 4.3.4.1.

3.2.5 Summary

Based on the above observations, to deploy the chargers that maximally reduce the idle time of taxicabs, we need to i) consider the density and functionality of buildings and their respective influence weights on the appearance of passengers, ii) measure the passenger frequency in a region from the region's passenger appearance time series, and iii) estimate the taxicabs' SoC based on the taxicabs' traffic flows. Considering these factors, we will find a solution in Section 3.3 for the following problem.

Problem: Given a road network comprised of a set of regions G, and taxicabs' trajectory datasets $\{Tr\}$, how to select regions to deploy chargers with the minimum cost so that the expected SoC of the taxicabs at each landmark is no less than a threshold, and the taxicabs have high probability of discovering passengers while being charged?

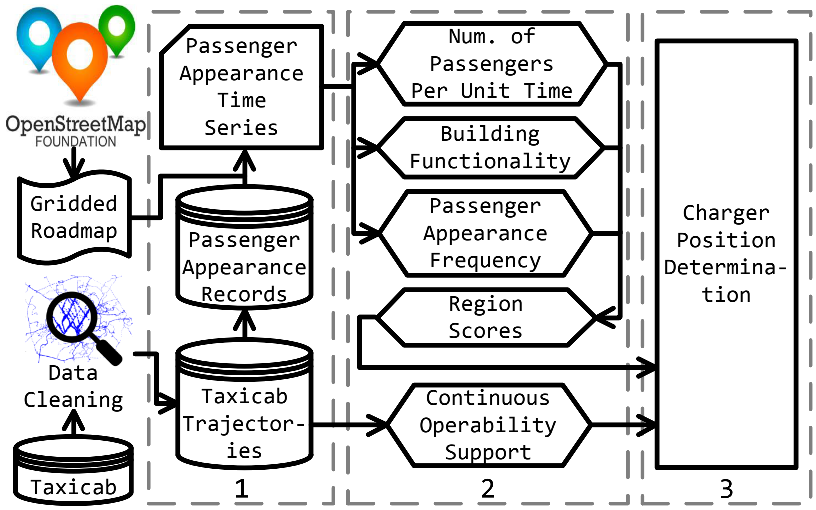

Figure 3.11: Framework of *PickaChu*.

3.3 System Design of PickaChu

3.3.1 Framework of PickaChu

PickaChu consists of the following three stages as shown in the three dashed boxes in Figure 3.11.

1. Map gridding & information derivation. First, the entire city area is partitioned into a *Gridded Roadmap* consisting of several equal-sized regions. Also, the taxicab dataset is cleaned up (e.g., filtering out positions out of the actual range of Shenzhen, redundant positions). Then, based on the cleaned data, we derive the *Taxicab Trajectories*, which will be used for extracting passenger requests and building traffic models. From the taxicabs' change of occupancy status from 0 to 1, we extract the *Passenger Appearance Records* (i.e., location and time). Finally, based on the *Gridded Roadmap* and the *Passenger Appearance Records*, we calculate the *Passenger Appearance Time Series* for each region.

2. Measuring likelihood of passenger appearance (Section 5.3.4). Based on the output from the first stage, we consider the *Number of Passengers Per Unit Time*, the *Building Functionality*, and the *Passenger Appearance Frequency* for each region to assign *Region Scores* to regions to measure their likelihood of passenger appearance.

3. Charging position determination (Section 4.3.4.1 and Section 4.3.4.2) We first use the lengths of the trajectories to model the *Continuous Operability Support* using KDE, which is used to estimate the taxicabs' expected SoC at different regions. Then, we formulate a multi-objective optimization problem to solve the wireless charger deployment problem, and its solution is the *Charger Position Determination* (i.e., where and how many wireless opportunistic chargers we should deploy).

3.3.2 Assumptions

Above all, we have the following assumptions for EVs:

1. Each EV that expects the charging service provided by the stationary wireless chargers is equipped with a receiver coil (source: [55, 71, 78]).
2. Each taxicab is equipped with a navigation system, which generates trajectories during the driving of the vehicle (source: [135]). Each taxicab is willing to report its driving trajectory to a central traffic control center for traffic information analysis (i.e., passenger appearance analysis, SoC consumption estimation). A trajectory is periodically updated whenever the vehicle starts driving.
3. The deployed stationary chargers are only available for taxicabs and work in a first-come-first-served manner (source: [14, 42]). For the deployment of stationary wireless chargers for private vehicles, travel trajectory data of private vehicles and detailed analysis are needed, which is not the focus of this work and left as a future direction.

3.3.3 Measuring Passenger Appearance

In the following, we firstly introduce how *PickaChu* estimates the likelihood of passenger appearance via a weighted sum of building functionalities. Then, we elaborate how *PickaChu* measures the frequency of passenger appearance in a region. Finally, we design a scoring mechanism for measuring each region's likelihood of passenger appearance.

3.3.3.1 Building Functionality

Different regions have different densities of buildings with different functionalities (e.g., *Residential* buildings, *Commercial* buildings). For example, the region in a central business district is likely to be filled with office buildings and shopping centers where passengers frequently appear, while the region in a residential area is likely to be filled with dwellings where a large number of passengers only appear during specific hours. Correspondingly, we use a weighted sum of building functionalities within a region to measure the buildings' potential contribution to passenger appearance.

We set the weight of a building class as the hourly average number of passengers that appeared nearby (e.g., within 100 meters) each building in the class throughout the dataset. For example, according to Figure 3.5 of our trace analysis, the weights of the building classes are: *Residential*=0.9, *Commercial*=0.7, *Civic*=2.0, *Basics*=0.2, *Professional* =4.4, and *Tourism*=0.2.

Suppose C is the set of the building classes in a region $\boldsymbol{g_i}$, and $\mathrm{P}_i(c)$ is the probability function of building class c, i.e., the percentage of buildings with building class c in $\boldsymbol{g_i}$. $\mathrm{w}(c)$ is the passenger appearance weight of building class c. We define the weighted sum of the building functionalities in $\boldsymbol{g_i}$ as:

$$\bar{H}_i = \frac{B_i}{B_{max}} \sum_{c \in C} \mathrm{w}(c)\mathrm{P}_i(c) \tag{3.1}$$

where B_i is the total number of buildings in $\boldsymbol{g_i}$, and B_{max} is the maximum number of buildings in a region among all the regions, i.e., $B_{max} = \max_{\boldsymbol{g_i} \in G} B_i$. Suppose a region has the following composition: {*Residential* (20%), *Commercial* (5%), *Civic* (20%), *Basics* (5%), *Professional* (10%), *Tourism* (40%)}, and $B_i = 100$, $B_{max} = 500$. Its weighted sum of the building functionalities is $\frac{100}{500} \times (0.9 \times 0.2 + 0.7 \times 0.05 + 2.0 \times 0.2 + 0.2 \times 0.05 + 4.4 \times 0.1 + 0.2 \times 0.4) = 0.23$. From Section 3.2.2, we know if a region has more heavy-weighted buildings, it has a larger H_i, meaning it tends to have more passengers.

3.3.3.2 Frequency of Passenger Appearance

When deploying chargers, we hope that when a taxicab arrives at a charger at a random time, it has a high probability of discovering a passenger nearby. It means that the region has a high frequency of passenger appearance and the number of passengers should be high at a time. As shown in Section 3.2.3, a passenger appearance time series can be considered as being composed by a group of patterned time series with different frequencies. We call the area size (i.e., the number of passengers) of a pattern (i.e., Y value in Figure 3.8) the *magnitude* of the pattern. Thus, we need to i) derive passenger appearance frequency, ii) derive the patterns with a high magnitude, and iii) find a way to measure the global frequency given multiple patterns. For tasks i) and ii), we use the approach introduced in [106]. For task iii), we design a metric. The details are introduced below.

In Section 3.2.3, we show that we can detect the potential patterns and their frequencies of a region's passenger appearance time series through DFT. However, DFT may generate false frequencies in the periodogram [63]. AutoCorrelation Function (ACF), another method for detecting repeated patterns, can avoid false detection of frequencies of a time series [106], but may result in the detection of integer times of true periods (i.e., reciprocal of the frequencies) [63]. For example, in addition to the true frequency of a pattern, say 1/30, the frequencies, which are integer multiples of 1/30 (i.e., {1/60, 1/90, ...}), are also falsely considered as the frequencies of this pattern. Therefore, solely using DFT or ACF cannot accurately determine the true frequencies in a time series. To more accurately find the patterns, we adopt the approach in [106] that combines the results from DFT and ACF to identify frequencies.

Below, we first present how to derive patterns with significant magnitude [106] from the periodogram generated by DFT. We then present how to get the intersection of the two groups of frequencies from DFT and ACF as the final detected frequencies. Finally, we propose a method that combines all the frequencies to get a global metric to evaluate the frequency of passenger appearance in a region.

(1) *Deriving patterns with significant magnitude.* As shown in Figure 3.8, some patterns have an extremely low magnitude. Therefore, we first determine the base magnitude and then derive the patterns with magnitude larger than the base magnitude [106]. Considering that any random time series has patterns with certain magnitudes [106], we use its maximum magnitude (denoted by p_i^{max}) as the base magnitude. In a region $\boldsymbol{g_i}$, the passenger appearance time series is defined as: $x_i(n), n = 0, \ldots, N-1$, where N is the total number of samples and $x_i(n)$ is the value of the n^{th} sample. To create random time series, we randomly shuffle the original $x_i(n)$ into a new sequence $\tilde{x}_i(n)$. To ensure 99% confidence level on the selection of the base magnitude, we repeat the shuffling for 100 times and record the maximum magnitude each time. Finally, we choose the 99^{th} value as the base magnitude.

(2) *Determining global frequency.* In step (1), for $\boldsymbol{g_i}$, we select potential significant patterns with frequencies denoted by $F_i^{DFT} = \{f_i^1, f_i^2, \ldots, f_i^{m'}\}$. Then we use ACF to identify the patterns with frequencies denoted by $F_i^{ACF} = \{f_i^1, f_i^2, \ldots, f_i^{m''}\}$. The final frequency set is calculated by: $F_i = F_i^{DFT} \cap F_i^{ACF}$.

(3) *Measuring passenger request frequency in a region.* Suppose the magnitudes of the significant patterns with frequencies $F_i = \{f_i^1, f_i^2, \ldots, f_i^m\}$ in the time series are $P_i = \{p_i^1, p_i^2, \ldots, p_i^m\}$. Since the magnitude of a pattern reflects how significant this pattern is to the entire time series, we use the weighted sum of the frequencies of the

significant patterns to describe passenger appearance frequency in each region. We call it region $\boldsymbol{g_i}$'s weighted frequency of passenger appearance and denote it by $\bar{F}_i$.

$$\bar{F}_i = \sum_{k=1}^{m} \frac{p_i^k}{\sum_{j=1}^{m} p_i^j} \cdot f_i^k. \tag{3.2}$$

For example, consider a time series which has two significant patterns with magnitudes of 2 and 3, and frequencies of 1/10 and 1/20, respectively. The weighted frequency of this region is calculated as $\frac{2}{5} \times \frac{1}{10} + \frac{3}{5} \times \frac{1}{20} = \frac{7}{100}$.

3.3.3.3 Likelihood of Passenger Appearance

PickaChu assigns scores to the regions to show their likelihood of passenger appearance considering the above metrics. We favor the regions with more passengers, and higher frequency of passenger appearance. Therefore, we define the score of a region, say $\boldsymbol{g_i}$, as:

$$\rho(\boldsymbol{g_i}) = (\frac{\bar{x}_i}{\bar{x}_{min}})^{\alpha} \cdot \bar{F}_i^{\beta} \cdot \bar{H}_i^{\gamma} \tag{3.3}$$

where $\bar{x}_i = \frac{\sum_{n=0}^{N-1} x_i(n)}{N}$ is the average number of passengers over all the N samples of $\boldsymbol{g_i}$, $\bar{x}_{min}$ is the minimum average number of passengers in a region among the regions, $\bar{F}_i$ is $\boldsymbol{g_i}$'s weighted frequency of passenger appearance, $\bar{H}_i$ is the weighted sum of building functionalities in $\boldsymbol{g_i}$, and α, β, and γ are constants that control the respective influence of the three metrics. We scale $\bar{x}_i$ by $\bar{x}_{min}$ to constrain the scores of the regions that have few passengers, which have almost no contribution on increasing the score. To find the best values for α, β, and γ, we vary each variable within a certain range (e.g., [1, 5]) and test different combinations of the values. Specifically, we use each combination to determine the deployment of the chargers and run our experiment for 1 hour randomly chosen among the 24 hours of a day. Then, we choose the combination of the values that results in the minimum time duration of the idle phases on the vehicles (i.e., cruising, seeking for chargers and charging) as the final setting. We find $\alpha = 1.2$, $\beta = 2$ and $\gamma = 1$ is the best combination for the case of Shenzhen.

Table 3.1: Comparison between two regions.

	$\boldsymbol{g_1}$	$\boldsymbol{g_2}$
$\bar{x}_i$	110	22
$\bar{F}_i$	1/10	1/2
Composition	1 airport 1 barn	2 houses
Building wgt	Professional=4.4 Basics=0.2	Residential=0.9
W/o building	11	11
W/ building	25.3	9.9

Note that the region scores calculated by Equation (3.3) is not the optimal way to reflect the likelihood of passenger appearance, and it is only a heuristic approach. It is difficult to find the optimal way to describe the distribution of the likelihood of passenger appearance in different regions. In order to make the scores more accurately reflect the likelihood of passenger appearance, in addition to using parameters $\bar{x}_i$ and $\bar{F}_i$, we further consider the weighted sum of the building functionality ($\bar{H}_i$) that also reflects the number of passengers in a region. In other words, parameter $\bar{H}_i$ enlarges the difference between the regions with higher likelihood of passenger appearance and the regions with low likelihood of passenger appearance. That is, the distribution of region scores calculated by Equation (3.3) is closer to the actual distribution of the likelihood of passenger appearance in different regions. In spite of the simplicity of this approach, it is helpful for differentiating the likelihood of passenger appearance in the regions. We use a simple example to show the effectiveness of additionally considering parameter $\bar{H}_i$. Suppose we have two regions, say $\boldsymbol{g_1}$ and $\boldsymbol{g_2}$, with different compositions of buildings, of which details are summarized in Table 3.1. We can see that in $\boldsymbol{g_1}$, there is an airport (50% of the buildings, classified as *Professional*), and a barn (the other 50% of the buildings, classified as *Basics*); while in $\boldsymbol{g_2}$, there are 2 houses (100% of the buildings, classified as *Residential*). Suppose the weights of the building classes are: *Professional*=4.4, *Basics*=0.2, and *Residential*=0.9. For simplicity for this example, we set $\alpha = \beta = \gamma = 1$. Without considering buildings, the region scores are $\rho(\boldsymbol{g_1}) = 110 \times \frac{1}{10} = \rho(\boldsymbol{g_2}) = 22 \times \frac{1}{2} = 11$, which means we cannot differentiate which region is better for picking up passengers. The reason that $\boldsymbol{g_1}$ has the same region score as $\boldsymbol{g_2}$ even though $\boldsymbol{g_1}$ has an airport (i.e., *Professional* building class), which has a high frequency of passenger appearance, is because the low frequency of passenger appearance of the barn makes the frequency of passenger appearance of region $\boldsymbol{g_1}$ low. The region scores calculated with considering buildings are $\rho(\boldsymbol{g_1}) = 110 \times \frac{1}{10} \times (\frac{1}{2} \times 4.4 + \frac{1}{2} \times 0.2) = 25.3$, and $\rho(\boldsymbol{g_2}) = 22 \times \frac{1}{2} \times 0.9 = 9.9$. The result shows that $\boldsymbol{g_1}$ is better than $\boldsymbol{g_2}$ for picking up passengers, which is consistent with our intuition that regions with airports are more likely to have high and constant flows of passenger appearances. This example shows that the additional consideration of buildings in Equation (3.3) can help more accurately reflect the likelihood of passenger appearance.

3.3.4 Supporting Continuous Operability

One of our objectives in the charger deployment is to ensure that the taxicabs can reach a nearby charger when their SoC is about to be exhausted (e.g., below 20%). To this end, we need to infer the taxicabs' expected SoC at each region given certain regions are installed with wireless chargers. KDE can be used to describe the taxicabs' probability of reaching a region from another region based on their distance in the road network. Also, the SoC of a taxicab is a function of the distance from the taxicab's source landmark to the destination landmark. Then, the expected SoC of a taxicab at a landmark in the road network can be calculated. We present the details below.

Since taxicabs' mobility patterns imply their traffic flows between certain locations [120], we feed their trajectories into a KDE model to infer the Probability Density Function (PDF) of the distribution of the trajectory lengths as in Equation

(4.7). Given a trajectory length d, the KDE model outputs the probability that a taxicab takes a trajectory with length d.

$$\hat{f}(d) = \frac{1}{R \cdot h} \sum_{t=0}^{R-1} K(\frac{d - d_t}{h}); \ -\infty < d < \infty, \tag{3.4}$$

where R is the total number of the taxicab trajectories, d_t is the length of the t^{th} trajectory, h is the smoothing parameter influencing the estimation accuracy of the KDE and is determined according to the MISE criterion [107], $K(\cdot)$ is the kernel function whose value decays with the increasing of d, which is set to the Gaussian function based on [60, 114, 115].

According to the state-of-the-art EV energy consumption model [57], the energy consumption of a taxicab (E_c) is primarily determined by air drag (E_{air}) and rolling resistance (E_{roll}):

$$\begin{aligned} \Delta E_c &= \Delta E_{air} + \Delta E_{roll} \\ &= c_w v^2 \Delta l + c_e \kappa g \Delta l \end{aligned} \tag{3.5}$$

where c_w is the air drag coefficient determined by vehicle front surface area; v is the driving speed; Δl is the distance that the taxicab has moved; c_e is the rolling resistance coefficient; κ is the taxicab's mass; and g is the gravity acceleration.

Suppose the taxicabs have the same battery capacity, E_0, and each taxicab gets fully charged before leaving a charger. We define the shortest distance between two regions as the distance of the shortest route between their respective central landmarks, which are the landmarks located the nearest to the middle of the two regions, respectively. Given a taxicab starting from a charger, based on Equation (4.9), its residual energy at a location, which is d distance away from the charger through the shortest route, can be estimated as $E_r^d = E_0 - \sum_{t=0}^{R'-1}(c_w v_t^2 + c_e \kappa g) l_t$ [57], where R' is the number of road segments of the shortest route, and v_t and l_t are the speed limit and length of the t^{th} road segment, respectively. The taxicab's SoC at the location

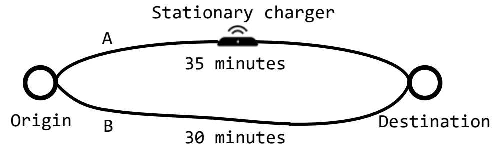

Figure 3.12: EV drivers' routing choice behavior.

can be represented as:

$$SoC(d) = \begin{cases} E_r^d/E_0, & \text{if } E_r^d \geqslant 0 \\ 0, & \text{otherwise.} \end{cases} \tag{3.6}$$

We use a natural number μ_i to denote the number of chargers deployed in region $\boldsymbol{g_i}$. We set $b_i = 0$, if $\mu_i = 0$; $b_i = 1$, if $\mu_i \geqslant 1$. Then, the expected SoC of the taxicabs at a region $\boldsymbol{g_j} \in G$ is:

$$\overline{SoC}(\boldsymbol{g_j}) = \sum_{i=0}^{M-1} \hat{f}(d_{i,j}) SoC(d_{i,j}) b_i, \tag{3.7}$$

where M is the total number of regions, and $d_{i,j}$ is the distance of the shortest route from $\boldsymbol{g_i}$ to $\boldsymbol{g_j}$.

3.3.5 Describing Drivers' Routing Choice

Charging facility presence might affect EV drivers' routing choice in a way that they are more likely to choose routes with charging facilities to mitigate range anxiety [38, 51]. Therefore, the deployment of new wireless chargers may affect the traffic distribution on the existing road network due to the mutual interaction between the location of charging facilities and the resultant network traffic flow. For example, as shown in Figure 3.12, there are 2 candidate routes with approximate distances between the EV's origin landmark and destination landmark. Given the well-known range anxiety of EVs [19, 73, 91], the EV driver might choose route A, which has a charging lane, even if its travel time cost (35 minutes) is a bit longer than that of route B (30 minutes). The decision of choosing whether to charge on the way or drive directly to the destination depends on two factors: the travel time cost and the benefit brought by charging facilities. Therefore, it is necessary to consider EV drivers' routing choice behavior in formulating the charger deployment optimization problem.

Previous studies on EV drivers' routing behavior have confirmed that for an EV driver, the probability of choosing a candidate route can be described with a multinomial logit model [19, 73, 91]. Specifically, the model estimates the EV driver's probability of choosing a route as below:

$$P_u^w = \frac{\exp(\epsilon \frac{1}{T_u^w} + \varepsilon y_u^w)}{\sum_{k \in U^w} \exp(\epsilon \frac{1}{T_k^w} + \varepsilon y_k^w)}, \forall u \in U^w, w \in W, \tag{3.8}$$

where P_u^w is the probability of choosing the route u among all the candidate routes between the origin-destination (O-D) pair w; T_u^w is the travel time cost of the route u between the O-D pair w; y_u^w is the binary variable indicating the presence of chargers on the route u, $y_u^w = 1$ if there is at least one charger in u, $y_u^w = 0$ otherwise; U^w is the set of all feasible routes of the O-D pair w reflected in all the historical trajectory data; W is the set of all possible O-D pairs on the road network; ϵ and ε are the scaling parameters for travel time cost and the presence of chargers, respectively, which describe the routing decision sensitivity in terms of travel time cost and the presence of chargers. In practice, ϵ and ε are calibrated by using survey data. In this study, we follow the settings of these parameters as recommended in [91]: $\epsilon = 0.1$ and $\varepsilon = 0.8$. According to Equation (3.8), the longer travel time cost a route has, the lower probability an EV driver will choose the route, and vice versa. This is consistent with the real-world driver's expectation of minimizing the travel time cost.

According to [20, 38], the travel time cost of a candidate route consists of the driving time of normal road segments (t_u^d), the driving time of charging lanes (t_u^c) and the waiting time at the charging lanes (t_u^w). The driving time of normal road segments included in the route u can be calculated as:

$$t_u^d = \sum_{n=0}^{N_u^R-1} \frac{l_n}{v_n}, \tag{3.9}$$

where N_u^R is the number of road segments of the route u, v_n and l_n are the speed limit and length of the n^{th} road segment, respectively.

The time spent at stationary chargers consists of the EVs' waiting time before charging and charging time. Let λ_i denote the arrival rate of EVs at the chargers located at landmark $\boldsymbol{p_i}$ (i.e., the number of EVs arriving at $\boldsymbol{p_i}$ for charging per time unit), which is actually the vehicle flow rate of $\boldsymbol{p_i}$. Let μ_i denote the service rate of the chargers located at landmark $\boldsymbol{p_i}$ (i.e., the number of EVs that the chargers can charge per time unit), which is calculated as $\mu_i = n_i/T_c$ [45, 48], where n_i is the number of chargers at the landmark and T_c is the time required to fully charge an EV from 0% to 100% SoC. Thus, an EV's charging time at the charging lane is:

$$t_u^c = 1/\mu_i. \tag{3.10}$$

The utilization ratio of the chargers is $\xi_i = \lambda_i/\mu_i$. According to the M/M/1 queuing theory [36, 38], the EVs' waiting time at the chargers is:

$$t_u^w = \begin{cases} \frac{\xi_i/\mu_i}{1-\xi_i}, & \text{if } \xi_i < 0 \\ \xi_i, & \text{otherwise.} \end{cases} \tag{3.11}$$

Finally, the travel time cost of route u can be calculated as:

$$T_u^w = t_u^d + y_u^w(t_u^c + t_u^w). \tag{3.12}$$

3.3.6 Optimization Problem

Our objective is to minimize the total deployment cost of the chargers, maximize the opportunity of picking up passengers at the charger positions, and meanwhile ensure that at each region, the expected SoC of a taxicab is higher than a threshold η (e.g., 20%). η is determined so that a taxicab can reach the nearest charger with η SoC left. We can set η to be a relatively high value, so that the taxicabs are always operable with high confidence. Meanwhile, the charging rate of the deployed chargers must be able to support the power demands from all the taxicabs. According to Equation (4.9), we can derive the battery consumption rate for each taxicab as $\phi = \frac{\Delta E_c}{\Delta t} = c_w v^3 + c_e \kappa g v$. Hence, the battery consumption rate depends on the speed limit of every road segment. That is, as the speed limit v increases, the battery consumption rate increases. To derive the maximum battery consumption rate ϕ_{max}, we use the maximum speed limit v_{max} of the entire road map. Finally, the optimization problem is formulated as:

$$\begin{aligned}
\text{minimize} \quad & \sum_{\boldsymbol{g_i} \in G} \omega_0 n_i \\
\text{maximize} \quad & \sum_{\boldsymbol{g_i} \in G} \rho(\boldsymbol{g_i}) n_i \sum_{w \in W} \sum_{u \in U_w^i} \bar{f}_u^i P_u^w \\
\text{subject to} \quad & \overline{SoC}(\boldsymbol{g_i}) \geqslant \eta, \forall\, \boldsymbol{g_i} \in G \\
& \mathcal{C} \sum_{\boldsymbol{g_i} \in G} n_i \geqslant \phi_{max} V \\
& n_i \in \mathbb{N}, \forall\, \boldsymbol{g_i} \in G,
\end{aligned} \tag{3.13}$$

where ω_0 is a constant representing the unit cost of deploying a charger, $\mathcal{C}$ is the charging rate of one charger, and V is the total number of taxicabs driving in the road map. $\bar{f}_u^i$ is the average vehicle flow rate (i.e., average vehicle visit frequency) at $\boldsymbol{p_i}$, which is caused by the vehicles that drive through route u, recall that U_w^i is the set of historical routes that pass through landmark $\boldsymbol{p_i}$, W is the set of all possible O-D pairs on the road network. This problem tries to minimize the total deployment cost of the chargers and maximize the total region scores covered by the chargers with two constraints: i) the expected SoC at any region is no less than threshold η, and ii) the total charging rate of the deployed chargers is not less than the total battery consumption rate of the electric taxicabs. Given source location $\boldsymbol{g_i}$ and destination location $\boldsymbol{g_j}$, the coefficient $\hat{f}(d_{i,j})SoC(d_{i,j})$ in Equation (4.12) is determined. Therefore, we can use a constant λ_{ij} to represent $\hat{f}(d_{i,j})SoC(d_{i,j})$. As a result, the optimization problem (3.13) is actually a classic Multi-objective Integer Programming (MIP) problem, and its optimal solutions can be found through a branch-and-bound search [2]. We can use an existing solver (i.e. JuMP [68], MultiJuMP [79]) to obtain its integer-feasible solution. After solving the optimization problem, we obtain the number of chargers (μ_i) in each selected region for charger deployment. For each selected region, we rank the landmarks within the region by their daily average number of passenger requests in descending order, and assign the μ_i chargers to the top ranked μ_i landmarks accordingly.

Note that the more passengers appear in a region (i.e., larger $\rho(\boldsymbol{g_i})$), the more opportunity the taxicabs will have in picking up the passengers in the region [134]. Meanwhile, the chargers will attract vacant taxicabs to wait in the region, namely create the opportunity of picking up passengers for the taxicabs. Therefore, our optimization problem has considered maximizing the opportunity of picking up passengers for the regions. In our future work, we will explore the accurate relationship between the likelihood of passenger appearance and the distribution of vacant taxicabs to better describe the opportunity of picking up passengers in the regions.

3.3.7 Taxicab Dispatching

During the driving process, the taxicabs follow the rules below in order to quickly discover passengers.

1. If a vacant taxicab finds that its SoC is below certain level θ (e.g., 80%), it moves to the nearest charger and randomly selects a period of waiting time (e.g., 5 to 30 minutes), which is the usual waiting time of taxicab drivers [134].
2. When a taxicab's SoC is below η (e.g., 20%), it seeks the nearest charger to get

a full recharge. Note the charging rate of the state-of-the-art vehicular wireless charging system, say $\mathcal{C}$, is 150 kW [48]. This means for a taxicab with a battery capacity of 75 kWh, it can be charged with 20% of SoC within around 7 minutes, which is consistent with the length of time that the taxicabs usually spend on waiting for passengers [123]. In this case, the time required for fully recharging a taxicab is around 30 minutes. Note a full charge can only support a taxicab to drive for around 300 km. However, a taxicab in a metropolitan road network usually needs to drive 800 km in one day [123]. This means that a taxicab needs to charge around 3 times (i.e., roughly 2 hours) to support its daily operation, during which it cannot serve any passenger. Therefore, instead of letting a taxicab be idle for such a long time, we let it charge opportunistically while waiting for passengers.

3. When a vacant taxicab's SoC is above θ, it cruises between chargers to seek passengers.

4. When a taxicab receives a passenger request before or during charging, if its SoC is above η and is sufficient for the travel and subsequent charging, it will stop charging and pick up the passenger; otherwise, it declines the request since maintaining operability has the highest priority. Note that once the taxicab starts to serve a passenger request, it won't stop to charge again until it completes the current request. For the detailed scheduling of the taxicabs, we refer to existing taxicab dispatching methods [122, 125, 134].

5. Our charger deployment ensures that there are chargers in less popular regions because the deployed chargers need to maintain the taxicabs' SoC to be above the threshold. However, the taxicabs may not want to serve in less popular regions. To motivate the taxicabs to stay in less popular regions more often, we specify the unit charging price in less popular regions to be lower (e.g., \$0.11 per kWh), and the unit charging price in popular regions to be higher (e.g., \$0.22 per

kWh). We leave the exploration of the optimized pricing strategy for balancing the taxicabs to our future work.

Since a taxicab only waits for 5 to 30 minutes at a charger, cruises between chargers to seek passengers, and meanwhile our charger deployment makes it very likely for a taxicab to pick up a passenger while waiting, the taxicabs are moving around and able to serve the passengers widely distributed in the city. Note the above parameters can be adjusted according to different service requirements. *PickaChu* can easily adopt the taxicab dispatching strategies in previous works [122, 125, 134], which is not our focus in this dissertation. In a centralized dispatching system, when the system receives a passenger's request, it will find the nearest vacant taxicab and notify it of the pick-up location [134]. In a distributed dispatching system [122, 125], a taxicab receives passenger request from nearby taxicabs through vehicle-to-vehicle communication, and decides the route to the location.

Though we allocate different numbers of chargers to different regions, it is still possible that when a taxicab arrives at a charger, it must wait in a waiting queue. Currently, the number of chargers in each region is determined based on the likelihood of passenger appearance. Therefore, each taxicab can quickly pick up a passenger and leave the charger. Namely the case of a taxicab waiting for an available charger should be rare. Moreover, we let each taxicab start looking for an available charger as long as its SoC is below 80%, and it will keep moving between the chargers until it finds an available charger. Thus, the taxicab will not just wait at a charger position for its turn of charging. Therefore, the possible waiting time caused by an unavailable charger is included in the seeking time for charger. We will further study how to optimize the number of chargers at a charging position so that the taxicabs' seeking time caused by looking for an available charger can be minimized.

In the current design of PickaChu, we mainly focus on regular passenger appearance with stable periods (e.g., airport passenger flows, daily rush hours). For disruptions or unplanned events, we rely on existing taxicab dispatching methods [122, 125, 134] to guide the taxicabs to adapt to the variation of passenger appearance frequency. We leave the comprehensive solution of this problem as our future work. The chargers are deployed one time. When the long-term traffic flows in the city change significantly, the wireless chargers need to be re-deployed.

3.4 Performance Evaluation

3.4.1 Comparison Methods

To evaluate *PickaChu*'s performance in reducing the idle time and supporting the continuous operability of electric taxicabs in a city, we compare it with a representative charging station deployment algorithm: Optimal Charging Station Deployment [62] (*OCSD* in short), and a representative taxicab guiding system: cruising on purpose (*pCruise* in short) [125]. We also evaluate the performance of existing deployment of plug-in charging stations in Shenzhen (*Baseline* in short) as the baseline.

To make the methods comparable, we assume that they all use the same wireless chargers. In *OCSD*, based on the analysis of taxicab mobility, the chargers are deployed to minimize the taxicabs' average seeking time for the nearest charger. To make methods comparable, in *PickaChu*, the deployment of chargers is determined by our optimization solution with the same cost as in *OCSD*. To demonstrate that *PickaChu* can further reduce the deployment cost, we also evaluated *PickaChu* with its optimization problem solution that minimizes deployment cost (denoted by *OptPickaChu*). We let *OCSD*, *PickaChu*, *OptPickaChu*, and *Baseline* all use the centralized taxicab dispatching system explained in Section 3.3.7. As *OCSD* and *Baseline* do not have a strategy to guide pick-ups, the taxicabs wander around in the road network to discover passengers before receiving notifications. In *pCruise*, the taxicabs share passenger information and cruise on the route with the most passenger requests. By communicating with its nearby taxicabs, each taxicab creates a cruising graph, which is the taxicab's nearby road network with vertices representing intersections, and edges weighted by the probability of finding a potential passenger. The probability is calculated as the number of unserved passenger requests over the total number of passenger requests found on the route. Then it uses the cruising graph to select the route that has the maximum probability of finding a passenger. In *pCruise*, we use the same charger deployment as that in *OCSD*. In all the methods, when a taxicab's SoC is below 20%, it drives to the nearest charger to get a full recharge, during which they won't serve passengers.

3.4.2 Experiment Settings

Parameter Settings: The parameters related to chargers, vehicles, and batteries are listed in Table 3.2. As BYD e6 is a widely used vehicle model among the taxicabs in Shenzhen [62], we use it to determine the parameters for taxicabs. With the most recent research implementations (e.g., Oak Ridge National Laboratory [85]), it is expected that within a 10-year timeframe, it is possible to reach a charging rate over 100kW for EV wireless charging. Therefore, we use 150kW as the charging rate of a stationary charger. After solving the optimization problem, *OptPickaChu* selects 93 regions out of 557 regions to deploy 350 wireless opportunistic chargers. *PickaChu* selects 125 regions to deploy 480 chargers, as shown in Figure 3.13. We observe that *OptPickaChu* results in fewer chargers than *PickaChu* since *OptPickaChu* additionally aims to minimize deployment cost. We can see that *PickaChu*'s deployment is generally consistent with the distribution of the existing 81 charging stations, which means it is extensible from the current charger deployment scheme. As for the cal-

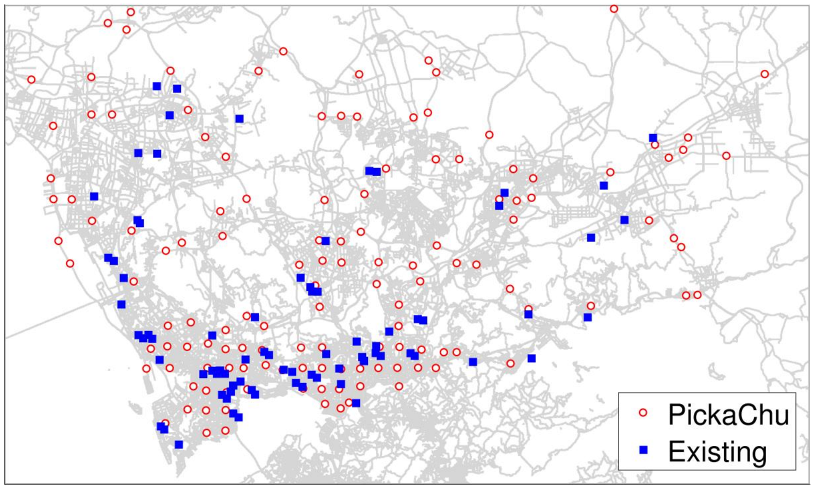

Figure 3.13: Comparison of deployed chargers.

culation of revenue and cost, the unit electricity cost of driving was set to \$0.5/mile, the unit service loss cost of charging (which is the possible loss of revenue earning opportunity) was set to \$0.1/hour, and the unit revenue of traveling with passengers was set to \$1.5/mile.

Table 3.2: Table of parameters.

Parameters	Setting	Source
Charging rate $\mathcal{C}$	150 kW	Chen *et al.* [20, 31, 113]
Charger unit price ω_0	\$30,000	Chen *et al.* [20]
Air drag coefficient c_w	0.3	Kurczveil *et al.* [57]
Rolling resistance coefficient c_e	0.01	Kurczveil *et al.* [57]
Mass of a taxicab κ	2,020 kg	Tian *et al.* [104]
Gravity acceleration g	9.8 m/s^2	Tian *et al.* [104]
Battery capacity of a taxicab E_0	75 kWh	Tian *et al.* [104]
SoC threshold η	20%	Author's assumption
Vacant SoC threshold θ	80%	Author's assumption
Maximum speed limit v_{max}	60 mph	Tian *et al.* [104]
Scaling parameters of drivers' choice behavior ϵ and ε	$\epsilon = 0.1$ and $\varepsilon = 0.8$	Riemann *et al.* [91]

Simulation Settings: With the deployment schedule, we use SUMO [56] to simulate the operation of 1,000 taxicabs on Shenzhen's road network for 24 hours in multiple days, which are January 12 (Monday), March 10 (Tuesday), May 13 (Wednesday), July 16 (Thursday), September 18 (Friday), November 21 (Saturday) and December 13 (Sunday) in 2015. These days are representative because they are unrelated to each other, belong to 4 different seasons, and cover weekdays and weekends [121]. In SUMO, taxicabs drive by following the traffic model we built in Section 4.3.4.1. The location and time of passenger requests follow the actual passengers' requests happened on January 12, March 10, May 13, July 16, September 18, November 21 and December 13 in 2015. We converted OpenStreetMap road network of Shenzhen to a SUMO road network file. We assume that each taxicab can only serve one passenger in a travel [125].

We use the movement records of the taxicabs mentioned in Section 2.2 for performance evaluation. Below, Figure 3.15 to Figure 3.32 demonstrate the metrics of the vehicles under different hours on July 15, 2015. Figure 3.33 to Figure 3.35 demonstrate the metrics of vehicles in multiple days, which are January 12 (Monday), March 10 (Tuesday), May 13 (Wednesday), July 16 (Thursday), September 18 (Friday), November 21 (Saturday) and December 13 (Sunday) in 2015. Specifically, we measured the following metrics:

- *Ratio of an operation phase*: the average hourly ratio of the time duration of respective operation phase (i.e., cruising, travel, seeking chargers, charging) of all the taxicabs. For an operation phase, we first record the average hourly ratio of each taxicab during the day. Then, we calculate the average of the ratios of all the taxicabs. We also show the CDF of vehicles in terms of the time duration for each operation phase.
- *Revenue*: the daily average revenue earned by all the taxicabs through traveling with the passengers. It is calculated by multiplying all the taxicabs' daily traveling distance with the unit revenue of traveling with passengers. We also show the CDF of vehicles in terms of the daily revenue for traveling phase.
- *Cost*: the sum of the daily average cost of the electricity consumed by all the taxicabs through driving (i.e., cruising, seeking chargers, and traveling) and the daily average service loss cost caused by charging. The cost of cruising, seeking chargers and

traveling is calculated by multiplying the driving distance of respective phase with the unit electricity cost of driving. The cost of charging is calculated by multiplying the charging time with the unit service loss cost. We also show the CDF of vehicles in terms of the daily cost for each idle operation phase.

- *Vehicle SoC*: we measure the SoC of each taxicab at each hour during a day, and calculate the median, 5^{th} percentile and 95^{th} percentile values to compare the performance of the methods in supporting the continuous operability of taxicabs.
- *Overall energy supply overhead*: the energy supply overhead on all chargers in kWh. We measure it under different hours during a day to observe different methods' charging pressure on the power grid.
- *The number of served passengers*: the number of passengers served by the taxicabs. We measure it under different hours during a day to compare the performance of the methods in serving passengers.

3.4.3 Validation of Likelihood of Passenger Appearance

To validate the effectiveness of our method on estimating the likelihood of passenger appearance, we measured the error ratios between the actual number of passenger appearances and the estimated likelihood (scores) of passenger appearance in different regions with the historical passenger appearance data of 7 different days, which are January 12 (Monday), March 10 (Tuesday), May 13 (Wednesday), July 16 (Thursday), September 18 (Friday), November 21 (Saturday) and December 13 (Sunday) in 2015. These days are representative because they are unrelated to each other, belong to 4 different seasons, and cover weekdays and weekends [121]. Specifically, since these two metrics have different units, we first normalize them to have values between 0 and 1 (Min-Max Normalization) [34]. Then, we calculated the error ratio between the two metrics as:

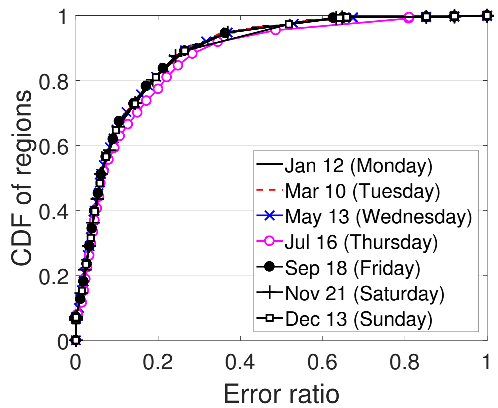

Figure 3.14: Distribution of error ratios in all regions.

$$ER = \frac{|v_p - v_\rho|}{v_\rho} \cdot 100\%, \tag{3.14}$$

where v_p and v_ρ represent the values of the same region for the normalized actual number of passenger appearances and the normalized likelihood (score) of passenger appearance, respectively. Figure 3.14 shows the distribution of error ratios between the normalized average actual number of passenger appearances per day and the normalized likelihood (score) of passenger appearance in all regions. We can see that on most days (except Jul 16), our method of estimating the likelihood of passenger appearance can achieve an error ratio lower than 20% in more than 80% of the regions. This means that the estimated scores reflect the passenger appearance in most regions with a low error.

3.4.4 Experimental Results

3.4.4.1 Ratio of Each Operation Phase

Figure 3.15 shows the average hourly ratio of each operation phase of all the taxicabs throughout a day. We see that for all the idle operation phases (i.e., cruising, seeking and charging), *PickaChu* has the lowest ratio. We also see that compared with *pCruise*, *OCSD* and *Baseline*, the cruising time in *PickaChu* is greatly reduced. Cor-

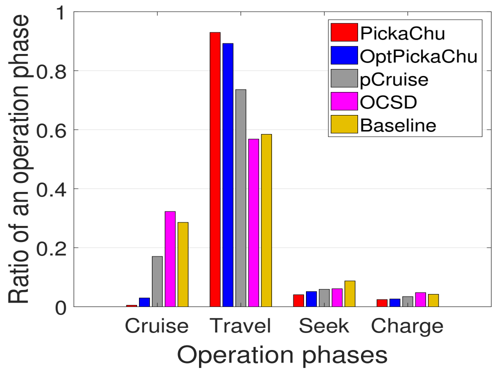

Figure 3.15: Ratio of each operation phase.

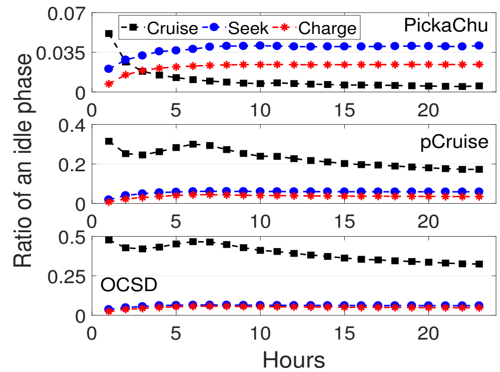

Figure 3.16: Ratio of each idle phase ratio over time.

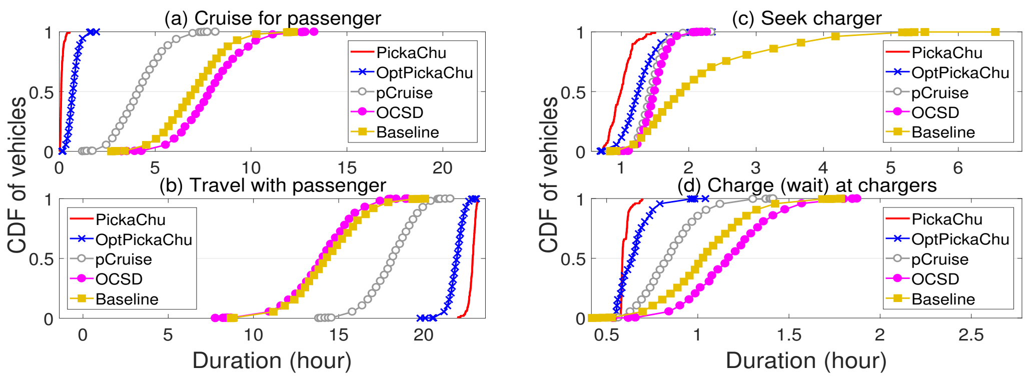

Figure 3.17: CDF on the durations of different operation phases.

respondingly, the time that *PickaChu*'s taxicabs spend on traveling with passengers on board (92%) is about 15% higher than that of *pCruise* (77%), 35% higher than that of *OCSD* (57%), and 33% higher than that of *Baseline* (59%). In *OCSD*, to discover passengers, the taxicabs must wander around in the road network, which increases cruising time. What's worse, with more time spent on cruising, the taxicabs have to charge more frequently to remain operable, which leads to higher ratios of seeking phase and charging phase than the other methods. As for *pCruise*, the taxicabs are always guided to the route with the highest probability of discovering passengers, which greatly reduces cruising time. However, the effective discovery of passengers still causes the taxicabs to waste much time on approaching the potential passengers. Compared with *Baseline*, only *OCSD* spends more time on cruising, which is caused by its inefficient discovery of passengers. But we also notice that *Baseline*'s time of

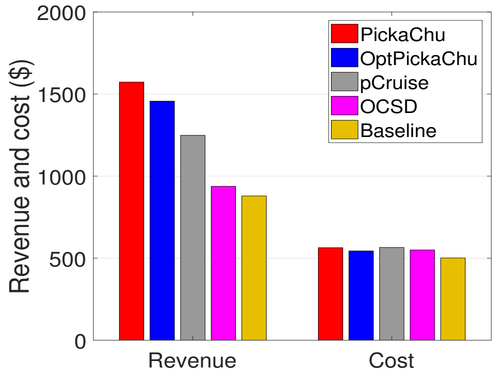

Figure 3.18: Revenue and cost of each method.

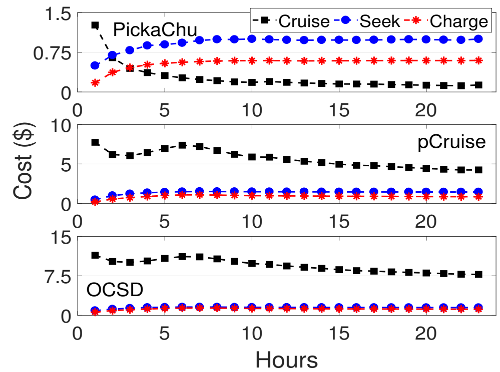

Figure 3.19: Cost variation of each idle phase over time.

seeking chargers ranks the highest, which means Shenzhen's current deployment of charging stations needs improvement in accessibility. In *PickaChu*, since the taxicabs are allowed to stay at an opportunistic charger for some time, and the regions with chargers have high likelihood of passenger appearance, many taxicabs find passengers during their stay. Compared to *pCruise*, this strategy further reduces the time wasted on cruising for passengers and saves energy for the taxicabs. We notice that compared with other methods, *PickaChu* also reduces the charger seeking time. This is because that taxicabs cruise between chargers, and are less likely to exhaust their power.

Figure 3.16 shows the variation of the ratios of the idle phases by hour throughout a day. We can see that in *pCruise* and *OCSD*, the taxicabs have to spend a large portion of time on cruising during each hour. Also note that there are small bumps on the cruising time curves in *pCruise* and *OCSD*. This is because there are not enough passenger pick-up requests appearing between 05:00 and 07:00, so the ratios of cruising phase in *pCruise* and *OCSD* are increased during these hours. In contrast, in *PickaChu*, except for the first few hours, during which most of the taxicabs do not need to get charged, and keep cruising between the regions with opportunistic chargers, the time on cruising is largely replaced with the time of seeking chargers and charging in the following hours.

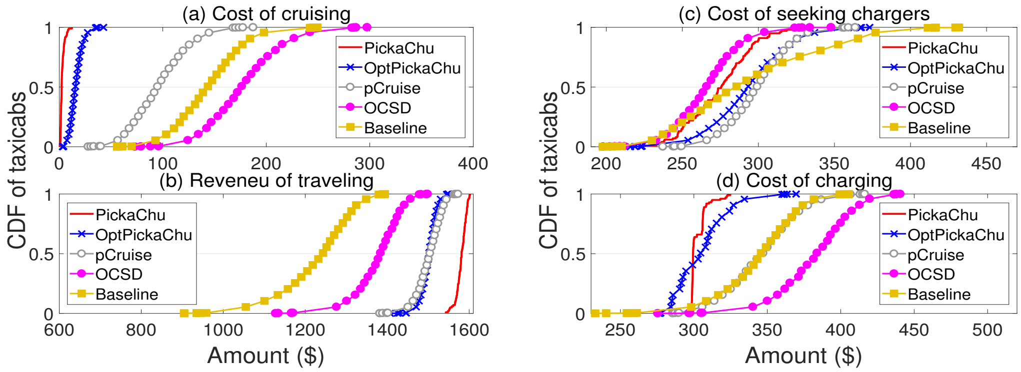

Figure 3.20: CDF on the cost/revenue of different operation phases.

Figure 3.17 demonstrates the CDF of the taxicabs on the time durations of different phases. Figure 3.17 (a) shows that the taxicabs' cruising phase durations in *PickaChu* (< 1 hour) are much shorter than those of the other methods. Figure 3.17 (b) shows that the taxicabs' traveling phase durations in *PickaChu* and *OptPickaChu* (> 20 hours) are significantly longer than those of the other methods. This is caused by their difference in operation strategies. Figure 3.17 (c) shows that due to the same deployment of chargers in *pCruise* and *OCSD*, they have similar distributions of seeking phase durations (1 hour $\sim$ 2.5 hours). *Baseline* has much longer seeking phase durations (1 hour $\sim$ 6.5 hours), which means that the current charger deployment needs improvement. In Figure 3.17 (d), all the taxicabs in *PickaChu* have much shorter charging phase durations (< 0.8 hours) than the others, which means it also reduces the need for recharge. Except for the seeking phase, the distribution of other operation phase durations in *PickaChu* is much more concentrated than the others, which further proves the consistency of *PickaChu*'s effectiveness on all the taxicabs. We also see that *OptPickaChu* is slightly worse than *PickaChu* in reducing idle operation time, though it still outperforms other methods. This shows that *PickaChu* can achieve better performance on operation efficiency even with relatively lower deployment cost than the others.

In addition, we also measured the average revenue resulted from the traveling

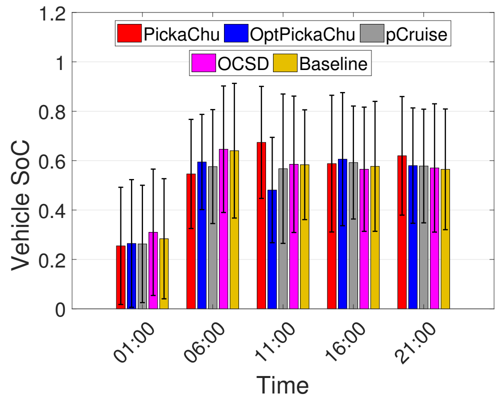

Figure 3.21: Vehicle SoC.

phase, and the average cost resulted from the other idle phases during the day, which are shown in Figure 3.18. We can see that compared with *pCruise*, *OCSD* and *Baseline*, *OptPickaChu* and *PickaChu* can increase the average revenue of all the taxicabs' by approximately more than \$250, \$500 and \$600 per day, respectively, with almost the same average cost. We also measured the changes of the costs of different methods under various hours, which are shown in Figure 3.19. The reason is the same as that of Figure 3.16. We also measured the distribution of the revenues, and the distribution of the costs of the taxicabs, which are shown in Figure 3.20. We can see that most of the taxicabs in *PickaChu* and *OptPickaChu* spend less than \$50 on cruising and less than \$300 on seeking chargers, which are less than those of the other methods. The taxicabs' costs spent on seeking chargers in *PickaChu* and *OptPickaChu* are comparable to those of the other methods. However, the revenues of the taxicabs in *PickaChu* and *OptPickaChu* (> \$1,400) are conspicuously higher than those of the other methods.

3.4.4.2 SoC Maintenance of Taxicabs

We measured the SoCs of all the taxicabs at each hour throughout a day. As we cannot show all the SoCs in a figure, we plot the median, 5^{th} and 95^{th} percentiles of SoCs of all the taxicabs at a few time points in Figure 3.21. We see that *OptPickaChu*

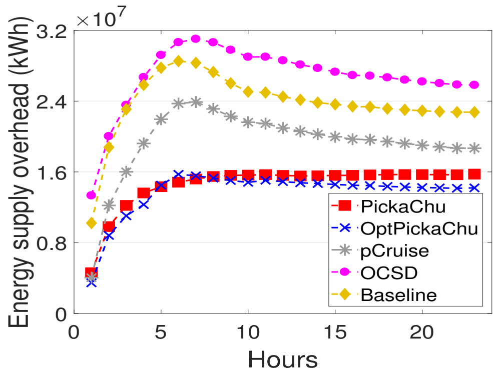

Figure 3.22: Energy supply overhead.

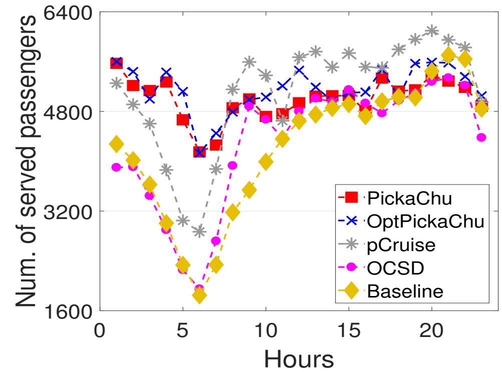

Figure 3.23: Num. of served passengers.

and *PickaChu* maintain almost the same SoC levels as the other methods. However, as observed in Section 4.4.3.1, the taxicabs in the other methods spend more time on idle phases, which results in a lower energy efficiency and lower profits. Note that *OptPickaChu* provides a comparable SoC as the other methods during most of the time, although it has fewer deployed chargers. This demonstrates its effectiveness on minimizing the deployment cost while still guaranteeing the SoC of taxicabs.

3.4.4.3 Overall Energy Supply Overhead

Figure 3.22 shows the overall energy supply overhead of different methods under different hours throughout a day. The results follow: *OCSD*>*Baseline*>*pCruise*>*PickaChu* ≈*OptPickaChu*. We can see that *PickaChu* and *OptPickaChu* result in the least pressure on the power grid given the same number of taxicabs. Rather than cruising for passengers as *pCruise*, *Baseline* and *OCSD*, the taxicabs in *PickaChu* and *OptPickaChu* can wait at the chargers for their next passengers. Moreover, since the taxicabs in *OCSD* and *Baseline* cannot effectively harvest passengers from chargers, they drive more idle trips and require more charging.

It is worth mentioning that in the first few hours, the energy supply overhead increases significantly. For *pCruise*, *Baseline* and *OCSD*, the peak that appears between 05:00 and 07:00 is caused by the lack of passengers. Taxicabs start with 100% SoC. Since there are few passengers during 00:00-07:00, the taxicabs in *pCruise*, *Base-*

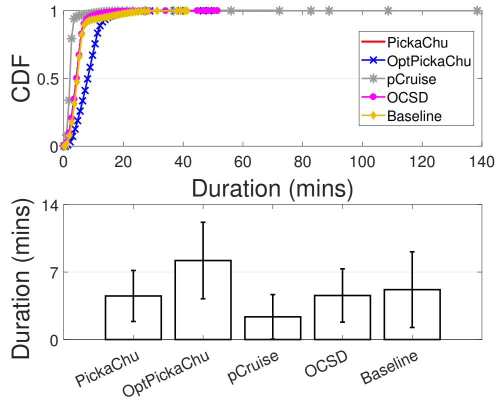

Figure 3.24: Waiting time of passengers.

line and *OCSD* keep cruising for passengers and their SoC keeps decreasing. Finally, all taxicabs exhaust their SoC and recharge at about the same time, resulting in a peak in charging overhead. After then, their SoC exhausts at different times caused by different passengers. Therefore, they charge at different times, resulting in no peaks in charging overhead. The energy supply overhead in *PickaChu* and *OptPickaChu* stabilize more quickly, which reflects their resilience against the variation of passengers.

3.4.4.4 Service Performance

Figure 3.23 shows the numbers of served passengers of different methods during different hours throughout a day. We see that during the hours with relatively fewer requests (01:00-08:00), the results follow: *PickaChu*>*OptPickaChu*>*pCruise*> *OCSD*≈*Baseline*. After then, *pCruise* can serve slightly more passengers ($<$ 1,000) than *PickaChu*, *OCSD* and *Baseline*. Figure 3.24 shows the distribution of the waiting time of the passengers (upper part), and the average, 5^{th} and 95^{th} percentiles of the waiting time of the passengers (lower part) in different methods. We can see that the passengers' average waiting time in *OptPickaChu* (8 minutes) is longer than the other methods. Since there are fewer chargers in *OptPickaChu*, so the chargers are more sparsely distributed in the road network. Since the vacant taxicabs cruise be-

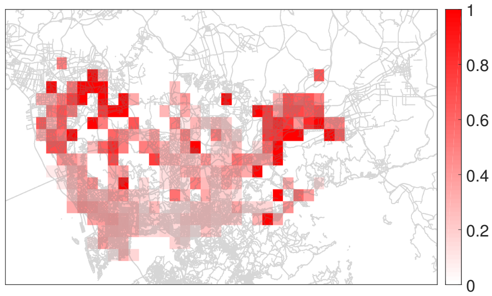

Figure 3.25: Heat map of service rates.

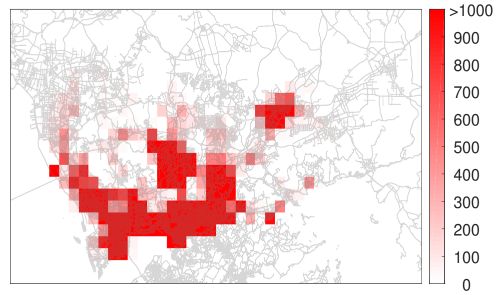

Figure 3.26: Heat map of passengers.

tween the chargers, the waiting time of the passengers in the regions without chargers is usually very long, which results in the longer average waiting time of passengers in *OptPickaChu*. We also find that the results of *PickaChu* (5 minutes), *OCSD* (5 minutes), and *Baseline* (6 minutes) are comparable to each other, and the result of *pCruise* is the shortest (2 minutes). In *PickaChu*, most of the passengers are picked up in the regions with chargers. Since the distance from the taxicabs to the passengers is bound by the region size (i.e., 2,000 meters), the passengers' waiting time is not very long. In *OCSD* and *Baseline*, the taxicabs randomly cruise in the road network, which means most of the passengers are picked up during the cruising of the taxicabs. Thus, the passengers' waiting time is comparable to that of *PickaChu*. In *pCruise*, the taxicabs are always cruising on the routes with the maximum probability of finding a passenger, so the passengers have the shortest waiting time.

When there are few pick-up requests, *PickaChu* serves more passengers than *pCruise*. This is because in *pCruise*, through vehicle-to-vehicle communication, a taxicab may not discover sufficient passengers to generate an effective cruising graph for guidance. On the contrary, the taxicabs in *PickaChu* wait at the regions with high likelihood of passenger appearance, which helps the taxicabs efficiently discover passengers. When there are many pick-up requests, the taxicabs in *pCruise* can easily discover requests. Hence, *pCruise* can serve more passengers than *PickaChu* during this time, but at the cost of more energy consumption, as mentioned in Section 3.4.4.3. We see that *PickaChu* always outperforms *OCSD* and *Baseline*, which spend more

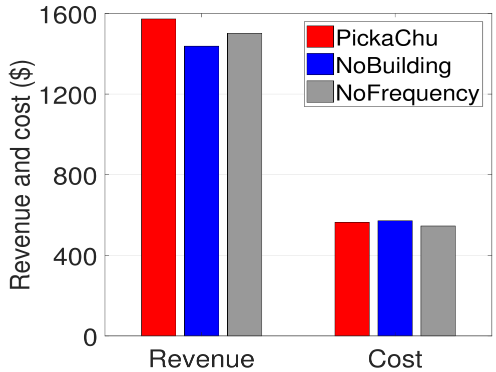

Figure 3.27: Effectiveness of components.

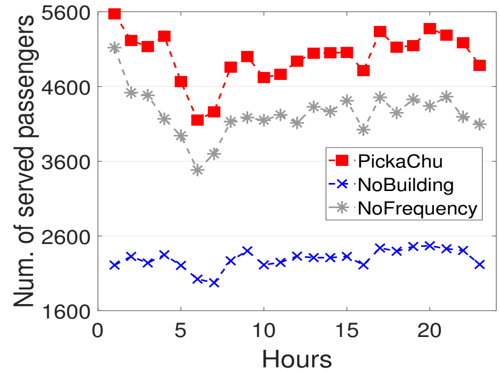

Figure 3.28: Served passengers.

time on cruising, seeking and charging. In addition, *OptPickaChu* provides service performance comparable to *PickaChu*, although *PickaChu* deploys more chargers. This is because the redundant chargers do not significantly benefit the discovery of passenger requests. This shows the effectiveness of *OptPickaChu* on minimizing the deployment cost while achieving our objectives.

Figure 3.25 shows the service rate (i.e., ratio between the number of served passengers and the total number of passenger requests) of each region. Figure 3.26 shows the distribution of daily average passenger requests in the regions. We can see that even for the distant regions with rare appearance of passengers (e.g., northwestern regions), the service rates were kept at high levels. Namely, the distribution of service rates is balanced among the regions. Note the service rates in the southern regions are relatively low. This is because in the simulation, the 1,000 taxicabs, which is limited by the simulator, cannot serve all the passenger requests.

3.4.4.5 Effectiveness of Components

As discussed in Section 4.3.3.3, the additional consideration of building functionalities ($\bar{H}_i$) in calculating the region scores in Equation (3.3) can help more accurately reflect the likelihood of passenger appearance in different regions, and then better guide the deployment of wireless chargers. Additionally considering the frequency of passenger appearance in Equation (3.3) serves the same purpose. To demonstrate the effective-

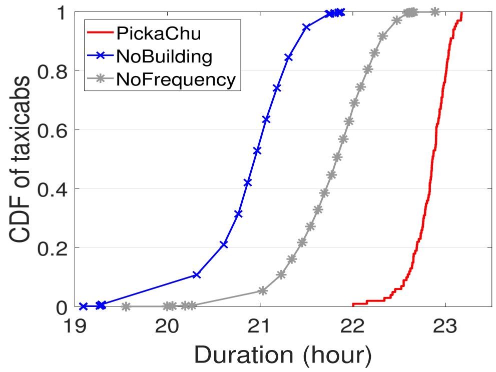

Figure 3.29: Travel phase durations.

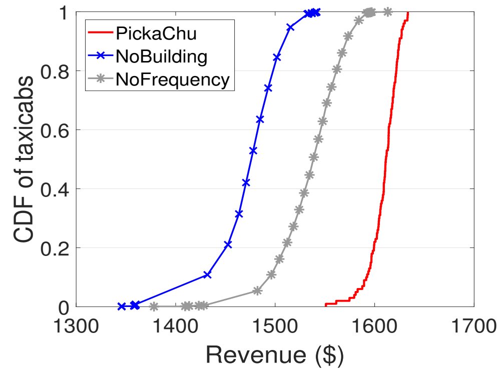

Figure 3.30: Distribution of taxicabs' revenues.

ness of these two components, we recalculated the score of each region ($\rho(\boldsymbol{g_i})$) without multiplying the weighted sum of the building functionalities (denoted as *NoBuilding*), and without multiplying the weighted sum of the passenger appearance frequencies (denoted as *NoFrequency*). Based on the new region scores, we redetermined the deployment of chargers, and measured the average costs and revenues of the taxicabs during the day as shown in Figure 3.27. In addition, we also measured the number of passengers served by the taxicabs in different methods under different hours as shown in Figure 3.28, and the distribution of the travel phase durations of the taxicabs as shown in Figure 3.29 and the distribution of the revenues of the taxicabs as shown in Figure 3.30.

We can see that compared with *NoBuilding* and *NoFrequency*, *PickaChu* increases the average revenue by \$150 and \$75 per taxicab, respectively, while the costs are almost equal. Also, *PickaChu* can serve at most 1,000 more passengers than *NoFrequency*, and at most 2,500 more passengers than *NoBuilding*. This is because with considering these two components, the region scores can more accurately reflect the likelihood of passenger appearance and the resultant charger deployment in *PickaChu* can provide higher opportunity of picking up passengers for the taxicabs.

3.4.4.6 Impact of the Number of Chargers

Our optimization problem outputs the selected regions for deploying chargers, and the number of chargers at each selected region. To illustrate the impact of the total number of chargers on the taxicabs' operation efficiency, from the optimally selected regions, we randomly picked 10 to 90 regions to deploy the chargers, while the number of chargers per region remains the same as that in the optimization output. We then measured the average, 5^{th} and 95^{th} percentiles of the revenues and the costs of the taxicabs under various total numbers of chargers, which is shown in Figure 3.31. We can see that along with the increasing of the total number of chargers, the average revenue of the taxicabs keeps increasing, and the average cost of the taxicabs keeps reducing. This is because the more chargers deployed, the less idle miles the taxicabs need to drive in seeking the chargers, which reduces the taxicabs' cost. Meanwhile, the taxicabs' opportunity of picking up passengers also increases with the increased number of chargers, which increases the taxicabs' revenue.

We also measured the distribution of the numbers of the chargers in the regions, which is shown in Figure 3.32. We can see that there are fewer regions deployed in *OptPickaChu* than in *PickaChu* (93 vs. 125), and the majority of the regions in *OptPickaChu* have 3 chargers, and the majority of the regions in *PickaChu* have 4 chargers. This is because *OptPickaChu* has smaller total deployment cost, it must deploy fewer chargers per region so that the chargers can be deployed to a sufficient number of regions to support the SoC of the taxicabs. While *PickaChu* has a higher budget, so it can select more regions to deploy wireless chargers and deploy more chargers per region.

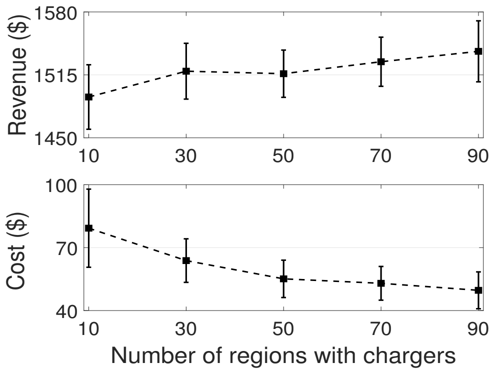

Figure 3.31: Impact of the number of regions with chargers.

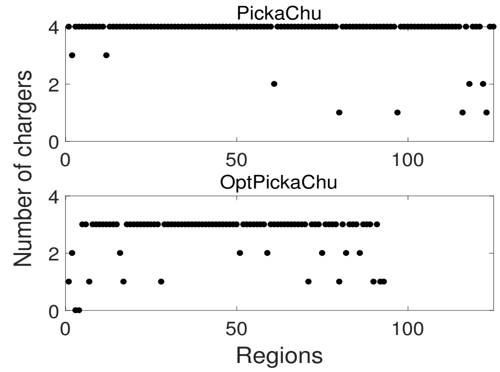

Figure 3.32: Distribution of the number of chargers in regions.

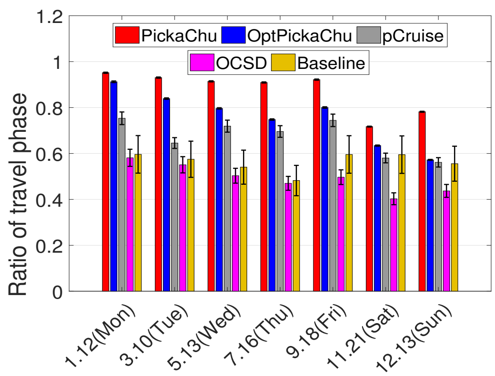

Figure 3.33: Ratios of travel phase of all vehicles in different days.

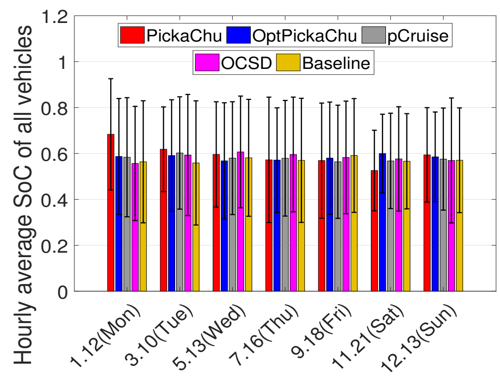

Figure 3.34: Hourly average SoC of all vehicles in different days.

3.4.4.7 Performance Evaluation on Multiple Days

To further validate the effectiveness of our charger deployment method under different scenarios, we measured the ratio of travel phase and hourly average SoC of all the vehicles on different days. Figure 3.33 shows the median, 5^{th} and 95^{th} percentiles of the ratios of travel phase of all the vehicles on different days. Figure 3.34 shows the median, 5^{th} and 95^{th} percentiles of the hourly average SoC of all the vehicles on different days. In these experiments, we assume that all the taxicabs are fully charged at the beginning of a day. This assumption is reasonable because many previous studies have confirmed that most EVs are fully charged overnight at their home or dispatch center [10, 49]. In addition, we also measured the impact of considering building functionality and the frequency of passenger appearance on the ratio of travel phase of the vehicles on different days. The measurement results are illustrated in Figure 3.35.

From Figure 3.33, we can see that the median values of the ratios of travel phase of the vehicles generally follow: *PickaChu*>*OptPickaChu*>*pCruise*>*OCSD*≈*Baseline* on weekdays. The only exceptions are on weekends where the ratios of travel phase significantly drop under all methods. This is because that the appearance positions of passengers on weekends are quite different with those on weekdays. The charger positions cannot provide sufficient passenger pick-up opportunities as on weekdays, which causes the taxicabs to drive less time with passengers onboard (i.e., shorter travel phase). To let the taxicabs fully adapt to the changed appearance positions, a dispatching method that schedules the driving and charging of taxicabs according to the real-time distribution of passenger pick-up requests is needed, which is the focus of Chapter 5. From Figure 3.34, we can see that the median values of the SoC of the vehicles in *PickaChu* and *OptPickaChu* are generally the same as those of the other methods on different days, which is consistent with Figure 3.21. This result demonstrates that although the taxicabs cannot pick up sufficient passengers by temporary parking at chargers during weekends, the deployed chargers can still maintain the SoC levels of the taxicabs. Note that the maintaining of the taxicabs' SoC is at the expense of the taxicabs' extra time spent on seeking chargers and charging. Although Figure 3.15 has already shown that many taxicabs can pick up sufficient passengers during their stay at an opportunistic charger, which greatly shortens their extra time spent on seeking chargers and charging, the passenger discovery ability of taxicabs is significantly dependent on the positions of the chargers. In the scenarios with a much more different passenger appearance pattern than the charger deployment (e.g., weekends, holidays), a dispatching as CD-Guide (Chapter 5) is needed.

To confirm the impact of considering building functionality and the frequency of passenger appearance on the ratio of travel phase of the vehicles under differ-

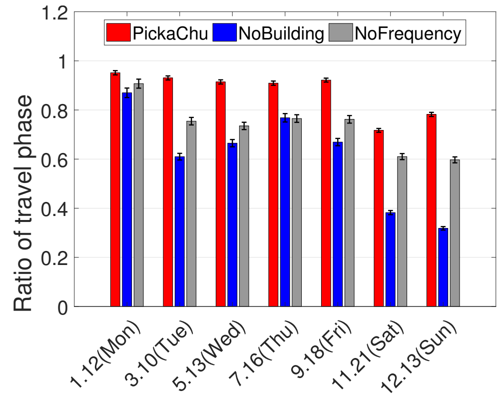

Figure 3.35: Impact of building functionality and passenger appearance frequency on charger deployment in different days.

ent scenarios, we redeployed the chargers without multiplying the weighted sum of the building functionalities (denoted as *NoBuilding*), and without multiplying the weighted sum of the passenger appearance frequencies (denoted as *NoFrequency*) in Equation (3.3). The results are illustrated in Figure 3.35. We can see that the median values of the ratios of travel phase of the vehicles generally follow *PickaChu*>*NoBuilding*≈*NoFrequency* on weekdays. We also notice that although the ratios of travel phase under all methods drop on weekends, *NoBuilding* suffers from much more drop compared with the others. This result shows that although the passenger appearance positions on weekends differ significantly with those on weekdays, building functionality is a relatively more stable indicator of passenger appearance.

3.5 Summary

The idle time of electric taxicabs is wasteful against making profits and energy consumption. Wireless charging techniques enable EVs to be charged at their parked positions. Our proposed *PickaChu* is the first work that aims at both maximally reducing the taxicabs' idle time and supporting the continuous operability of the taxicabs through proper deployment of wireless opportunistic chargers. Our analytical results on a metropolitan-scale taxicab dataset lay the foundation of the design of *PickaChu*. We assign scores to regions to represent the likelihood of passenger appearance in the regions, and model taxicab mobility to calculate the expected SoC of the taxicabs in each region. We design a multi-objective optimization problem to minimize the total deployment cost of chargers, maximize the passenger pick-up opportunity at the chargers, and ensure the continuous operability of the taxicabs. We conducted trace-driven experiments on SUMO to verify the performance of *PickaChu*. Compared with the previous methods, *PickaChu* reduces the taxicabs' daily average idle time by 81% and increases the taxicabs' daily revenue by more than 50% under the same charger deployment cost. When minimizing the charger deployment cost, *PickaChu* reduces the number of chargers by 27%, but still reduces the taxicabs' daily average idle time by 61% and increases the taxicabs' daily revenue by more than 40%.

The components of *PickaChu* can also be used for the planning of many existing charging facilities, such as fast charging stations, and battery swapping stations. In future work, we will explore some other region partitioning methods to improve the charger deployment (e.g., considering building size, city layout plan, and possible waiting queue length). We will also consider the pattern of passenger appearance to guide the taxicab pick-ups proactively before receiving passenger requests.

Chapter 4

Deployment of Dynamic Wireless Chargers

To fulfill metropolitan transit demands, public transportation EVs (e.g., buses), although only have limited battery capacity, must be continuously driving without recharging downtime [23]. As discussed in Chapter 1, a dynamic wireless charger is suitable to charge electrified buses and customized transit vehicles, since their driving routes are fixed or pre-determined by a ride-hailing service. A road segment deployed with a dynamic wireless charger is called a wireless charging lane. It however brings up a new challenge: how to deploy dynamic wireless chargers (i.e., determine the locations and lane lengths) in a metropolitan road network to minimize the deployment cost while enabling EVs to be continuously operable on the roads. By operable, we mean that an EV's residual energy measured by State of Charge (SoC) (i.e., percentage of stored energy) is non-zero. Although there have been multiple works proposed for optimally deploying plug-in charging stations [5, 26, 58, 93, 108, 119, 137], the methods cannot be applied to deploying dynamic wireless chargers because of their different charging approaches. Therefore, in this chapter, we propose *CatCharger*, an approach that uses Categorization and clustering of vehicle traffic attributes (i.e., passing velocity, visiting frequency) to determine the deployment of dynamic wireless Chargers considering metropolitan-scale charging demands of electrified buses and customized transit vehicles.

The remainder of this chapter is organized as follows. Section 4.1 identifies the background and challenges in the design of *CatCharger*. Section 4.2 presents our metropolitan dataset measurement results. We describe the main design of *CatCharger* in Section 4.3 and present our experiment evaluation in Section 4.4. Section 4.5 concludes this chapter with remarks on our future work.

4.1 Background

Several previous works [5, 26, 137] deploy charging stations based on the demands deduced from models (e.g., queueing theory, driver preference, and parking patterns). Bae *et al.* [5] proposed to deploy charging stations through analyzing the spatial and temporal dynamics of charging demand profiles at potential positions using the fluid dynamic model. Zheng *et al.* [137] formulated an optimization problem trying to maximize the number of EVs charged while minimizing the life cycle cost of all the stations. Eisel *et al.* [26] aimed at dealing with drivers' range anxiety (i.e., fear of being unable to reach destination due to insufficient charging opportunities) by transforming the drivers' preference in charging into planning of stations.

Further, several traffic flow based charging station deployment algorithms have been proposed [58, 93, 108, 119]. Lam *et al.* [58] formulated the station placement as a vertex cover problem, proved its NP-hardness and proposed four solutions. Wang *et al.* [108] determined constraints (e.g., driving range, traffic volume) from EV traffic statistics, and formulated and solved a multi-objective location optimization problem to maximize the coverage of EV traffic. Sánchez-Martín *et al.* [93] proposed to deploy charging stations at the positions with many parking events and suitable parking time length with the minimum deployment cost to offer EVs enough charging opportunities. Yao *et al.* [119] formulated a problem trying to minimize deployment cost to maximize the covered EV traffic flow.

However, the methods for deploying plug-in charging stations cannot be used for deploying wireless charging lanes due to their different charging approaches as explained in the beginning of this chapter. There are two main challenges that need to be addressed in handling the dynamic wireless charger deployment problem:

(1) **Reducing charging lane length.** The charging lanes need to be as short as possible in order to reduce the deployment cost, while still enabling EVs to be fully charged when they pass a lane. However, how to select locations for charging lane deployment to achieve this objective is challenging.

(2) **Reducing the number of deployed charging lanes.** The problem of determining the locations of the charging lanes on a metropolitan road network to maintain the continuous operability of the EVs on roads, while minimizing the number of deployed charging lanes, is non-trivial.

4.1.0.1 Vehicle Velocity at Charging Lanes Matters

The amount of energy transmitted to an EV from a wireless charging lane (E) equals: $E = L \cdot r/v$, where L denotes the length of the charging lane, r denotes its energy supply rate, and v denotes the vehicle's speed passing through the charging lane.

Since EVs with different battery capacities may pass a charging lane with various speeds, to ensure that any EV can be charged certain amount of energy after it passes a charging lane with a speed slower than a certain value (average vehicle passing speed in this paper), we can manually specify an expected minimum charge amount threshold E_{min} (e.g., the 50%, 80%, or 100% of the EVs' maximum battery capacity). That is, any EV can be charged with at least E_{min} if it passes through the charging lane with a speed slower than the average vehicle passing speed at the charging lane. A larger E_{min} enables the charging lanes to maintain higher SoC levels in application, but requires higher cost (i.e., longer charging lane length) and is limited by technology issues [45], and vice versa. Thus, the value of E_{min} should be adjusted according to city planner's expectations. Therefore, when a landmark i with average passing speed $\overline{v}_i$ is chosen to deploy a charging lane, its length is determined to meet the above condition:

$$L_i = \frac{E_{min}}{r}\overline{v}_i. \tag{4.1}$$

Note $\frac{E_{min}}{r}$ is a constant, so the charging lane length (L_i) is directly determined by vehicle average passing speed $(\overline{v}_i)$. Since a longer charging lane leads to higher deployment cost [48, 50, 83], the charging lanes should be placed at the positions with the slowest passing speed. Then, the charging lane has the shortest length that can fully charge passing EVs.

4.1.0.2 Vehicle Visit Frequency and Multi-source Vehicle Traffic Matter

To keep the EVs operable at any location in the city without downtime, the placement of charging lanes must cover the majority of the EV traffic. Therefore, the selection of the charging positions should also consider EV visit frequency. Meanwhile, to support the operability of all EV-based public transit services, considering a single source of vehicle traffic may generate bias and we must consider all sources of vehicle traffic. Our datasets meet this requirement.

4.2 Dataset Analysis

A road network is essentially a directed graph, in which nodes represent intersections and edges represent road segments [135]. The movement records of a vehicle are continuous. We first generate the driving trajectory of each vehicle. We view a

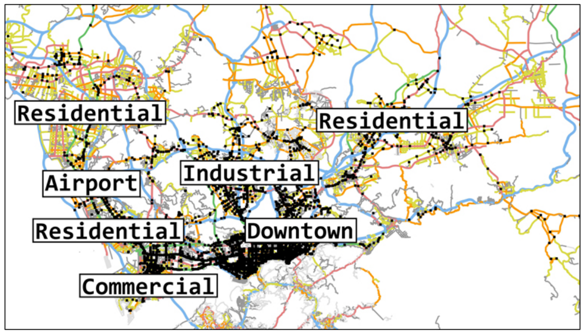

Figure 4.1: Distribution of potential positions for placing charging lanes.

vehicle has finished its previous trajectory if it stops at a location for more than 10 minutes. Thus the stopping locations cut the movement records into multiple trajectories. Since vehicles usually change movement at intersections, we map each position record to its nearest landmark (in Euclidean distance). Then, a vehicle trajectory can be represented by a sequence of landmarks [121]. We define vehicle trajectory as:

Definition 5 *A vehicle n_i's trajectory is a sequence of time-ordered spatial positions, $Tr_i : \{(\boldsymbol{p_0}, t_0), (\boldsymbol{p_1}, t_1), \ldots, (\boldsymbol{p_m}, t_m)\}$, where each position is represented by a latitude and a longitude $\boldsymbol{p_j} = (lat_j, lon_j)$.*

Through measurement, we found that the range and the average of vehicle visit frequency at a landmark are $[0/day, 96,637/day]$ and $3,840/day$, and the range and the average of vehicle passing speed in a landmark are $[0km/h, 142km/h]$ and $20km/h$. Figure 4.1 shows the distribution of landmarks (black dots) whose vehicle visit frequency is higher than $10^4/day$, and vehicle passing speed is lower than $60km/h$. The territory of Shenzhen consists of 7 functional regions (e.g., commercial, residential). We can see that each region has several candidate landmarks with both high vehicle visit frequency and slow passing speed.

Figure 4.2 shows the Cumulative Distribution Function (CDF) of average vehicle passing speed and average vehicle visit frequency per day of each landmark. Figure 4.3

plots the density distribution of vehicle passing speed with respect to (w.r.t.) vehicle visit frequency to illustrate the distribution of positions with both slow vehicle passing speed and high vehicle visit frequency. In Figure 4.2, we see that the landmarks with vehicle visit frequency higher than $10^4/day$ only take less than 25% of all the landmarks, and the landmarks with vehicle passing speed less than $60km/h$ take up about 80% of all the landmarks. In Figure 4.3, we can see the landmarks with both low vehicle passing speed ($60km/h$) and high vehicle visit frequency ($10^4/day$) take up a small portion within the red square circle. Additionally, even for the landmarks with high average vehicle visit frequency, their actual vehicle visit frequency may vary a lot. Considering that the charging lane length is determined after deployment, a landmark with a relatively more stable vehicle visit frequency is more suitable for deploying wireless charging lanes since there will be continuous flows of EVs passing through them (e.g., landmarks nearby train station, airport). Therefore, we also measured the variance of the vehicle visit frequency of the landmarks in the square circle of Figure 4.3. The measurement results are illustrated in Figure 4.4. We can see that although the standard deviation of vehicle visit frequency at around 80% of the landmarks is lower than 1,000, the standard deviation of vehicle visit frequency at the other 20% landmarks can be as high as 10,000 in the worst case. Even for some landmarks with extremely high average vehicle visit frequency, their actual vehicle visit frequency can vary significantly. This means that the variance (standard deviation) of vehicle visit frequency of the landmarks needs to be considered in measuring the suitability of deploying wireless charging lanes.

In addition, we also measured the variance of vehicles' passing speed at the landmarks. The results are illustrated in Figure 4.5. We can see that the variances of vehicles' passing speed differ a lot in different regions. More than 40% of the positions have a variance of vehicle passing speed higher than $20km/h$, and the variance can

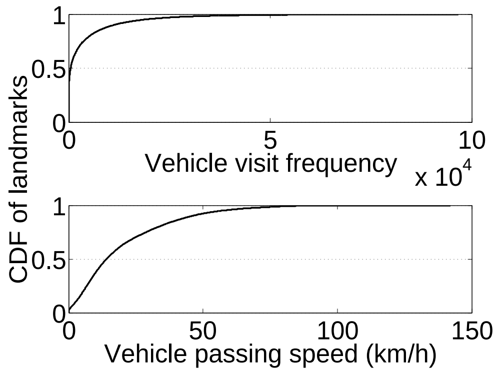

Figure 4.2: Average vehicle passing speed & daily vehicle visit frequency.

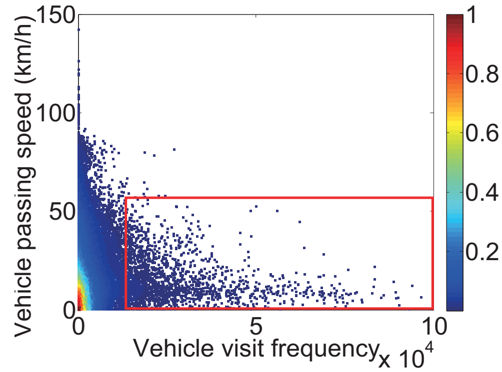

Figure 4.3: Density scatter of vehicle passing speed w.r.t. vehicle visit frequency.

be as high as $50km/h$. It means that if we solely determine the charging lane length by vehicles' average passing speed at these positions, the deployed charging lane may not be able to fully charge most vehicles passing through the positions. However, simply deploying charging lanes with the maximum possible length to ensure all the vehicles can be fully charged is unrealistic due to high deployment cost. Therefore, in addition to average vehicle passing speed, we need to also consider the variance of vehicle passing speed at the potential charging positions. The above observations motivate us to find an innovative method to properly extract candidate charging lane placement positions considering the diversity in vehicle passing speed and visit frequency, and their distribution in different regions. The details will be elaborated in Section 5.3.4.

Average vehicle flow rate of a landmark is defined as the average number of vehicles driving through the landmark per unit time [6, 35]. From the definition of average vehicle flow rate of a landmark, it equals to the product of average vehicle density and average vehicle passing speed on the landmark. A landmark with a high vehicle flow rate means that there are many vehicles that pass through the landmark per unit time, and the vehicles can pass the landmark with a relatively high velocity (i.e., no traffic congestion). Thus, it is usually a good indicator on how well a charging facility can serve EVs. Therefore, in addition to vehicle visit frequency, we also measured the

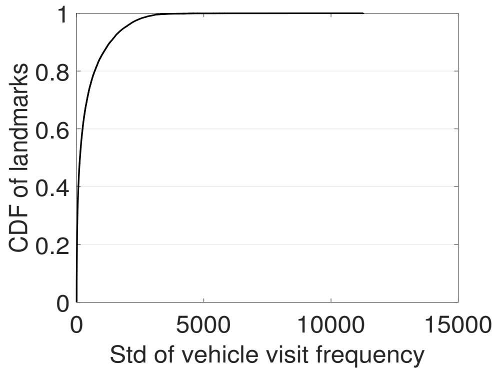

Figure 4.4: Variance of vehicle visit frequency of landmarks.

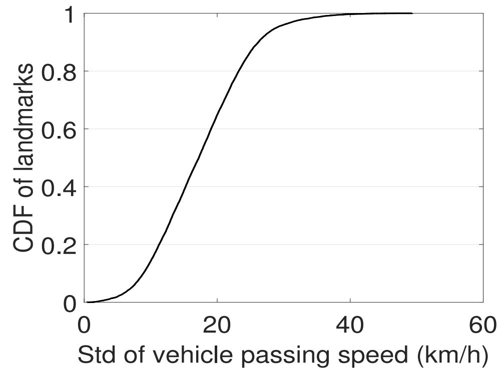

Figure 4.5: Variance of vehicle passing speed of landmarks.

average vehicle flow rate of all the landmarks. We consider the landmarks in the red square in Figure 4.3 as potential candidate landmarks (i.e., landmarks with vehicle visit frequency higher than $10^4/day$ and vehicle passing velocity lower than $60km/h$). We also measured the average vehicle flow rate of the candidate landmarks. The CDF of the measurement results are illustrated in Figure 4.6. The black curve is the measurement results of all the landmarks. The red dashed curve is the measurement results of candidate landmarks suitable for deploying in-motion wireless chargers. We can see that the black curve is about to reach 1 at a vehicle flow rate of $1000/h$ (i.e. almost all landmarks have a vehicle flow rate that is less than $1000/h$). About 80% of all the landmarks have a vehicle flow rate less than $125/h$. About 60% have a vehicle flow rate less than $62/h$. The trend of the result is similar to that in Figure 4.2.

From the measurement results of candidate landmarks (i.e., red dashed curve in Figure 4.6), we can see that its general trend is similar to that of the black curve but shifts to the right significantly. This means that the potential candidate landmarks typically have much higher average vehicle flow rate than other landmarks. Specifically, the CDF is about to reach 1 at a vehicle flow rate of $2500/h$. About 80% of all candidate landmarks have a vehicle flow rate less than $750/h$. About 60% of all candidate landmarks have a vehicle flow rate less than $625/h$. We can see that although all the candidate landmarks have a much higher vehicle flow rate than other

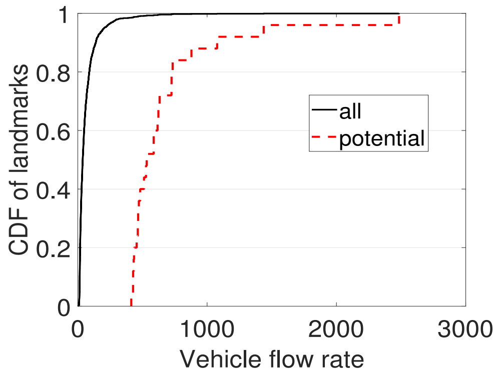

Figure 4.6: Distribution of vehicle traffic flow rate of landmarks.

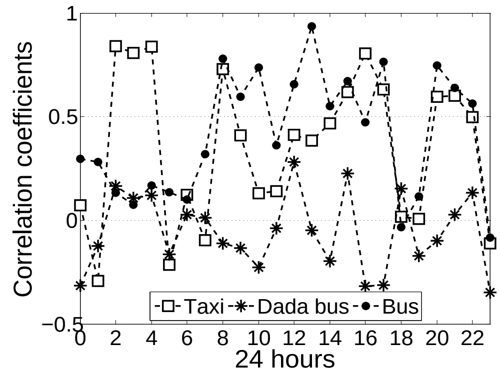

Figure 4.7: Correlation between each vehicle source and public transit traffic.

landmarks, their vehicle flow rates still vary a lot. We must consider deploying in-motion wireless chargers to the positions with the highest vehicle flow rate to ensure the total charging capability of the deployed chargers. In Section 4.3.4.2, we will explicitly explain how we consider the average vehicle flow rates of candidate landmarks in determining the locations to deploy wireless charging lanes.

We further compare the mobility of each vehicle source with the total public transit mobility to demonstrate the necessity of using multiple sources of vehicle mobility in collecting traffic statistics. We define an activity of a vehicle as a position change in the vehicle's trajectory. Then, we calculate the average number of the activities of each kind of vehicles during each hour throughout a day for one month. Next, we use the Pearson correlation coefficient [87] to measure their respective correlation to the total movement activity of public transit vehicles (i.e., bus+taxi+Dada bus), as shown in Figure 4.7. The result shows that during morning hours (i.e., 00:00∼06:00), the activity of taxis is more correlated with the public transit mobility than bus and Dada bus, which means that the taxis play the main role in public transit service during this period of time. This is because most bus lines and customized transits are not in service during this period. Starting from 07:00, the correlation between the bus and the public transit mobility is higher than the others. This is because the buses are in service after this time point, so they represent the public transit mobility

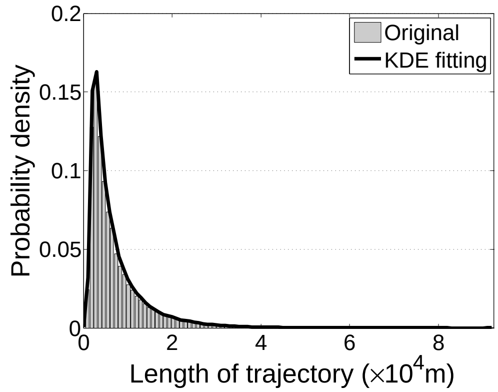

Figure 4.8: Distribution of trajectory lengths & estimation of KDE.

the most. Since the operation of Dada buses is driven by crowdsourced requests, so they do not operate throughout 24 hours. Therefore, it has low correlation to the public transit traffic at many time points in the figure. We see that at around 12:00, 13:00 and 18:00, the correlation of Dada buses to the public transit mobility is close to the others. It means that during these times, Data buses provide a majority service to meet the public transit demands, and the mobility of the Dada buses must be considered in measuring the public transit demands that the charging lanes need to satisfy.

Considering that the vehicles' trajectories reflect their traffic between different locations [120], and the length of a trajectory determines the energy consumption, we calculated the length of the trajectories of each vehicle in one month. The distribution of the collected trajectory lengths is shown in Figure 4.8. We can see that most of the trajectories are less than 10,000 meters. The long trajectories are mostly generated by buses, as they drive continuously on scheduled routes when in service. However, the distribution of the trajectory lengths cannot be simply modeled using a parametric distribution. Since KDE is a non-parametric method to estimate the probability density function of a random variable, we feed the lengths of the trajectories to the KDE model to infer the vehicles' probability of reaching each landmark in the road network. The curve in Figure 4.8 represents the distribution fitting result from the

KDE. The KDE is a function of the trajectory length. Based on a trajectory's length, we can calculate an EV's residual energy after it drives through the trajectory. Then, using the probability of reaching each landmark from the KDE, we can estimate the expectation of residual energy of EVs at each landmark on the road network given deployed charging lanes. Then, we can formulate an optimization problem that aims to maintain the expected residual energy above a threshold at each landmark with the minimum charging lane deployment cost.

Summary: We observed that different landmarks have different vehicle passing speeds and vehicle visiting frequencies. We conclude that the determination of wireless charging lane positions needs to: (i) consider vehicle passing speed since it determines the deployment cost of the charging lane required for fully charging EVs, (ii) consider vehicle visit frequency since it determines the landmark's capability of serving charging demands, and (iii) comprehensively analyze vehicle mobility from various types of vehicles to ensure that the deployed charging lanes can meet the charging demands from various vehicles. This conclusion motivates us to design a novel approach using multi-source vehicle mobility to extract candidate positions suitable for placing wireless charging lanes, and properly choose the positions so that they can meet all the charging demands of EVs with the minimum deployment cost. We find a solution for the charging lane placement challenge as follows:

Solution: Given a road network comprised of a set of landmarks LM, and trajectory datasets of multiple sources of vehicles $\{Tr\}$, we first extract candidate positions from LM that have both slow passing speed and high visit frequency (i.e., short length of charging lane required for fully charging an EV and high capability for serving charging demands). We then further select positions to place charging lanes to ensure that the expected residual energy of EVs at each landmark is no less than a threshold with the minimum deployment cost.

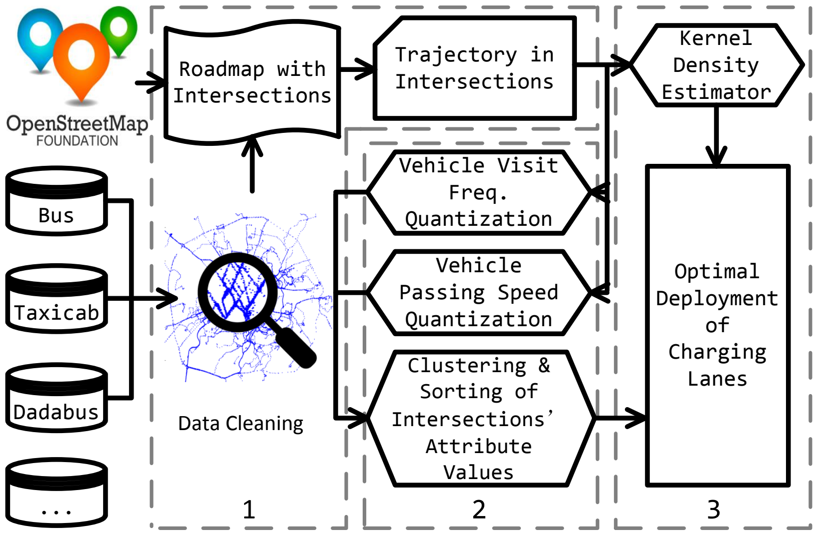

Figure 4.9: Framework of *CatCharger*.

4.3 System Design of CatCharger

As shown in Figure 4.9, the *CatCharger* consists of following three stages (highlighted as three dashed boxes):

1. **Vehicle mobility normalization** (Section 5.3.3). First, we need to apply the *Data Cleaning* on the vehicle datasets. Then, based on *OpenStreetMap*, we extract all intersections (landmarks) and generate the *Roadmap with Intersections*. Finally, by mapping each position record to respective nearest intersection (in Euclidean distance), we represent a vehicle's mobility by a *Trajectory in Intersections*.
2. **Charging lane location candidate extraction** (Section 5.3.4). With the data output from the first stage, we apply the *Vehicle Visit Frequency Quantization* and the *Vehicle Passing Speed Quantization* to generate the traffic attribute values for each intersection. Then, we apply the *Clustering & Sorting of the Intersections' Attribute Values* to extract the intersections with both high vehicle visit frequency and short required charging lane length.
3. **Charging lane location determination** (Section 4.3.4). We first use the lengths of the trajectories to build the *Kernel Density Estimator* (KDE), which is used to

estimate the vehicles' traffic at different landmarks. Then we formulate an optimization problem to solve the wireless charging lane deployment problem, and its solution outputs the locations and lane lengths for *Optimal Deployment of Charging Lanes*.

4.3.1 Assumptions

Above all, we have the following assumptions for EVs:

1. When an EV needs to recharge its battery, it will drive to the nearest charging lane for charging. If necessary, the EV will utilize a charging guidance method [72, 104] to direct its driving route to the most suitable charging station, which is not the focus of *CatCharger*.
2. The EVs' traffic pattern during the time when they do not demand charging (i.e., the EVs' trajectories between their origin and destination) will remain similar as the EVs' traffic pattern before the deployment of dynamic wireless chargers. This is reasonable because that the daily transit demand of city population, which determines the traffic pattern of the EVs, remains relatively stable among different days (source: [14, 135]).
3. On a charging lane, an EV driver can only drive a relatively low passing speed between a maximum allowable speed and a minimum speed limit. The former is specified according to the planned charging lane length determined by Equation (4.1), while the latter is a predetermined constant no greater than the former (source: [19]).

4.3.2 Vehicle Mobility Normalization

The original movement records of vehicles are mixed with noises (e.g., records with duplicated GPS position, timestamp and etc., and records with GPS positions out of the area range of Shenzhen), so we first need to clean the datasets by removing the duplicated records. Moreover, as a road network can be abstracted into intersections and road segments [135], we map each position record to its nearest intersection in Euclidean distance. Finally, the original position records generated by the vehicles in a time period (Figure 4.10 for 07:00–07:30 on July 1, 2015) are normalized to sequences of landmarks (Figure 4.11).

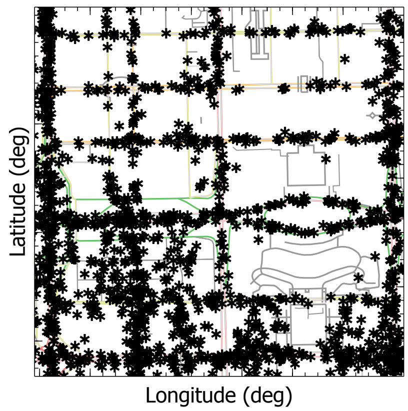

Figure 4.10: Original mobility.

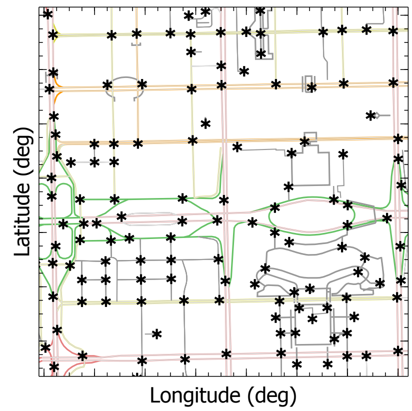

Figure 4.11: Normalized mobility.

4.3.3 Charging Lane Location Candidate Extraction

Vehicle visit frequency on different landmarks varies in different regions [124]. For example, the vehicle visit frequency of a landmark in Downtown is generally much higher than a landmark in an Industrial region. The deployment of charging lanes still needs to consider the charging demands in Industrial areas as well in order to support the traffic of the EVs on the entire road network. For this purpose, considering that the landmarks belonging to the same region usually have similar attribute values (i.e., average vehicle passing speed, daily vehicle visit frequency), we cluster such landmarks to one group. Since the landmarks in each group have similar attribute values, they are almost equally important in deploying location selection. We then choose groups with better attribute values for deploying charging lanes. Next, from each group, we further extract the landmarks with the best attribute values from different regions. Finally, the extracted candidate landmarks are the ones with high suitability for deploying charging lanes, and geographically distributed in different functional regions.

In the following, we first introduce how *CatCharger* categorizes attribute values, and then clusters the landmarks using the entropy minimization based clustering method.

4.3.3.1 Categorization of Original Mobility Data

As previously indicated, we need to consider two attributes of the landmarks (i.e., vehicle passing speed, and vehicle visit frequency) in the deployment. But directly clustering the landmarks with different numerical attributes is non-trivial because it is not easy to define "closeness" between the attributes based on the Euclidean distance. For example, given three landmarks: $A(50km/h, 10000/day)$, $B(50km/h, 9000/day)$ and $C(100km/h, 10000/day)$. With K-means using Euclidean distance, C is more similar to A than B, though actually A is more similar to B because they require the same charging lane length and have high vehicle visit frequency.

To handle this problem, we propose to properly categorize the attribute value range into several intervals, with each interval representing a range of speed (v) and visit frequency (f). Jang *et al.* [48] used a speed variance of $5km/h$ in determining the charging lane length, so we use it in categorizing speeds. As for vehicle visit frequency at landmarks, since there are around 51,000 vehicles being considered, we use 1,000 as the categorization interval. Each interval has an ID. Thus, the attributes are categorized into IDs like:

$$\begin{aligned} v :& \{0, 0 \sim 5km/h\}, \{1, 5 \sim 10km/h\}, \ldots, \\ f :& \{0, 0 \sim 1000/day\}, \{1, 1000 \sim 2000/day\}, \ldots. \end{aligned} \tag{4.2}$$

Each attribute has the form <attribute ID, description>. For example, the attributes of a landmark with an average vehicle passing speed of $3km/h$ and a daily average vehicle visit frequency of $1500/day$ are represented as $\{0, 1\}$.

4.3.3.2 Clustering of Landmarks

After categorization, each landmark is described with two attribute IDs. *CatCharger* clusters the landmarks with the most similar attribute values into one group. We use entropy, which measures categorical disorder (i.e., dissimilarity of attribute IDs within a group) [7] for clusering. Let's take the attribute of vehicle passing speed as an example. Suppose a group has two landmarks with attribute IDs $\{0\}$ and $\{1\}$, respectively. F is a discrete random variable representing an attribute (e.g., average vehicle passing speed), $A(F)$ is the set of the attribute IDs of F in a group (e.g., 0, 1), and $p(f)$ is the probability function of F, namely the ratio of the attribute ID in the group (e.g., 0.5). The entropy of the attribute $H(F)$ within the group is defined as:

$$H(F) = -\sum_{f \in A(F)} p(f) \log_2(p(f)), \tag{4.3}$$

where $-\log_2(p(f))$ measures the dissimilarity of the attribute in the group. The entropy of the two landmarks in the example is $\frac{1}{2}\log_2 2 + \frac{1}{2}\log_2 2 = 1$. Higher dissimilarity between two landmarks' attribute IDs leads to a larger entropy. Since each landmark has two attributes, the entropy of a cluster C_i can be calculated as the sum of the entropies of the two attributes:

$$H(C_i) = H_i(F_0) + H_i(F_1). \tag{4.4}$$

Suppose all candidate landmarks LM are clustered into k clusters $\mathcal{C} = \{C_0, \ldots, C_{k-1}\}$. To measure the quality of the clustering, we use the weighted sum of the entropies of all clusters as the expected entropy resulted from the clustering. The weight for each cluster is calculated as $\frac{|C_i|}{|LM|}$, where $|\cdot|$ means the number of landmarks in the set. Thus, the expected entropy is calculated by:

$$\overline{H}(\mathcal{C}) = \sum_{k=0}^{k-1} \frac{|C_i|}{|LM|} H(C_i). \tag{4.5}$$

Given a set of landmarks for clustering, we first find all possible clustering arrangements, and then choose the one with the minimum expected entropy. For example, assume that we have a set of landmarks, $\boldsymbol{lm_0} = \{1, 2\}$, $\boldsymbol{lm_1} = \{0, 2\}$, and $\boldsymbol{lm_2} = \{2, 1\}$, and we want to form two clusters. We find all possible clustering arrangements, and then choose the one with the minimum expected entropy. Table 4.1 shows all possible arrangements of the landmarks. Since the first clustering results in the minimum expected entropy, it results in the best clustering quality.

Table 4.1: Table of clusters.

Cluster ID	Member landmarks	H	Exp. Entropy
Cluster 0	$\boldsymbol{lm_0}$ $\boldsymbol{lm_1}$	1.0	0.66
Cluster 1	$\boldsymbol{lm_2}$	0.0	
Cluster 0	$\boldsymbol{lm_0}$ $\boldsymbol{lm_2}$	2.0	1.33
Cluster 1	$\boldsymbol{lm_1}$	0.0	
Cluster 0	$\boldsymbol{lm_0}$	0.0	1.33
Cluster 1	$\boldsymbol{lm_2}$ $\boldsymbol{lm_1}$	2.0	

As a result, the optimal clustering strategy renders clusters whose member landmarks have the least dissimilar attribute IDs between each other. Unfortunately, such a clustering strategy is difficult to execute because it is NP-complete [77]. Then, *CatCharger* instead follows a heuristic method introduced in [7] to approximate the best solution. The steps of the landmark clustering are as follows:

(i) *Initialization:* To cluster landmarks into k groups, we must start with k most dissimilar landmarks. But directly extracting such k landmarks from the entire set of landmarks is non-trivial. To handle this problem, we take a sample S from the set of landmarks LM ($|S| \ll |LM|$). In S, we enumeratively calculate the entropy generated by each pair of landmarks, and place the two landmarks that generate the maximum entropy in two clusters (C_0, C_1) as the two starting clusters. Then, the remaining $k-2$ starting landmarks will be incrementally found as the ones that are most dissimilar with the already determined ones.

(ii) *Incremental clustering:* After the initialization, the remaining $|LM|-k$ landmarks will be clustered to the respective starting landmark that renders the minimum total expected entropy (Equation (4.5)) one by one.

The major problems with such heuristic clustering include: i) how to select the sample S, ii) how to determine the number of clusters k, and iii) incrementally clustering the landmarks may deteriorate the clustering quality. For i), we randomly select $\gamma\%$ (e.g., 10%) of the landmarks from every functional region of Shenzhen, and combine them as the sample because each region needs several charging positions to support the EV traffic. For ii), within the sample, we follow the algorithm developed in [18] to find the most suitable k that results in the maximum difference in entropy changing rate, of which complexity is $O(|S|^2)$. As for iii), we repeat the clustering steps (in which landmarks are randomly picked) for several times and choose the result with the minimum entropy.

4.3.3.3 Extracting Top Ranked Landmarks from Clusters

Note the required length of charging lane i (L_i) can be calculated by Equation (4.1) based on the average passing speed of a landmark. Since the shorter charging lane a landmark requires, and the higher vehicle visit frequency the landmark has, the more suitable it is for placing a charging lane. In Section 4.2, we also verified that the variance (standard deviation) of the vehicle visit frequency and the variance (standard deviation) of the vehicle passing speed of the landmark are two important factors that will influence how stable the landmark can provide charging service to EVs once it is equipped with a wireless charging lane. Generally, the less variance of vehicle visit frequency and the less variance of vehicle passing speed a landmark has, the more stable a wireless charging lane can serve many EVs and fully charge the EVs at this landmark. Therefore, we need to extract landmarks that have short charging lane length, high vehicle visit frequency, and small variance of vehicle visit frequency and vehicle passing speed. Then, we define the rank of a landmark $\boldsymbol{lm_i} \in C_j$ as:

$$R(\boldsymbol{lm_i}) = \frac{\log(\frac{\bar{f}_i}{\sigma_i^f})}{L_i \sigma_i^v}, \tag{4.6}$$

where $\bar{f}_i$ is the average vehicle visit frequency at $\boldsymbol{lm_i}$, σ_i^f is its standard deviation, and σ_i^v is the standard deviation of vehicle passing speed at $\boldsymbol{lm_i}$. Thus, the larger $\bar{f}_i$ and the smaller L_i that $\boldsymbol{lm_i}$ has, and meanwhile the smaller σ_i^v and σ_i^f the landmark has, the higher rank it will have. We use logarithmic value of $\bar{f}_i$ because $\bar{f}_i$ is generally much larger than L_i. To ensure the suitability of selected landmarks, we need to remove landmarks with low ranks. For this purpose, we calculate the average rank of each group, and then remove groups with ranks lower than a threshold. Next, we order the landmarks in each group in decreasing order of the rank. In one group, if there are several landmarks in one region, we remove the low-rank landmarks. Finally, we select the top ranked $\eta\%$ (e.g., 10%) of the landmarks from each group, and use them as the candidates for charging lane deployment, which are denoted as $\widetilde{LM} = \{\boldsymbol{lm_0}, \boldsymbol{lm_1}, \ldots, \boldsymbol{lm}_{|\widetilde{\boldsymbol{LM}}|}\}$.

4.3.4 Charging Lane Location Determination

To determine the deployment plan on the selected candidate locations, we first use the KDE, which is fed with vehicle mobility, to infer the EVs' expected residual energy at each landmark given that certain landmarks are installed with charging lanes. Then, we formulate an optimization problem that aims to minimize the total cost of deployment while ensuring that the EVs can have a certain level of expected residual energy when they arrive at each landmark. This residual energy level enables an EV to move to its nearest charging lane.

4.3.4.1 Inferring Expected Residual Energy

KDE can be used to describe the vehicles' probability of reaching a landmark on the road network given a source landmark. Also, the residual energy of a vehicle is a function of the distance from the vehicle's source landmark to the destination landmark. Then, the expected residual energy of a vehicle at a landmark in the road network can be calculated. We present the details below.

Since vehicles' mobility patterns imply their traffic at certain locations [120], we feed the vehicles' trajectories into a KDE model to infer the probability density function (PDF) of the distribution of the trajectory lengths as in Equation (4.7), namely the trip lengths that need to be supported.

$$\hat{f}_h(d) = \frac{1}{mh}\sum_{i=0}^{m-1} K(\frac{d-d_i}{h});\ -\infty < d < \infty, \tag{4.7}$$

where m is the number of sample trajectories, d_i is the length of the i^{th} trajectory, and h is the smoothing parameter influencing the estimation accuracy of the KDE and is determined according to the MISE criterion [107]. $K(\cdot)$ is the kernel function whose value decays with the increasing of d. It is set to the Gaussian function as in Equation (4.8) based on [60, 61].

$$K(\frac{d-d_i}{h}) = \frac{1}{\sqrt{2\pi}}\exp\left[-\frac{(d-d_i)^2}{2h^2}\right]. \tag{4.8}$$

According to the state-of-the-art EV energy consumption model [57], the energy consumption of a taxicab (E_c) is primarily determined by air drag (E_{air}) and rolling resistance (E_{roll}). Therefore, the consumption rate is:

$$\begin{aligned}\Delta E_c &= \Delta E_{air} + \Delta E_{roll} \\ &= c_w v^2 \Delta l + c_e \kappa g \Delta l\end{aligned} \tag{4.9}$$

where c_w is the air drag coefficient determined by vehicle front surface area; v is the driving speed; Δl is the distance that the taxicab has moved; c_e is the rolling resistance coefficient; κ is the taxicab's mass; and g is the gravity acceleration.

According to Equation (4.1), any EV can be at least charged to the expected charge amount threshold E_{min} if it drives through a charging lane with a speed slower than the landmark's average vehicle passing speed. Given an EV starting from a charger, based on Equation (4.9), its residual energy (i.e., SoC) at a location, which is d distance away from the charger through the shortest route, can be estimated as [57]:

$$E_r^d = E_{min} - \sum_{n=0}^{N^R-1} (c_w v_n^2 + c_e \kappa g) l_n, \tag{4.10}$$

where N^R is the number of road segments of the shortest route, and v_n and l_n are the speed limit and length of the n^{th} road segment, respectively. Then, the EVs' SoC at the location can be represented as:

$$SoC(d) = \begin{cases} E_r^d / E_0, & \text{if } E_r^d \geqslant 0 \\ 0, & \text{otherwise.} \end{cases} \tag{4.11}$$

Thus, given a binary integer x_i to denote whether a candidate landmark $\boldsymbol{lm_i} \in \widetilde{LM}$ is installed with a charging lane or not, the expected SOC of EVs at a landmark $\boldsymbol{lm_j} \in LM$ in the road network is:

$$\overline{SOC}(\boldsymbol{lm_j}) = \sum_{i=0}^{|\widetilde{LM}|-1} \hat{f}(d_{i,j}) SOC(d_{i,j}) x_i, \tag{4.12}$$

where $d_{i,j}$ is the shortest route distance from $\boldsymbol{lm_i}$ to $\boldsymbol{lm_j}$.

4.3.4.2 Formulating Optimization Problem

Our objective is to minimize the total deployment cost through properly selecting landmarks from $\widetilde{LM}$ to install charging lanes while ensuring that at each landmark, the expected residual energy of an EV is higher than a threshold η (e.g., 20%). The threshold is determined so that an EV uses the residual energy to reach the nearest charging lane. We can set η to be a relatively high value, so that the taxicabs are always operable with high confidence. Meanwhile, the charging rate of the deployed chargers must be able to support the power demands from all the EVs. According to Equation (4.9), we can derive the battery consumption rate for each EV as $\phi = \frac{\Delta E_c}{\Delta t} = c_w v^3 + c_e \kappa g v$. Hence, the battery consumption rate depends on the speed limit of every road segment. That is, as the speed limit v increases, the battery consumption rate increases. To derive the maximum battery consumption rate ϕ_{max}, we use the maximum speed limit v_{max} of the entire road map. In Section 4.2, we have identified that vehicle traffic flow rate is an important indicator of the charging service capacity of deployed in-motion wireless charging lanes, and different landmarks have various vehicle traffic flow rates. Therefore, in addition to the above objective of minimizing the charger deployment cost, we also have another optimization objective to maximize the average vehicle traffic flow rate covered by the deployed wireless charging lanes. Finally, the optimization problem can be formulated as below:

$$\text{minimize} \quad \sum_{\boldsymbol{lm_i} \in \widetilde{LM}} \omega_0 x_i L_i, \tag{4.13}$$

$$\text{maximize} \quad \sum_{\boldsymbol{lm_i} \in \widetilde{LM}} x_i \sum_{w \in W} \sum_{u \in U_w^i} \bar{f}_u^i P_u^w, \tag{4.14}$$

$$\text{subject to} \quad \overline{SOC}(\boldsymbol{lm_j}) \geqslant \eta, \forall\, \boldsymbol{lm_j} \in LM, \tag{4.15}$$

$$x_i L_i \leqslant L_i^{max}, \forall\, \boldsymbol{lm_i} \in \widetilde{LM}, \tag{4.16}$$

$$\mathcal{C} \sum_{\boldsymbol{lm_j} \in \widetilde{LM}} x_i \geqslant \phi_{max} N_v, \tag{4.17}$$

$$x_i \in \{0, 1\}, \forall\, \boldsymbol{lm_i} \in \widetilde{LM} \tag{4.18}$$

where ω_0 is a constant representing the cost of deploying a unit length of charging lane, $\mathcal{C}$ is the charging rate of one charger. $\bar{f}_u^i$ is the average vehicle flow rate (i.e., average vehicle visit frequency) at $\boldsymbol{lm_i}$, which is caused by the vehicles that drive through route u, recall that U_w^i is the set of historical routes between O-D pair w that pass through landmark $\boldsymbol{lm_i}$, W is the set of all possible O-D pairs on the road network, and N_v is the total number of EVs driving on the road network. This problem tries to minimize the total deployment cost of the in-motion wireless chargers

(Equation (4.13)), and maximize the average vehicle traffic flow rate covered by the deployed in-motion wireless chargers (Equation (4.14)) with three constraints: i) the expected residual energy of an EV is no less than a threshold η (Equation (4.15)), ii) each individual charging lane cannot exceed the maximum road segment length (denoted by L_i^{max}) allowed at its scheduled landmark (Equation (4.16)) [20, 45] and iii) the total charging rate of the deployed chargers is able to support the total battery consumption rate of all the EVs (Equation (4.17)).

Note the reason we filter candidate landmarks by their attribute values of vehicles' passing speed and visit frequency is that *CatCharger* does not consider the landmarks that require a too long charging lane to fully charge an EV or have low vehicle visit frequency. Therefore, the binary integers for the non-candidate landmarks are 0, namely $x_i = 0, \forall\, \boldsymbol{lm_i} \in LM \setminus \widetilde{LM}$. Given source landmark $\boldsymbol{lm_i}$ and destination landmark $\boldsymbol{lm_j}$, the coefficient $\hat{f}(d_{i,j})SoC(d_{i,j})$ in Equation (4.12) is determined. Therefore, we can use a constant θ_{ij} to represent $\hat{f}(d_{i,j})SoC(d_{i,j})$. As a result, the final multi-objective optimization problem is actually a classic Multi-objective Integer Programming (MIP) problem. Multi-Objective Evolutionary Algorithm based on Decomposition (MOEA/D) is effective for solving MIP problem with lower computational complexity than traditional multi-objective genetic local search algorithm [129]. Therefore, we employ MOEA/D to solve our formulated optimization problem. Generally, MOEA/D first uses the Tchebycheff approach [129] to decompose the MIP problem into several optimization sub-problems. Then, MOEA/D solves the sub-problems simultaneously and maintains the population of best solutions to each sub-problem during the evolution of solutions until the stop criteria has been reached.

4.3.4.3 Objective Transformation and Normalization

The first objective of the proposed model is to minimize the overall deployment cost of the chargers, while the second objective is to maximize the average vehicle traffic flow captured by the deployed chargers. Therefore, it is necessary to make the following transformation:

$$
\begin{aligned}
F(\boldsymbol{x}) &= [\min f_1(\boldsymbol{x}), \max f_2(\boldsymbol{x})]^T \\
&= \min[f_1(\boldsymbol{x}), -f_2(\boldsymbol{x})]^T
\end{aligned}
\tag{4.19}
$$

where $\boldsymbol{x} = \{x_i | \boldsymbol{lm_i} \in \widetilde{LM}\}$ is the vector of binary decision variables of all the candidate landmarks. $f_1(\boldsymbol{x}) = \sum_{\boldsymbol{lm_i} \in \widetilde{LM}} \omega_0 x_i L_i$ and $f_2(\boldsymbol{x}) = \sum_{\boldsymbol{lm_i} \in \widetilde{LM}} x_i \bar{v}_i \bar{f}_i$ are the two objective functions: Equation (4.13) and Equation (4.14), respectively. To make f_1 and f_2 comparable within the same scale, we normalize them as $\overline{f_i} = \frac{f_i - f_i^{\min}}{f_i^{\max} - f_i^{\min}}, \forall i = 1, 2$ where $f_i^{\max}$ and $f_i^{\min}$ are the maximum and minimum values of f_i, respectively. These values are obtained by solving the optimization problem with each single objective function as the optimization goal.

4.3.4.4 Solution Algorithm

The major steps of MOEA/D for solving the MIP problem are specified below in Algorithm (1). We follow [129] on utilizing the Tchebycheff approach to decompose the MIP problem into sub-problems. More technical details can be found in [129].

4.4 Performance Evaluation

4.4.1 Experiment Settings

We used our Shenzhen datasets to drive our experiments. We built a trace-driven simulator with Apache Spark 1.5.2 [4]. Since there are no previous methods that

Algorithm 1: Solution process of MOEA/D.

Input : MIP problem;
A stopping criterion;
The number of decomposed sub-problems N;
N weight vectors: $\theta^1, \ldots, \theta^N$;
The number of closest weight vectors T;

Output: EP, the external population, which stores non-dominated solutions found during each iteration;

Step 1) Initialization:
Set $EP = \varnothing$;
Obtain the T closes weight vectors to each weight vector through calculating the Euclidean distances between any two weight vectors $B(i) = \{i_1, \ldots, i_T\}$;
Initialize the solution population of each sub-problem $\boldsymbol{x}^1, \boldsymbol{x}^2, \ldots, \boldsymbol{x}^N$ and set $F^i = F(\boldsymbol{x}^i)$, where F^i is the objective function value of the i^{th} sub-problem;
Step 2) Update solutions of sub-problems:
for $i = 1, 2, \ldots, N$ **do**
    Randomly select two indices t, s from $B(i)$, and generate a new solution $\boldsymbol{y}$ from $\boldsymbol{x}^t$ and $\boldsymbol{x}^s$ by using genetic operators;
    Calculate the deployment cost resulted by $\boldsymbol{y}$ according to Equation (4.13), and calculate the vehicle flow rate captured by the charger deployment plan $\boldsymbol{y}$ according to Equation (4.14);
    Check whether a constraint is violated. If yes, decrease the objective function value resulted by $\boldsymbol{y}$ by a penalty mechanism;
    for $j \in B(i)$ **do**
        if $F(\boldsymbol{y}) < F(\boldsymbol{x^j})$ **then**
            Set $\boldsymbol{x^j} = \boldsymbol{y}$;
            Set $F^j = F(\boldsymbol{y})$;
        In EP, remove all the vectors dominated by $F(\boldsymbol{y})$;
        Add $F(\boldsymbol{y})$ to EP if no vectors in EP dominate $F(\boldsymbol{y})$;
    Step 3) Stop criteria checking and obtaining results:
    if stopping criterion is met **then**
        return final EP

handle the wireless charging lane deployment in a road network, we created two methods to compare with *CatCharger*: random placement (denoted by *Random*), and a method that maximally covers traffic flows (denoted by *MaxFlow*) [119]. In addition, we also evaluate the performance of a variance of *CatCharger* (denoted by *CatCharger+*), which considers the variances of vehicle visit frequency and vehicle passing speed in extracting the candidate landmarks, and the maximization of vehicle traffic flows in determining the landmarks for deploying in-motion wireless chargers.

In simulation, the battery capacities of the EVs follow a uniform distribution ranging from 5kWh to 10kWh [20]. We suppose every vehicle starts driving with full energy in battery at the beginning of a day. With the most recent research implementations (e.g., Oak Ridge National Laboratory [85]), it is expected that within a 10-year timeframe, it is possible to reach a charging rate over 100kW for EV wireless charging. Therefore, we use 150kW as the charging rate of a charging lane. The unit price of a charging lane is \$500/m [20, 48]. In *CatCharger*, the length of a charging lane is calculated by Equation (4.1). According to [20, 45], the length of a charging lane cannot exceed the maximum road segment length at its scheduled deployment landmark, which ranges from 100.4m to 926.7m based on the map information extracted from OpenStreetMap [84]. Since *Random* and *MaxFlow* do not have methods to determine the charging lane length, we suppose they deploy a maximally 500m-long charging lane (maximum length in *CatCharger*) at each charging landmark, which can charge 50% SoC for the EVs with a battery capacity smaller than 10kWh and a passing speed slower than 15km/h. For fair comparison, the deployment cost in *Random* and *MaxFlow* is the same as *CatCharger*. In *Random*, the locations for placing charging lanes are chosen randomly from the collection of landmarks. *MaxFlow* is for charging station deployment and we use it for charging lane deployment. We choose the landmark that covers the most traffic sequentially until the deployment cost is reached. *MaxFlow* is a traffic flow based method. Since traffic flow based methods can more accurately estimate the charging demands than the charging demand based methods [58], we do not include a charging demand based method for comparison. In landmark categorization (Section 4.3.3.1), the speed interval and the frequency interval are $5km/h$ and 1,000, respectively. In clustering initialization (Section 4.3.3.2), the ratio for selecting landmarks from every administrative region of Shenzhen, γ, is 10%. In candidate position extraction (Section 4.3.3.3), the ratio of the top ranked landmarks, ε, is 10%. The threshold of expected residual energy, η, is set to 20%. The expected minimum charge amount threshold E_{min} is set to 80% of the EVs' maximum battery capacity. As for the scaling parameters of drivers' choice behavior (i.e., ϵ and ε), we follow the settings as recommended in [91]: $\epsilon = 0.1$ and $\varepsilon = 0.8$. The parameters are listed in Table 4.2.

Table 4.2: Table of parameters.

Parameters	Setting	Source
Charging rate $\mathcal{C}$	150 kW	Chen *et al.* [20, 31, 113]
Charger unit price ω_0	\$500/m	Chen *et al.* [20]
Air drag coefficient c_w	0.3	Kurczveil *et al.* [57]
Rolling resistance coefficient c_e	0.01	Kurczveil *et al.* [57]
Mass of a taxicab κ	2,020 kg	Tian *et al.* [104]
Gravity acceleration g	9.8 m/s^2	Tian *et al.* [104]
Battery capacity of an EV E_0	5kWh – 10kWh	Tian *et al.* [33]
Ratio for selecting landmarks from regions γ	10%	Author's assumption
Ratio for selecting top ranked landmarks ε	10%	Author's assumption
Residual energy (SoC) threshold η	20%	Author's assumption
Expected minimum charge amount threshold E_{min}	80%	Author's assumption
Scaling parameters of drivers' choice behavior ϵ and ε	$\epsilon = 0.1$ and $\varepsilon = 0.8$	Riemann *et al.* [91]

We use the movement records of the taxicabs, buses and Dada buses mentioned in Section 2.2 for performance evaluation. Below, Figure 4.17 to Figure 4.19 demonstrate the metrics of the vehicles under different hours on July 15, 2015. Figure 4.20 to Figure 4.22 demonstrate the metrics of vehicles in multiple days, which are January 12 (Monday), March 10 (Tuesday), May 13 (Wednesday), July 16 (Thursday), September 18 (Friday), November 21 (Saturday) and December 13 (Sunday) in 2015. These days are representative because they are unrelated to each other, belong to 4 different seasons, and cover weekdays and weekends [121]. Specifically, we measured the following metrics:

- *Average ratio of operable vehicles.* The average ratio of vehicles that have residual energy above 0%. We measure this ratio, and different deployment costs to compare the ability of supporting EVs' operability and cost efficiency of different methods.
- *Average residual energy of vehicles.* The vehicles' average amount of energy (in percentage) left in the EVs' batteries. We measure it to compare the level of energy

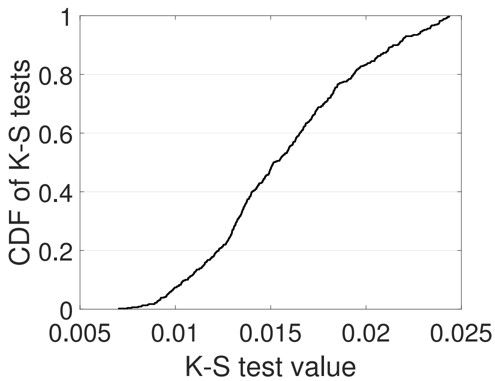

Figure 4.12: K-S test values of all the passed tests.

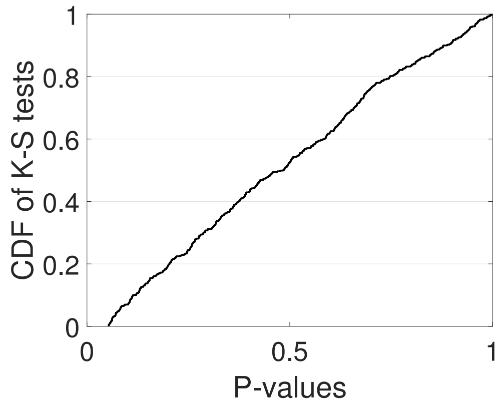

Figure 4.13: P-values of the passed tests.

that different methods can maintain.

- *Average number of charges of vehicles.* The average number of charges that the EVs receive per hour. We measure it to compare the methods' ability in offering charging opportunities to EVs.

- *Performance in distributing energy supply overhead.* The average amount of energy (in logarithmic scale) transferred per charging lane per hour. We measure it to compare the charging overhead generated by different methods. Meanwhile, we also measure the average number of charges (in logarithmic scale) occurred per charging lane per hour. We measure it to compare the energy supply opportunity generated by different methods. In addition, we also measure the CDF of the energy supply overhead over all charging lanes. We measure it to compare the balance of energy supply overhead of different methods.

4.4.2 Validation of The KDE Based Traffic Model

The validation of the KDE based traffic model is conducted by applying the One-sample Kolmogorov-Smirnov test (K-S test in short), which verifies whether the population CDF of the actual data (say $F(d)$) is equal to the hypothesized CDF (say $\hat{F}_h(d)$) [15, 65, 75]. Specifically, the K-S test value between $F(d)$ and $\hat{F}_h(d)$ is calculated by the following:

$$K = \max_{d}(|F(d) - \hat{F_h}(d)|), \tag{4.20}$$

where K is the K-S test value, and $\max_d$ is the maximum absolute difference between $F(d)$ and $\hat{F_h}(d)$. Then we use K to calculate the significance level by using an approximation formula or by interpolation in a table as in [75]. If the test approves the hypothesis that the $F(d)$ is similar to $\hat{F_h}(d)$ inferred by the KDE based traffic model (i.e. small K-S test value) at the significance level (measures the reliability of this test) of 5%, we view the observed distribution of trajectory lengths is consistent with the KDE based traffic model.

To validate that the CDF determined by our KDE based traffic model can describe the distribution of trip lengths during different days, we used the daily trip data of four months (January, April, July and October in 2015) as the dataset for parameter training, and the daily trip data of other four months (February, May, August and November in 2015) as the testing dataset for applying K-S tests. The training of the CDF is completed by using cross-validation maximum likelihood [37]. Then we applied K-S tests on each day's trip data of the testing dataset. The test pass rate is 91.8%. Figure 4.12 shows the CDF of the K-S test values of all the passed tests. We can see that all the passed tests have a K-S test value lower than 0.025, which means the maximum absolute difference between $F(d)$ and $\hat{F_h}(d)$ is quite small.

However, the test result only has a certain level of confidence to be reliable. Therefore, we need to further measure the p-value of the test. The p-value is the probability that the data samples will actually follow the target CDF (i.e., the CDF determined by the KDE), which measures the doubt on the test result. A small p-value (e.g., less than 0.1 in our case) means that even if the trajectory lengths passed the K-S test, the validity of the test is in doubt [75]. Figure 4.13 shows the p-values of all the passed tests. We can see that more than 85% of the passed tests resulted in a p-value higher than 0.1. This means most of the test results are reliable. Therefore,

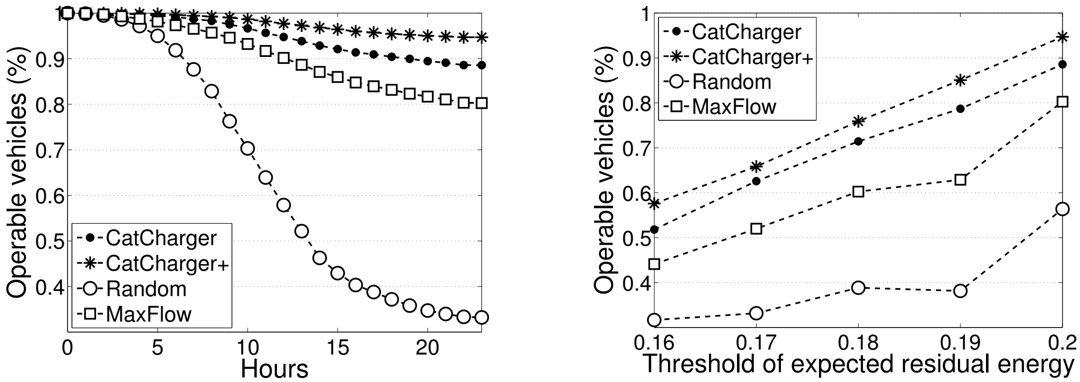

(a) Operable vehicles over time. (b) Operable vehicles versus threshold.

Figure 4.14: Performance in supporting EV charging demands.

the actual distribution of trip lengths is consistent with the CDF determined by our KDE based traffic model.

4.4.3 Experimental Results

Based on the traffic data extracted from the 1-year long dataset mentioned in Section 2.2, from total 26,036 landmarks, *CatCharger+* chose 930 landmarks to deploy charging lanes, *CatCharger* chose 922, while *Random* and *MaxFlow* chose 228. Since *CatCharger* and *CatCharger+* place most of the charging lanes at positions with short required lane lengths, while *Random* and *MaxFlow* use the same deployment cost and set the length of each charging lane to the longest length in *CatCharger* and *CatCharger+*, so they result in much fewer charging lanes.

4.4.3.1 Average Ratio of Operable Vehicles

Figure 4.14(a) shows the average ratios of operable vehicles (SOC>0%) in each hour in a day during the month. Figure 4.14(b) shows the ratios of operable vehicles resulted from different residual energy thresholds. In both figures, the ratios follow: *CatCharger+*>*CatCharger*>*MaxFlow*>*Random*.

Figure 4.14(a) shows that at the beginning of a day, the dropping rate of the ratio of operable vehicles is slow because most of the vehicles are not in service and their batteries remain full. Starting from 06:00, the result drops dramatically because the EVs start driving on the road network, which consumes much battery. In *Random*, during the time between 06:00 and 14:00, the dropping rate is almost linear with the change of time, which means that many vehicles cannot be charged during this time. This observation demonstrates that *Random* cannot cover the traffic of most vehicles since it does not consider the mobility of vehicles in determining charging positions. After 15:00, the ratio of operable vehicles gradually stabilizes at around 30%. This is because the buses and Dada buses gradually stop service so their energy levels do not change anymore, while taxicabs are still driving on roads and get charged randomly. As for *MaxFlow*, since it deploys charging lanes at the landmarks with the most traffic flows, and each vehicle passing a charging lane can be fully charged, it can keep most vehicles operable most of the time. During the time between 06:00 and 14:00, the ratio of operable vehicles drops 15%. This is because *MaxFlow* does not consider maintaining the operability of the EVs. When the EVs drive to some landmarks not frequently visited by vehicles, they may not be able to get recharged. Similar to *Random*, after 15:00, the metric gradually stabilizes at around 80% due to the same reasons. *CatCharger* can keep most of the vehicles operable throughout the day. The stabilized ratio of operable vehicles stays at around 90% in the end of the day. *CatCharger* chooses landmarks that have both high average daily vehicle visit frequency and require short required charging lane length. Thus given the same objective of minimizing the total deployment cost, each charging position of *CatCharger* consumes low cost because it generally has shorter lane length. Therefore, *CatCharger* can offer more charging opportunities (positions) than the other two methods. These positions may not necessarily be the most frequently visited ones, but they altogether can support the continuous operability of the vehicles in the road network.

Figure 4.14(b) shows that the ratio of operable vehicles of *CatCharger* increases

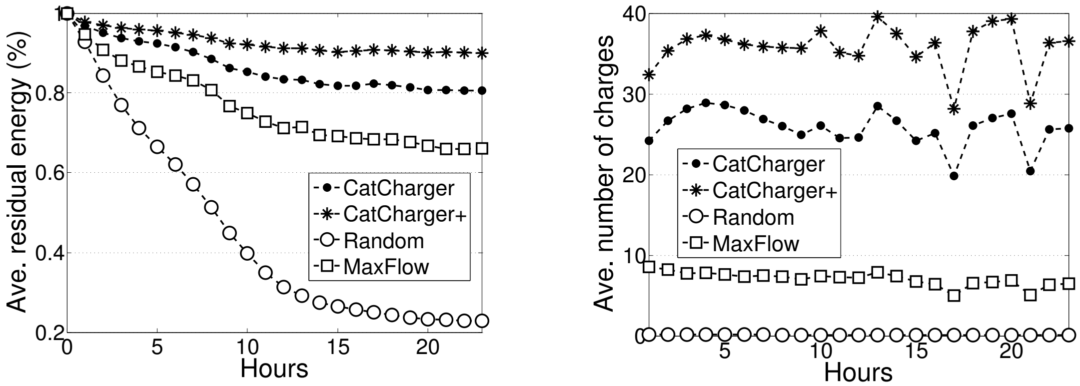

(a) Average residual energy.

(b) Avg number of charges of vehicles.

Figure 4.15: Performance in supporting EV charging demands.

linearly with the increase of the threshold of expected residual energy, since a higher residual energy guarantee increases the probability that an EV can be operable at any position. A higher expected residual energy threshold results in a higher deployment cost of the deployment solution. As a result, as the allowed deployment cost increases, the ratio of operable vehicles in *Random* and *MaxFlow* increases. The increase rate of *CatCharger* is higher than *Random* and *MaxFlow*, which means that *CatCharger* can more effectively plan the positions and lengths to maintain the highest ratio of operable vehicles given a deployment budget.

Since *CatCharger+* further considers the variances of vehicle visit frequency and vehicle passing speed, and the maximization of vehicle traffic flow at the chargers, the deployed chargers can fully recharge most EVs with their lane length since the EVs' passing speed at the charger landmarks does not vary a lot, and are free from vehicle traffic congestion. Therefore, *CatCharger+* can maintain the highest ratio of vehicles operable by the end of a day (Figure 4.14(a)) and under different residual energy thresholds (Figure 4.14(b)).

4.4.3.2 Average Residual Energy of Vehicles

Figure 4.15(a) shows the average residual energy of vehicles under different hours throughout a day. The results follow *CatCharger+*>*CatCharger*>*MaxFlow*>*Random*.

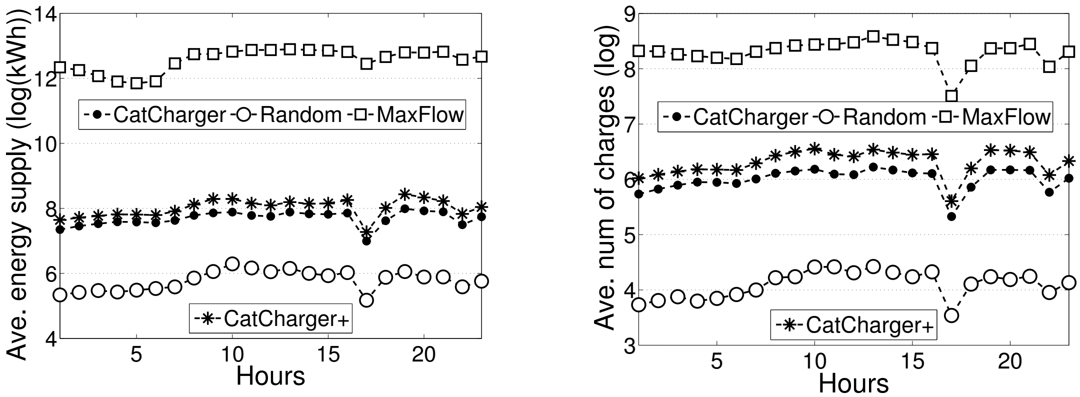

(a) Energy supply overhead.

(b) Num of charges of charging lanes.

Figure 4.16: Performance in distributing energy supply overhead.

The relationship between the methods and the changing trends of this metric are similar to those in Figure 4.14(a) due to the same reasons.

4.4.3.3 Average Number of Charges of Vehicles

Figure 4.15(b) shows the average number of charges of all vehicles under different hours throughout a day. The results follow *CatCharger+>CatCharger>MaxFlow>Random*. We can see that *CatCharger+* and *CatCharger* offer the most and second most charging opportunities to vehicles due to the same reasons as in Section 4.4.3.1. Note that the result of *Random* is almost 0. This is because only a small portion of the EVs can receive charging opportunities from *Random* deployment.

4.4.3.4 Performance in Distributing Energy Supply Overhead

Figure 4.16(a) shows the average energy supply overhead (i.e., amount of transferred energy) per landmark (in logarithmic scale) under different hours in a day. Figure 4.16(b) shows the average number of charges per landmark (in logarithmic scale) under different hours in a day. In both figures, the results follow *MaxFlow*$\gg$*CatCharger+ >CatCharger>Random*. *Random* has the lowest supply overhead because it fails to cover most of the vehicle traffic. *MaxFlow* suffers from a much larger average supply overhead. This is because *MaxFlow* aims to place charging lanes at the landmarks

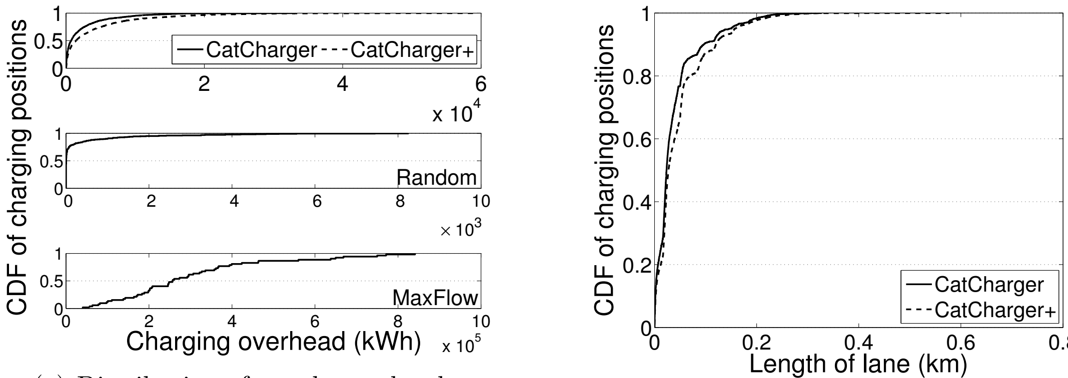

(a) Distribution of supply overhead.

(b) Distribution of charging lane length.

Figure 4.17: Performance in distributing energy supply overhead.

most frequently visited by vehicles. But the popular positions generally concentrate on a few areas. Moreover, the higher cost of a charging lane in *MaxFlow* results in fewer charging positions. Since *CatCharger* tries to deploy short charging lanes by considering vehicle passing speed, it leads to more charging lanes with a certain deployment cost. Also, it tries to cover most vehicle traffic. Then, vehicles in *CatCharger* can be more frequently charged at more landmarks, resulting in lower average energy supply overhead per landmark. *CatCharger+* further avoids deploying chargers at the landmarks with variant vehicle passing speed an vehicle visit frequency, and enables more EVs to receive recharge than *CatCharger*. Therefore, it achieves the highest results in both Figure 4.16(a) and Figure 4.16(b).

Figure 4.17(a) shows the CDF of the energy supply overhead over all charging lanes. Figure 4.17(b) shows the CDF of the length of the charging lanes deployed in *CatCharger* and *CatCharger+*, and *Random* and *MaxFlow* are not included since they have the same charging lane length. In Figure 4.17(a), we see that the distribution of energy supply overhead in *CatCharger* is more balanced than the others. In Figure 4.17(b), we see that most of the charging lanes in *CatCharger* and *CatCharger+* have lengths shorter than 0.1km due to the constraint 4.16. This result is consistent with the results in [12, 20, 45, 48]. From Figure 4.17(a), we see that in *CatCharger*, 80% of the charging lanes only need to supply less than 5,000kWh energy. This can be verified with Figure 4.17(b), in which 80% of the charging lanes have length shorter than 0.1km. In *Random*, most of the charging lanes have 0kWh supply overhead. While in *MaxFlow*, around 75% of the charging stations have supply overhead higher than 200,000kWh, which is caused by the fewer charging positions. These observations illustrate that *CatCharger* and *CatCharger+* can better balance the distribution of the energy supply overhead among charging lanes while satisfying the charging demands of EVs.

4.4.3.5 Impact of Variance of Vehicle Passing Speed and Visit Frequency

As discussed in Section 4.3.3.3, the additional consideration of the variance of vehicle visit frequency (σ_i^f) and the variance of vehicle passing speed (σ_i^v) in Equation (4.6) can help extract the candidate landmarks for charging lane deployment with more stable vehicle visit frequency and vehicle passing speed, and then better guide the deployment of in-motion wireless chargers. To demonstrate the impact of these two components, we recalculated the score of each landmark without considering the variance of vehicle visit frequency (denoted as *NoFreqVar*), and without considering the variance of vehicle passing speed (denoted as *NoSpdVar*). Based on the new landmark scores, we redetermined the deployment of chargers, and measured the average ratio of operable vehicles. The measurement results are illustrated in Figure 4.18. In addition, we also measured the average energy supply overhead per landmark under different hours in a day. The measurement results are illustrated in Figure 4.19.

From Figure 4.18, we can see that *CatCharger+* increases the final ratio of operable vehicles by the end of the day by 11.8% when compared to *NoFreqVar* and 8.6% when compared to *NoSpdVar*, respectively. This is because that *NoSpdVar* selects some landmarks with high variance of vehicle passing speed to deploy chargers. At the landmarks where the vehicle passing speed is very high during some time, the

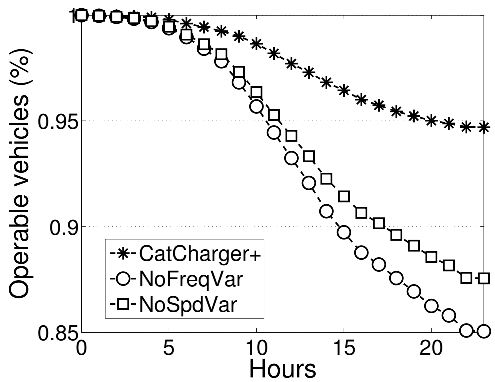

Figure 4.18: Impact of components on the ratio of operable vehicles.

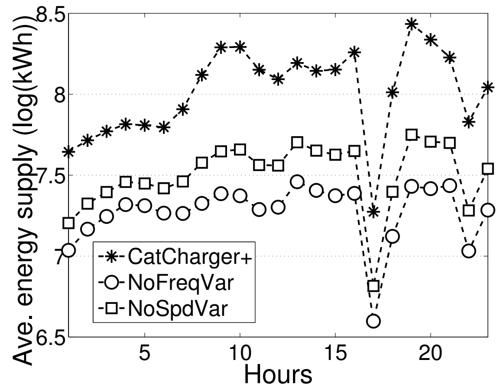

Figure 4.19: Impact of components on average energy supply overhead.

deployed chargers can not fully charge the EVs after they pass by, which made only around 87.5% of the vehicles remaining operable by the end of the day. Similarly, *NoFreqVar* selects some landmarks with high variance of vehicle visit frequency to deploy chargers. At the landmarks where the vehicle visit frequency is very low during some time, the deployed chargers can not serve the charging demand of many EVs, which resulted in that there are only around 85% of the vehicles remaining operable by the end of the day. Since the lack of considering vehicle visit frequency causes more EVs to fail to charge than the lack of considering vehicle passing speed, the ratio of operable vehicles in *NoSpdVar* is a bit higher than that in *NoFreqVar*.

From Figure 4.19, we can see that *CatCharger+* increases the average energy supply overhead of all the chargers by 10% when compared to *NoFreqVar* and 7% when compared to *NoSpdVar*, respectively. This is due to the same reasons as explained in Figure 4.18. The consideration of the variances of vehicle passing speed and vehicle visit frequency enables the deployed chargers to serve more EVs. Therefore, the charging energy supply overhead per charger is increased in *CatCharger+*. These measurement results verify that the consideration of the variances of vehicle passing speed and vehicle visit frequency is effective in selecting landmarks that are more suitable for deploying in-motion wireless chargers.

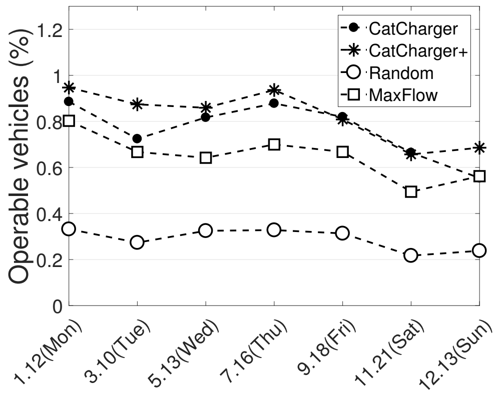

Figure 4.20: Ratio of operable vehicles by the end of different days.

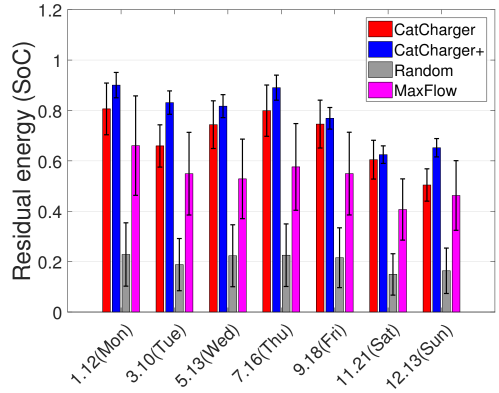

Figure 4.21: Residual energy of vehicles by the end of different days.

4.4.3.6 Performance Evaluation on Multiple Days

To validate the effectiveness of our charger deployment method under different scenarios, we measured the ratio of operable vehicles and residual energy of the vehicles by the end of different days. Figure 4.20 shows the ratios of operable vehicles by the end of different days. Figure 4.21 shows the median, 5^{th} and 95^{th} percentiles of the residual energy (i.e., SoC) of all the vehicles by the end of different days. In these experiments, we assume that all the vehicles are fully charged at the beginning of a day. This assumption is reasonable because many previous studies have confirmed that most EVs are fully charged overnight at their home or dispatch center [10, 49]. In addition, we also measured the impact of considering drivers' routing choice behavior on keeping the vehicles operable. The measurement results are illustrated in Figure 4.22.

From Figure 4.20, we can see that the ratios of operable vehicles generally follow: *CatCharger+*$\geqslant$*CatCharger*>*MaxFlow* >*Random* in different days. From Figure 4.21, we can see that the median residual energy of the vehicles follow: *CatCharger+*>*CatCharger* >*MaxFlow*>*Random* on different days. These results confirm that the charger deployment determined by our method can better support the continuous operability of EVs under various scenarios. We can also observe that the ratio of operable vehicles

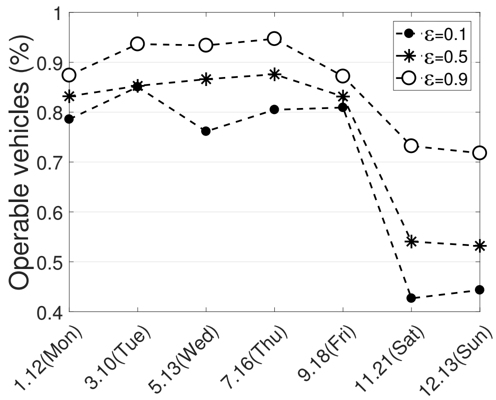

Figure 4.22: Impact of considering drivers' routing choice behavior.

and the vehicles' SoC significantly drop on weekends, especially for *CatCharger+* and *CatCharger*. This is because that the traffic pattern on weekends is quite different from that on normal weekdays. One possible reason to the significant change of traffic pattern is that during weekends, the appearance pattern of passengers significantly changes. Some EV drivers (e.g., electric taxicab drivers) need to change their regular route to cover the changed passenger appearance pattern. If the charger deployment plan fully considers the drivers' routing behavior and place more charging lanes on the routes which the drivers are willing to drive through during both weekdays and weekends, the determined charger deployment plan may provide more charging opportunities to the EVs.

To confirm the impact of considering drivers' routing choice behavior on determining the charging lanes, we vary the sensitivity of our optimization problem towards the availability of chargers. Specifically, since the parameter ε in Equation (3.8) describes how sensitive EV drivers are to driving a route equipped with charging facilities while making routing choices [91], we vary the value of ε between 0.0 and 1.0 and measured the ratios of operable vehicles in different days. From Figure 4.22, we can see that a larger value of ε generally increases the ratio of operable vehicles in all days. This is because that according to Equation (3.8), a larger value of ε will cause the route that has a shorter travel time cost to have higher weight of deploying chargers. We can also notice that increasing the value of ε brings only about 12.5% improvement on the ratio of operable vehicles during weekdays (i.e., Jan 12, Mar 10, May 13, Jul 16 and Sep 18), but brings about 75% improvement on the ratio of operable vehicles during weekends (i.e., Nov 21 and Dec 13). This means that despite the significant change of traffic pattern on weekends, the drivers still prefer to drive the routes with a relatively lower travel time cost. Increasing the value of ε enables the routes that are not frequently driven during weekdays to be covered with charging lanes, thereby significantly increases the charging opportunities of EVs during weekends. Note that Figure 4.20, Figure 4.21 and Figure 4.22 aim to compare how well the charger deployment can support the original driving routes of the vehicles without forcing them to spend extra effort in seeking for chargers. In reality, the vehicles that become out of SoC will change their original driving routes and seek for nearby chargers for battery replenishment.

4.5 Summary

The rapid development of vehicular WPT techniques brings up a new challenge of deploying wireless charging lanes in a metropolitan road network that support the continuous movement of vehicles with minimum deployment cost. Previous methods for deploying plug-in station are not qualified due to different charging approaches. Previous methods for deploying wireless charging lanes cannot handle the challenge in metropolitan scale. Our proposed *CatCharger* is the first work that tackles this challenge. Our analytical results on a dataset consisting of the mobility records of all public transit vehicles in the city of Shenzhen, China lay the foundation of the design of *CatCharger*. Using an entropy minimization based method, we conduct categorization and clustering on the intersections (landmarks), and extract the candidate positions for placing charging lanes that have low vehicle passing speed (hence short charging lanes) and high vehicle visit frequency (hence high covered traffic), and low variances of these two metrics. Then by using KDE to model vehicle mobility and to estimate the residual energy of EVs at a landmark, we formulate a multi-objective optimization problem to minimize the total deployment cost, maximize the vehicle traffic flow at the landmarks with chargers, and meanwhile ensuring the continuous operability of the vehicles on roads. We conducted trace-driven experiments to verify the superior performance *CatCharger* over other methods. In the future, we plan to consider more human activities that affect the movement of public transit vehicles (e.g., pickup requests).

Chapter 5

Dispatching and Charging Approach for Electric Taxicabs

Unlike buses which have determined driving routes, the profiting of taxicabs is highly dependent on efficient discovery of passengers. Also, the recharge of electric taxicabs must be properly considered in parallel with dispatching to minimize the taxicab's number of missed potential passengers during charging. Therefore, in addition to the proper deployment of chargers, it is necessary to develop an electric taxicab dispatching and charging methodology that can minimize the taxicab's number of missed potential passengers due to charging. The approach provides guidance for the taxicab on where to pick up a passenger or receive a recharge based on future passenger demand. Therefore, how to infer a future passenger demand with a sufficiently high accuracy, and utilize the inference result to optimize the charging of taxicabs becomes important. In this chapter, we propose *CD-Guide*, an electric taxicab *C*harging and *D*ispatching approach, which utilizes customized selection and training of suitable historical passenger demands, and reinforcement learning and multi-objective optimization to *Guide* an electric taxicab. By saying suitable historical data, we mean the data that are under the influence of random factors (e.g., weather, holiday) similar as current time.

The remainder of this chapter is organized as follows. Section 5.1 identifies the background and challenges in the design of *CD-Guide*. Section 5.2 presents our metropolitan dataset measurement results. We describe the main design of *CD-Guide* in Section 5.3 and present our experiment evaluation in Section 5.4. Section 5.5 concludes this chapter with remarks on our future work.

5.1 Background

Multiple urban passenger demand inference methods [29, 99, 126, 128] have been proposed. Fan *et al.* [29] proposed to decompose passenger demand into several patterns representing the influence of different random factors, and use the patterns to infer the number of population at specific times in each region. Shimosaka *et al.* [99] proposed to utilize a bilinear Poisson regression model, which considers random factors including day of week, holidays, etc., to predict passenger demand in a metropolitan scale. Zhang *et al.* [126] developed a customized online training model with both historical and real-time GPS position data of taxicabs to infer taxicab passenger demand. Zhang *et al.* [128] proposed a residual Convolutional Neural Network (CNN) based model to learn the influence of several random factors (e.g., weather, period and trend of passenger demand), and achieved a higher inference accuracy than previous methods. However, these methods have insufficient accuracy because they fail to catch the influence of all random factors.

Following the effort of passenger demand inference works, multiple taxicab dispatching works [111, 122, 123, 125, 134] have been proposed. Yuan *et al.* [122] introduced a method that schedules the pick-up locations with the shortest routes for taxi drivers and the waiting locations for passengers to reduce the cruising time. Zheng *et al.* [134] modeled the driving patterns (e.g., driving path, parking position and time) of vacant taxicabs with a non-homogeneous Poisson process to find the optimal waiting positions for passengers. Zhang *et al.* [123] proposed a method to estimate the revenue of each route, and guide the taxicab to the route with the maximum estimated revenue. Zhang *et al.* [125] proposed *pCruise*, in which each taxicab collects the passenger requests from nearby taxicabs and accordingly cruises on the routes with the maximum probability of finding a passenger. Xie *et al.* [111] further proposed *PrivateHunt*, which utilizes a Markov Decision Process to model the appearance of passengers and dispatches taxicabs to the positions with the maximum likelihood of potential passenger appearance. However, these methods push the taxicabs to cruise among the locations where passengers are likely to appear, but are not directly applicable for electric taxicabs because they cannot output the optimal decision on where to go and whether to get charged, which minimizes the number of missed passengers for the taxicabs.

To ensure efficient service of electric taxicabs, an electric taxicab dispatching and charging approach that can minimize the taxicab's number of missed potential passengers due to charging is expected. The approach provides guidance for a taxicab on where to pick up a passenger or receive a recharge based on future passenger demand. Therefore, how to infer future passenger demand with a high accuracy, and utilize the inference result to optimize the charging of taxicabs become important. However, how to generate a highly accurate inference result is challenging because it is difficult to consider the influence of all the random factors. What's more, how to utilize the inference result to design a charging optimization strategy for an electric taxicab, which minimizes the taxicab's number of missed potential passengers during charging, maximizes the taxicab's probability of picking up a passenger, and meanwhile prevents the taxicab from SoC exhaustion, is also non-trivial.

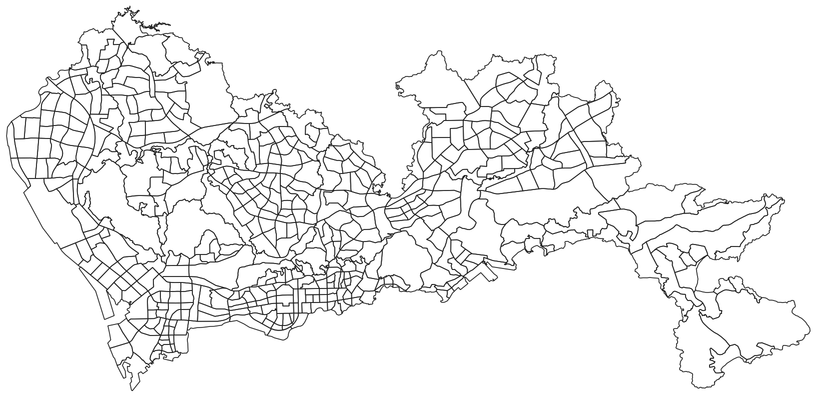

Figure 5.1: Gridded road map.

5.2 Dataset Analysis

5.2.1 Definitions

We represent the road network of Shenzhen with a directed graph, in which vertices represent landmarks (i.e., intersections or turning points), and edges represent road segments [124, 135]. For a road segment longer than 200 meters, which is the general length of a metropolitan road segment [135], we broke it into several road segments no longer than 200 meters, and set the breaking positions as new landmarks. Based on the road network, we introduce the following definition:

Definition 6 Region. *The road network is partitioned into a set of* $N^G = 496$ *regions* $G = \{g_0, g_1, \ldots, g_{N^G-1}\}$ *according to administrative region planning of Shenzhen city government, which is shown in Figure 5.1.*

We partition the timeline of a day into 48 30-minute-long time slots. Then, combining the taxicabs' movement records with the changes of their occupancy status, we extracted pick-up position and time (i.e., where and when occupancy status changes from "0" to "1") of each passenger and mapped it to the road network, and calculated the number of passenger pick-ups (i.e., passenger demand) in each region per time slot.

5.2.1.1 Suitability of Historical Data for Passenger Demand Inference

Although people's life routines repeat in daily manner, taxicab passenger demand in a time slot (e.g., 08:00-08:30) may vary in different days due to random factors (e.g., weather, ceremony). Considering this problem, previous passenger demand inference methods [29, 99, 126, 128] additionally take into account specific random factors as inputs in the passenger demand inference. However, the methods may not be able to observe all random factors, so generate insufficient inference accuracy. We notice that the influence of random factors has been reflected in historical passenger demands. Therefore, we can utilize historical passenger demands to catch the influence of all the random factors as training data. Suppose the time slot duration is 30 minutes, at 13:00, we predict demand at 13:30. To generate training data for the prediction, we select suitable historical passenger demand data at 13:30 in different days that is under the influence of random factors similar as the current time. A challenge here is how to find the historical data that is under the influence of random factors similar as current time, which is used to infer the passenger demand of the next time. For example, if we use a historical passenger demand of a normal working day to help infer the passenger demand in the next time slot in a holiday, the inference accuracy may not be high. Then one question is: given the actual passenger demand in current time slot of a region, how to extract the most suitable historical data for inferring the passenger demand of the region in the next time slot? Some previous studies [117, 123, 139] have shown that the spatial distribution of passenger appearance in a region is closely related to the distribution of buildings, since each passenger comes from a building with a high probability. Considering that the distribution of passengers can be represented with the histogram of the buildings where the passengers come from (called the passengers' *building tag*), we believe that the histogram of passengers' building tags can be an effective metric for extracting suitable historical data. Then,

Figure 5.2: A region with 18 buildings.

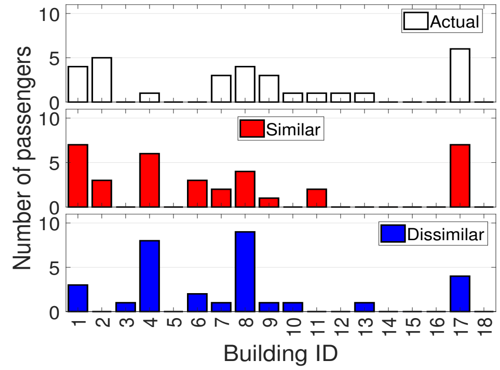

Figure 5.3: Comparison of histograms of passengers' building tags.

we can utilize the suitable historical data to train a passenger demand inference model to infer future passenger demand. By suitable historical data, we mean the data at the same current time (e.g., 13:00-13:30) in previous days that is under the influence of random factors (e.g., weather, holiday) as in current time (e.g., 13:00-13:30) today.

To prove the conjecture that the histogram of passengers' building tags is effective for extracting suitable historical data, we randomly selected a region with 18 major buildings, which is as shown in Figure 5.2, and conducted an experiment on inferring the region's passenger demand in different time slots of Mar 5, 2015. The general procedure is: (1) at current time slot of today (e.g., 13:00-13:30 on Mar 5, 2015), we select historical passenger demand data at the same time slot from previous 365 days before Mar 5, 2015 that is under the influence of random factors similar as the current time; (2) we utilize the selected historical passenger demand value in the next time slot (i.e., 13:30-14:00) as the predicted demand in the next time slot of today; (3) we repeat this prediction of passenger demand for each time slot throughout today (i.e., Mar 5, 2015).

For each passenger, we use the building nearest to (in Euclidean distance) his/her pick-up position as his/her building tag. Then we decompose the passenger demand in each time slot into a histogram of building tags, where each column represents a building tag and the column's height represents the number of passengers of the building tag. The "Actual" in Figure 5.3 illustrates an example histogram of region g_i's actual passenger building tags in the time slot 13:00-13:30. We use a vector $\mathbf{h}_i^c$ to represent this histogram, and a vector $\mathbf{h}_i^j$ to represent a histogram of g_i's passenger building tags on j^{th} day. For simplicity, we use $\mathbf{h}^c$ and $\mathbf{h}^j$ below for explanation, and we do not show the subscript i unless needed in the following sections. Both $\mathbf{h}^c$ and $\mathbf{h}^j$ are called a *building tag histogram vector*. We use the chi-square distance [22] between $\mathbf{h}^j$ and $\mathbf{h}^c$ as their similarity. Specifically, given the building IDs in g_i are $k = 1, 2, \ldots, N^B$, where N^B is the total number of buildings in g_i. Thus, $\mathbf{h}^j$ and $\mathbf{h}^c$ are two $N^B \times 1$ vectors. The chi-square distance between $\mathbf{h}^j$ and $\mathbf{h}^c$ is defined as

$$\chi_j^2 = \frac{1}{2} \sum_{b=1}^{N^B} \frac{(\mathbf{h}^j[k] - \mathbf{h}^c[k])^2}{\mathbf{h}^j[k] + \mathbf{h}^c[k]}. \tag{5.1}$$

where $\mathbf{h}^j[k]$ represents the k^{th} element in vector $\mathbf{h}^j$. The smaller χ_j^2 a previous demand has, the more similar it is to current status. For example, suppose $\mathbf{h}^c$ is composed of 404 passengers from *building1*, 262 passengers from *building2*, and 89 passengers from *building3*. Then $\mathbf{h}^c$ has the following representation: $\{$*building1* (404), *building2* (262), *building3* (89)$\}$. Suppose $\mathbf{h}^1$ has the following representation: $\{$*building1* (201), *building2* (500), *building3* (90)$\}$. The similarity between $\mathbf{h}^c$ and $\mathbf{h}^1$ is $\chi_1^2 = \frac{1}{2} \times (\frac{(404-201)^2}{404+201} + \frac{(262-500)^2}{262+500} + \frac{(89-90)^2}{89+90}) = 71.23$. Suppose $\mathbf{h}^2$ has the following representation: $\{$*building1* (401), *building2* (300), *building3* (100)$\}$. The similarity between $\mathbf{h}^c$ and $\mathbf{h}^2$ is $\chi_2^2 = \frac{1}{2} \times (\frac{(404-401)^2}{404+401} + \frac{(262-300)^2}{262+300} + \frac{(89-100)^2}{89+100}) = 1.61$. Since $\chi_2^2 < \chi_1^2$, $\mathbf{h}^2$ is more similar to $\mathbf{h}^c$.

Above, we have defined the similarity of histogram of passengers' building tags and how to utilize it for the selection of suitable historical data for training. We conducted an experiment to show the effectiveness of the method on extracting suitable historical demands. In the experiment, we use the historical data that has the most similar histogram (denoted as "Histogram") as the suitable historical data to predict demand value. For example, the "Histogram" in Figure 5.3 illustrates the histogram

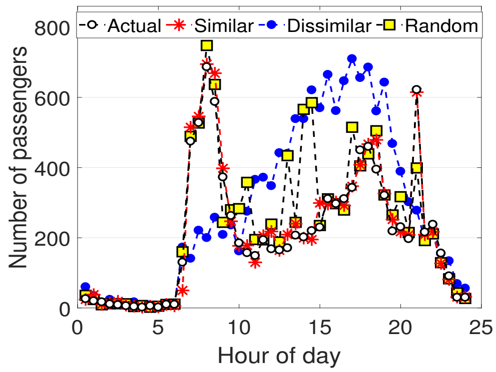

Figure 5.4: Comparison of suitability for passenger demand inference.

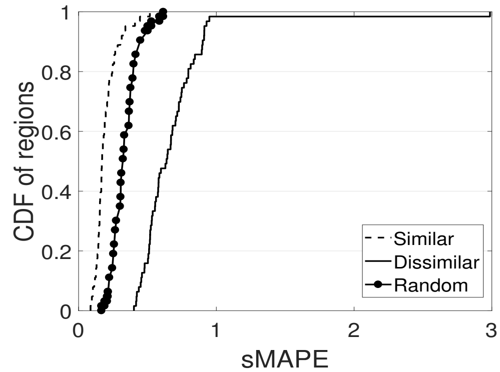

Figure 5.5: Distribution of sMAPEs.

of passenger building tags of a historical demand in the time slot 13:00-13:30 that has the most similar histogram to "Actual". Specifically, in the experiment, when inferring each time slot's passenger demand on Mar 5, 2015, we calculate and rank the χ_j^2 of all the previous demand data to select the most suitable historical data that has the minimum χ_j^2. Then, based on the passenger demand of current time slot denoted as the n^{th} time slot (e.g., 13:00-13:30), we use the demand value of "Histogram" in the next time slot denoted as the $(n+1)^{th}$ time slot (e.g., 13:30-14:00) as the predicted demand value in the $(n+1)^{th}$ time slot. Using this way, we predict the passenger demand of each time slot throughout the day. In addition, we also use a randomly selected historical passenger demand in the $(n+1)^{th}$ time slot as the predicted demand value (denoted by "Random"), which serves as the baseline. Figure 5.4 shows the demand values of "Actual" and prediction results of "Histogram". We can see that compared with the predicted demand values of "Random", the result of "Histogram" matches the values of "Actual" much more closely. This observation confirms that the histogram similarity of passengers' building tags is effective for extracting suitable historical data.

Some people may argue that we can simply compare the total number of passengers rather than the histogram of passengers' building tags to select the suitable historical demand. We also used the experiment to show that using the total number of passengers for comparison cannot guarantee that we can extract the most suitable historical data. Specifically, in the experiment, when inferring each time slot's passenger demand on Mar 5, 2015, we select the historical data, whose total number of passengers in current time slot (e.g., 13:00-13:30) is the most approximate to today's demand value in the same time slot, and utilize the data's demand value in the next time slot (e.g., 13:30-14:00) as the predicted demand value in the next time slot throughout the day (denoted as "Total"). The "Total" in Figure 5.3 illustrates the histogram of passenger building tags of a historical demand in the time slot 13:00-13:30 that has the most similar total number of passengers to "Actual". Figure 5.4 shows the passenger demand in different time slots of "Actual", and the predicted demands of "Total". We can see that the results of "Total" do not match the values of "Actual" during most time slots. During some time slots, the results of "Total" are even worse than those of "Random". This confirms that the total number of passengers does not qualify in extracting suitable historical data.

We further calculated the symmetric Mean Absolute Percentage Error of the inference results (i.e., sMAPE $= \frac{1}{N_s}\sum \frac{|\text{inferred demand}-\text{actual demand}|}{\text{inferred demand}+\text{actual demand}+1}$ [105, 132], where N_s is the number of time slots in a day, and 1 is to avoid division by zero as in [105, 132]) over all time slots for each region. The results are illustrated in Figure 5.5. We can see that the sMAPEs of the three methods generally follow: "Histogram"$<$"Random"$<$"Total". This result confirms that the histogram of passengers' building tags is an effective metric for differentiating the suitability of historical data. The experiment also confirms that the total number of passengers is not a reliable metric for selecting the most suitable historical data for training the inference model. In Section 5.3.3, we will elaborate how *CD-Guide* utilizes this metric to extract suitable historical training data and infer the passenger demand in the next time slot.

5.2.1.2 Variance of Taxicab Passenger Demand

Several previous works [101, 132] have confirmed that taxicab passenger demand in a region has a certain degree of regularity (e.g., weekly patterns), but also a certain degree of variance (i.e., fluctuation of demand values due to the influence of random factors), which constrains the maximum predictability of passenger demand in the region (i.e., the maximum accuracy that an inference algorithm can possibly achieve). However, these methods do not explain how to consider this maximum predictability of passenger demand inference and for taxicab charging optimization. Entropy of a time series is effective in measuring the degree of variance (i.e., fluctuation of demand values due to the influence of random factors) of the time series. Generally, the more various a taxicab passenger demand time series is, the larger entropy it will result in, and the less predictable it is. A region g_i's all historical taxicab passenger demands (i.e., passenger demand in each time slot from day 1 to today) can be represented as a time series: $\mathbf{D}_{\text{all}} = \{D_1, \ldots, D_a, \ldots, D_{N_A}\}$, where each element D_a is an observed historical passenger demand in a time slot, and N_A is the total number of collected demand values of g_i since the beginning of observation. For example, suppose we have been observing the passenger demand in g_i for 30 days, each day is partitioned into 48 time slots, thus $\mathbf{D}_{\text{all}}$ has $N_A = 30 \times 48 = 1440$ passenger demand records. Suppose the time series $\mathbf{D}_{\text{all}} = \{1, 2, 2\}$, then its subsequences are: {1}, {2}, {2} {1,2}, {2,2}. Its unique subsequences (s_a) are: {1}, {2} {1,2}, {2,2}. Following the definition of human mobility randomness in [101] and [132], the entropy of $\mathbf{D}_{\text{all}}$ is defined as:

$$E = -\sum_{s_a \subset \mathbf{D}_{\text{all}}} \Pr(s_a) \log_2(\Pr(s_a)), \tag{5.2}$$

where $\Pr(s_a)$ is the probability that a unique subsequence (e.g., $\{1\}$ is a unique subsequence of $\{1, 2, 2\}$) s_a appears in $\mathbf{D}_{\text{all}}$. For example, the probabilities that each unique subsequence of $\mathbf{D}_{\text{all}} = \{1, 2, 2\}$ appears in $\mathbf{D}_{\text{all}}$ are: $\Pr(\{1\}) = \frac{1}{5}$, $\Pr(\{2\}) = \frac{2}{5}$,

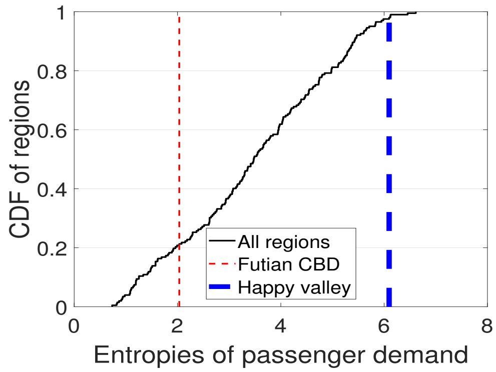

Figure 5.6: Distribution of passenger demand entropies.

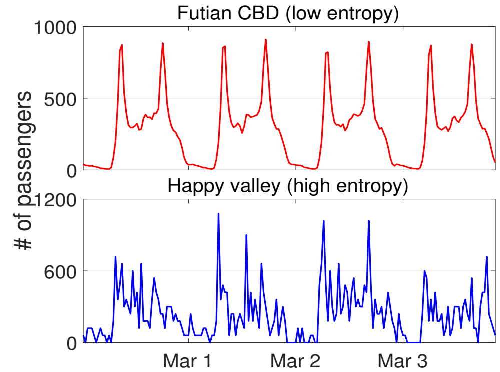

Figure 5.7: The number of passengers in two regions.

$\Pr(\{1,2\}) = \frac{1}{5}$ and $\Pr(\{2,2\}) = \frac{1}{5}$. The entropy of $\mathbf{D}_{\text{all}}$ is calculated as $\frac{1}{5}\log_2 5 + \frac{2}{5}\log_2 \frac{5}{2} + \frac{1}{5}\log_2 5 + \frac{1}{5}\log_2 5 = 1.92$. The fewer unique subsequences $\mathbf{D}_{\text{all}}$ has (i.e., lower similarity of historical passenger demand values), the smaller E will be.

We calculated the entropy of passenger demand time series (including all observed passenger demand values from Jan 1 to Dec 31, 2015) for each region by Equation (5.2). Figure 5.6 shows the CDF of the results. For comparison, we additionally illustrate the entropies of Futian Central Business District (Futian CBD), which is a business office region, and Happy valley, which is an entertainment region in Figure 5.6. The entropies of Futian CBD and Happy valley are 2.03 and 6.10, respectively. The numbers of passengers in these two regions from Mar 1 to Mar 3, 2015 are illustrated in Figure 5.7. We can see that the passenger demand in Futian CBD ($E = 2.03$) has a higher degree of variance, while the passenger demand in Happy valley ($E = 6.10$) has a lower degree of variance. This means for Shenzhen city, if a region has a passenger demand entropy lower than 2.03, it means the region's variance of passenger demand is lower than Futian CBD. If a region has a passenger demand entropy higher than 6.10, it means the region's variance of passenger demand is higher than Happy Valley. Back to Figure 5.6, we can see that 80% of the regions have a passenger demand entropy higher than 2.03 (red dashed line), which means that the passenger demand in these regions has a higher degree of variance than Futian CBD.

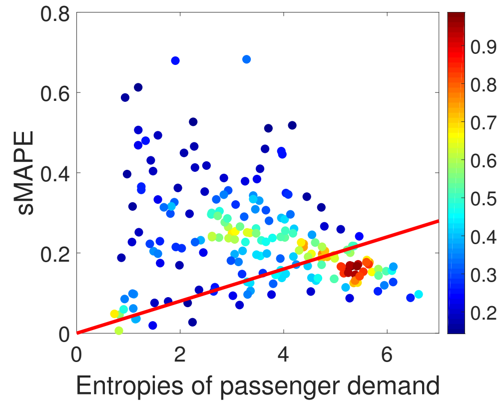

Figure 5.8: Scatter plot of passenger demand entropies vs. sMAPE.

We need to use the entropy of passenger demand to measure the different degrees of variance for the regions.

Recall that in Section 5.2.1.1, we have obtained the sMAPEs of the passenger demand inference result of "Similar" throughout all time slots of Mar 5, 2015 for all regions. To analyze the relation between the inference accuracy and the passenger demand entropy of the regions, we further drew a density scatter heat plot between the entropies of passenger demand and the sMAPEs of all regions, as shown in Figure 5.8. Each point represents a region. The warmer color a point has, the more concentrated it is with the other points, which have similar entropies of passenger demand and sMAPEs. We also drew a line across the points. We can see that most points are scattered around the line, which means that for the regions with a larger entropy, their inference error will be higher (i.e., lower inference accuracy) and vice versa. This result indicates that the maximum predicability of passenger demand in a region is dependent on the randomness of the region's historical passenger demand time series. The maximum predicability constrains the maximum accuracy of the region's passenger demand inference result. In Section 5.3.3.3 and Section 5.3.4, we will introduce how *CD-Guide* determines the maximum predictability of the inference result and considers it in taxicab dispatching and charging optimization.

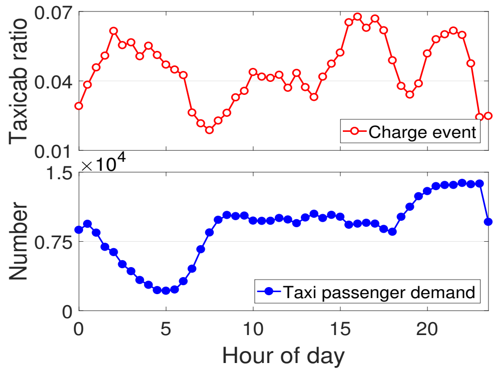

Figure 5.9: Taxicabs' charging events vs. passenger demand.

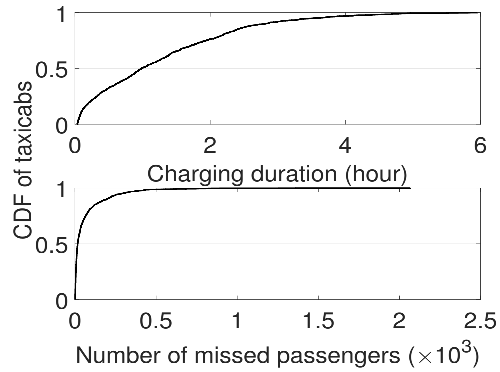

Figure 5.10: Distribution of charging event durations and number of missed passengers during charging.

5.2.1.3 Charging Time Must Be Considered in Taxicab Dispatching

In this section, we analyze the movement records of the 6,510 electric taxicabs in the Shenzhen dataset to detect the charging events of all taxicabs, and investigate whether the charging events affected the taxicabs' service. From the Shenzhen Transport Committee, we obtained the positions of all charging stations in Shenzhen. As in previous works [104, 120, 135], if a taxicab's movement record shows that it has stayed at a charging station for a long period of time (e.g., 10 minutes), we consider that it was charging at the station at that time. Therefore, we define the charging time of a taxicab at a charging station as the time duration that the taxicab stayed at the charging station.

We first measured the ratio of charging taxicabs over all the taxicabs in each time slot per day throughout the 365 days, and calculated the average ratio of charging taxicabs in each time slot over all the days. The measured results are illustrated in Figure 5.9 along with the average number of taxicab passengers in each time slot over all the days. We can see that the peak time of taxicabs' charging events usually happens at around 03:00-05:00, 09:00-13:00, 16:00-18:00 and 20:00-22:00. Obviously, most taxicabs tried to avoid the peak time of passenger demand at around 07:00-09:00 and 20:00-24:00 and arranged their charge time in late night (03:00-05:00) and afternoon (16:00-18:00), which results in the two highest peaks on the charging taxicab ratio curve. This charging strategy can help them reduce the loss of missing passengers during charging. However, due to several factors (e.g., limited battery capacity, too much driving without a passenger on board), there are still some taxicabs that have to charge at around 09:00-13:00 and 20:00-22:00, during which the taxicab passenger demand is still high. Such charging time selection may cause the taxicabs to lose potential passengers.

To confirm this conjecture, for each taxicab, we calculated its total duration of charging events in each day throughout the 365 days. During the charging event of each taxicab, we also measured the number of passengers that appeared within 500 meters around the taxicab. The reason we only count the passengers appeared within a 500-meter-range is that they can be picked up by a taxicab within roughly 2 minutes if the taxicab was not charging. The results are illustrated in Figure 5.10. We can see that about 50% of the taxicabs spent more than 0.83 hours on charging per day in average, and about 50% of the taxicabs missed more than 50 passengers per day in average. What's worse, about 10% of the taxicabs missed more than 300 passengers per day in average. These observations indicate that the dispatching of electric taxicabs must optimize the charging of electric taxicabs to help the taxicabs avoid missing potential passengers. In Section 5.3.4, we will elaborate how *CD-Guide* minimizes the taxicab's number of missed potential passengers due to charging.

5.3 System Design of CD-Guide

5.3.1 Framework of CD-Guide

CD-Guide consists of the following three stages as shown in the three dashed boxes in Figure 5.11:

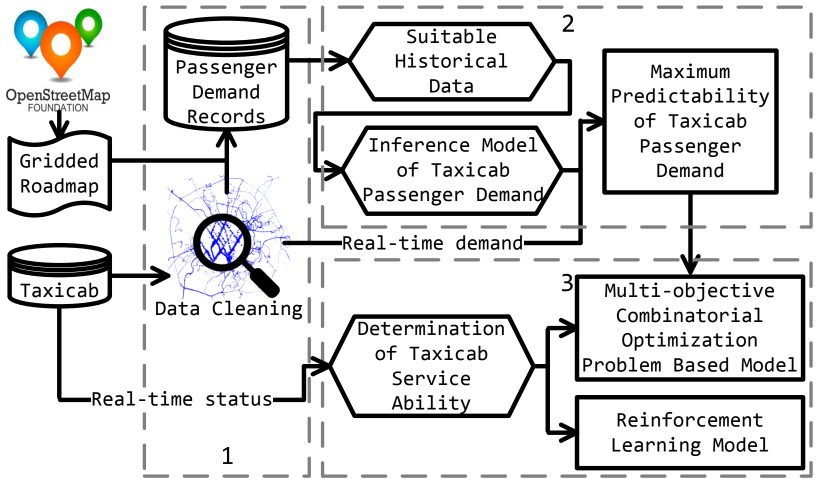

Figure 5.11: Framework of *CD-Guide*.

1. Map gridding & information derivation. First, the entire city area is partitioned into a *Gridded Roadmap* as shown in Figure 5.1. Also, the taxicab dataset is cleaned up (e.g., filtering out positions out of the actual range of Shenzhen, redundant positions). Then, based on the cleaned data, we derive the *Passenger Demand Records* of taxicabs in each region of the *Gridded Roadmap* as explained in Section 2.2.

2. Taxicab passenger demand inference (Section 5.3.3). Based on the output *Passenger Demand Records* from the first stage, we extract *Suitable Historical Data* that are under the influence of random factors similar as current time for each region. Then, we apply *Inference Model of Taxicab Passenger Demand* to infer demand value in the next time slot. Finally, we calculate the *Maximum Predictability of Taxicab Passenger Demand* for more accurate inference of passenger demand value.

3. Optimization of taxicab dispatching and charging (Section 5.3.4). For each taxicab, we first use its SoC and taxicab passenger demands in each region for the *Determination of Taxicab Service Ability* for each region. A taxicab's service ability in a region is defined as the ratio of passenger trips in a region after it arrives at the region until the end of the next time slot that its SoC can support. Then we develop two methods for taxicab dispatching and charging. In the first method, we utilize a *Multi-objective Combinatorial Optimization Problem Based Model* to decide which region the taxicab should drive to and whether to get charged in the region. In the second method, through using a taxicab's SoC and taxicab passenger demands as *state* and uses the taxicab's service ability to calculate the *reward*, we train and utilize the *Reinforcement Learning Model* to decide which region the taxicab should drive to and whether to get charged in the region.

5.3.2 Assumptions

Above all, we have the following assumptions for EVs:

1. Without losing generality and for the ease of calculating the number of missed passenger due to charging, we assume that if a taxicab requires a recharge, it will start charging as soon as it arrives at its dispatched region.
2. A taxicab will fully charge its battery in each recharge due to its limited charging opportunity.
3. For a region g_i, the passengers that appear before the arrival of the dispatched target taxicab will be picked up by other taxicabs. The passengers that appear in g_i after the taxicab's arrival time and before the end of the $(n+1)^{th}$ time slot are the pool of passengers that the taxicab can possibly pick up.

5.3.3 Taxicab Passenger Demand Inference

In the following, we firstly introduce how *CD-Guide* utilizes the distribution of passengers' building tags to select the historical passenger demands that are suitable for training the model for inferring the taxicab passenger demand in the next time slot. Then, we design an linear regression based model to infer the taxicab passenger demand in the next time slot. Finally, we elaborate how *CD-Guide* calculates the maximum predictability of passenger demand for more accurate inference of passenger demand value.

5.3.3.1 Extracting Suitable Historical Data

The analysis result in Section 5.2.1.1 has demonstrated that the historical passenger demand with a total number of passengers approximate to current passenger demand is not guaranteed to be suitable for training the inference model. Instead, we need to extract the historical passenger demands, of which histogram (distribution) of building tags is similar to current passenger demand, to train the inference model.

Specifically, given the building tag histogram vector of region g_i in current time slot (i.e., n^{th} time slot) of today ($\mathbf{h}^c(n)$), we first use Equation (5.1) to calculate its similarity (i.e., chi-square distance) to the historical building tag histogram vector of region g_i in the same time slot ($\mathbf{h}^j(n)$) of each day in the previous N^D days (e.g., 365 days). Then, we rank the historical passenger demands in previous N^D days by increasing order of their chi-square distance to $\mathbf{h}^c(n)$, and select the top ranked β (e.g., 10%) days' passenger demands as training data. Finally, we obtain a sequence of N^d suitable previous passenger demands during n^{th} time slot from the total N^D historical passenger demands: $\{D^j(n)|j = 1, 2, \ldots, N^d\}$, where $D^j(n)$ represents the taxicab passenger demand in region g_i during n^{th} time slot on j^{th} day, and N^d is the number of days of the extracted suitable passenger demands. A larger N^D and β will increase the training computation overhead but may include the influence of more random factors that are similar as current time in the extracted suitable historical training data. To find the best values for them, we vary each variable within a certain range (e.g., [30, 60] for N^D and [5%, 15%] for β). We try different combinations of the N^D and β values, and choose the combination that achieves the minimum chi-square distance to $\mathbf{h}^c(n)$ as the final values of N^D and β. In implementation, we determine these parameters offline.

5.3.3.2 Inference Model of Taxicab Passenger Demand

We want the inference model to utilize the extracted suitable historical data (i.e., $\{D^j(n)|j = 1, 2, \ldots, N^d\}$) to infer passenger demand in the next time slot of today (i.e., $D^c(n+1)$). The analysis results in Section 5.2.1.1 have demonstrated that for the historical passenger demand with a building tag histogram similar to that of current passenger demand, their trend of passenger demand in the next time slot will also be similar. Thus, if the training output in current time slot is close to current passenger demand (i.e., $D^c(n)$), we can use this model to estimate the demand value in the next time slot (i.e., $D^c(n+1)$) with a high accuracy. Therefore, we propose a taxicab passenger demand inference model based on the linear regression of the extracted suitable historical passenger demands.

The general procedures of training the inference model consists of: (1) we first input $\{D^j(n)|j = 1, 2, \ldots, N^d\}$ as the training data to the inference model, and learn the parameters of the inference model to minimize the error between the training output and current passenger demand $D^c(n)$. Once the best parameters are determined, the training of the inference model is complete. (2) Then we input the suitable historical data in $(n+1)^{th}$ time slot (i.e., $\{D^j(n+1)|j = 1, 2, \ldots, N^d\}$) to the inference model to infer the passenger demand in $(n+1)^{th}$ time slot of today (i.e., $D^c(n+1)$).

Considering that $D^j(n)$ is actually the sum of passenger demand contributed by each building $k \in g_i$, we use its corresponding building tag histogram vector $\mathbf{h}^j(n)$ to represent $D^j(n)$. Let $H(n)$ be a $N^B \times N^d$ matrix with each column representing the building tag histogram vector of an extracted suitable historical passenger demand in n^{th} time slot. That is, $H(n) = [\mathbf{h}^1(n), \mathbf{h}^2(n), \ldots, \mathbf{h}^{N^d}(n)]$. Note that N^B is the total number of buildings in g_i. Let $\mathbf{w}$ be a $N^d \times 1$ weight vector of the N^d days' extracted suitable passenger demands. As a result, a $N^B \times 1$ vector $H(n)\mathbf{w}$ is the model's training output for $\mathbf{h}^c(n)$, which is the building tag histogram vector on today in n^{th} time slot (i.e., ground truth). Thus, the key objective for training the inference model is to find an optimal $\mathbf{w}$ that minimizes the error between $\mathbf{h}^c(n)$ and $H(n)\mathbf{w}$ as follows:

$$\mathbf{w}^* = \underset{\mathbf{w}}{\operatorname{argmin}}(\mathbf{h}^c(n) - H(n)\mathbf{w})'(\mathbf{h}^c(n) - H(n)\mathbf{w}), \tag{5.3}$$

where $()'$ means matrix transpose, and $\mathbf{w}^*$ is the optimal solution, which can be obtained by least-square fitting [17]. Finally, the building tag histogram vector of g_i during the next time slot $t+1$ is

$$\mathbf{h}^c(n+1) = H(n+1)\mathbf{w}^*. \tag{5.4}$$

The inferred total taxicab passenger demand in g_i during the next time slot of today (i.e., $D^c(n+1)$) is obtained by summing the elements in $\mathbf{h}^c(n+1)$. That is, $D^c(n+1) = \sum_{NB} \mathbf{h}^c(n+1)$.

5.3.3.3 Maximum Predictability of Taxicab Passenger Demand

The data analysis result in Section 5.2.1.2 have illustrated that the maximum predictability of a region's future passenger demand value is dependent on the randomness (entropy) of the region's historical passenger demand time series, and measures how reliable the passenger demand inference result is. For example, if a region has the maximum predictability of 0.7 (denoted by $P^{\max} = 0.7$), it means that the maximum probability we can correctly infer the passenger demand in the next time slot is 0.7, for the other 30% of the cases, we cannot correctly infer the future demand value due to random factors. That is, the inference result has the probability of 70% to be reliable at maximum. Then, one question is: how to determine the maximum predictability of the passenger demand for each region and consider it in the optimization of electric taxicab dispatching and charging? In this section, we elaborate how

CD-Guide determines the maximum predictability of the region's passenger demand value.

We first compute the entropy of historical passenger demand time series E by Equation (5.2) for each region offline to save real-time computation overhead. Suppose the number of unique taxicab passenger demand values in $\mathbf{D}_{\text{all}}$ is N^u. For example, for $\mathbf{D}_{\text{all}} = \{1, 2, 2\}$, $\mathbf{D}_{\text{all}}$ only has $N^u = 2$ unique demand values: 1 and 2. That is, N^u is the number of possible values that a future taxicab passenger demand (e.g., $D^c(n+1)$) can have. Among the N^u demand values, only one value is correct. Suppose the probability that we can accurately infer the demand value of $D^c(n+1)$ is $P^{\max}$ (i.e., the maximum predictability of a future passenger demand value in g_i). Thus, the probability that we will inaccurately infer the demand value is $1 - P^{\max}$ [101, 132]. According to [101, 132], we assume the probability of inferring the remaining inaccurate $N^u - 1$ possible demand values follows a uniform distribution. That is, the probability of inaccurately inferring any one of the other $N^u - 1$ possible values is $\frac{1-P^{\max}}{N^u-1}$, then E can be also calculated as the entropy resulted from accurate case and inaccurate case:

$$
\begin{aligned}
E &= -P^{\max}\log_2(P^{\max}) - \sum_{N^u-1}\frac{1-P^{\max}}{N^u-1}\log_2(\frac{1-P^{\max}}{N^u-1}) \\
&= -P^{\max}\log_2(P^{\max}) - (1-P^{\max})\log_2(1-P^{\max}) + (1-P^{\max})\log_2(N^u-1)
\end{aligned}
\tag{5.5}
$$

Since E is known, and N^u can be determined from $\mathbf{D}_{\text{all}}$, thus $P^{\max}$ can be obtained by solving Equation (5.5). Finally, the maximum predictability of the passenger demand value $D^c(n+1)$ is determined as $1 - P^{\max}$. Since we expect to dispatch the taxicab to the region with a relatively higher predictability of passenger demand (i.e., higher inference accuracy, $1 - P_i^{\max}$ should be as low as possible), we adjust the passenger demand value $D^c(n+1)$ to be $\widetilde{D}^c(n+1) = \frac{D^c(n+1)}{1-P_i^{\max}}$ in later optimization of taxicab dispatching and charging.

5.3.4 Optimization of Taxicab Dispatching and Charging

Based on the passenger demand inference result output from Section 5.3.3, we next elaborate how *CD-Guide* determines the service ability of a taxicab in a region g_i based on its current SoC, and how *CD-Guide* decides which region the taxicab should drive to and whether to get charged in the region. In the following sections, we use subscript i to mark all the parameters related to g_i.

5.3.4.1 Determination of Taxicab Service Ability

When dispatching a taxicab to pick up its next passenger, we expect that the taxicab has enough SoC to support the trip of its next passenger. This is because that the trip length of the passenger determines the energy consumption of the taxicab. Intuitively, the trip lengths of civilians in a city are relatively stable during the same time slot among different days due to life routines. For example, Jack usually goes from home to working place at 08:00, and leaves from working place to home at 18:00. Therefore, from the suitable historical data of a region g_i extracted from Section 5.3.3.1 (i.e., $\{D_i^j(n)|j = 1, 2, \ldots, N_i^d\}$), we collect the distribution of possible passenger trip lengths at specific time (e.g., 13:10) in the next time slot in previous days, and use it as an estimation of the distribution of passenger trip lengths in the next time slot of today. We collect this distribution for each region g_i, and calculate the taxicab's service ability in g_i (i.e., ratio of future passenger trips that a taxicab's current SoC can support). Specifically, suppose current SoC of a taxicab is SoC, and the lower bound of a taxicab's SoC is $SoC_{\min}$ (e.g., 20%), which is set to ensure that the taxicab will have enough remaining SoC to go to the nearest charging position upon the exhaustion of its battery. The taxicab's service ability during specific time duration within a time slot (e.g., [13:10, 13:20] within time slot 13:00-13:30) in g_i is calculated as:

$$\Phi_i(SoC|[t_s, t_e]) = \Pr\{SoC - c_e(l_i^d + l_i^p) > SoC_{\min}|t_s \leqslant t_i^p \leqslant t_e\}, \tag{5.6}$$

where c_e is the energy consumption rate (i.e., the amount of SoC consumed by unit length of driving) of the taxicab, l_i^d is the driving distance from the taxicab's current position to the nearest position in region g_i, and l_i^p is the trip length of a passenger in region g_i. Therefore, $SoC - c_e(l_i^d + l_i^p)$ is the remaining SoC after the taxicab arrives at g_i. t_i^p is the appearance time of a passenger in g_i, t_s is the start time of the time duration, t_e is the end time of the time duration. Equation (5.6) can be equivalently transformed into the following form:

$$\Phi_i(SoC|[t_s, t_e]) = \Pr(l_i^p < \frac{SoC - SoC_{\min} - c_e l_i^d}{c_e}|t_s \leqslant t_i^p \leqslant t_e), \tag{5.7}$$

which means that based on the current SoC of the taxicab SoC, the taxicab can support passenger trip lengths shorter than $\frac{SoC - SoC_{\min} - c_e l_i^d}{c_e}$ during specific time duration $[t_s, t_e]$. Recall that we assume the maximum pool of passengers that the taxicab can possibly pick up in region g_i consists of passengers that will appear in the region within n^{th} and $(n+1)^{th}$ time slots. That is, the actual pool of passengers that the taxicab can support with its current SoC during a specific time duration $[t_s, t_e]$ (e.g., the taxicab's charging time duration) is $\Phi_i(SoC|[t_s, t_e])(\widetilde{D}_i^c(n) + \widetilde{D}_i^c(n+1))$. From the estimated distribution of future passenger trip lengths, we can calculate Φ_i for each region g_i during specific time duration for a taxicab. Then we extract the regions that have $\Phi_i > 0$ and define them as the set of candidate regions for dispatching the given taxicab:

$$\widetilde{G} = \{g_i \in G|\Phi_i > 0\}, \tag{5.8}$$

which means that the taxicab can afford the trip length of at least one passenger in these regions. Recall that the taxicab's total number of potential passengers in each candidate region of $\widetilde{G}$ is weighted by the taxicab's service ability (i.e., $\Phi_i(SoC|[t_s, t_e])(\widetilde{D}_i^c(n) + \widetilde{D}_i^c(n+1)))$.

5.3.4.2 Optimization Models

From the analysis result of Section 5.2.1.3, we know that if a taxicab simply waits until complete exhaustion of battery to get fully charged, it will miss a lot of potential passengers during its long charging time. It would be better if a taxicab gets charged at the time slots with few passengers without waiting until complete exhaustion of battery. Therefore, the **problem** is: *how to determine the action of the taxicab (i.e., which region to go and whether receive a recharge) to minimize the taxicab's number of missed potential passengers due to charging, maximize the taxicab's probability of picking up a passenger, and meanwhile prevents the taxicab from SoC exhaustion?* Below we introduce two solutions: the first method formulates and solves a Multi-objective Combinatorial Optimization Problem for the optimization of electric taxicab dispatching and charging; the second method utilizes Reinforcement Learning to determine the optimal action of an electric taxicab.

Multi-objective Combinatorial Optimization Problem based Model: We first formulate a multi-objective combinatorial optimization problem to achieve this goal. The inputs include the taxicab's candidate regions for dispatching ($\widetilde{G}$), and the inferred passenger demand that the taxicab can support with its current service ability. The outputs generated in the n^{th} time slot are: 1) which region the taxicab should drive to (denoted by x_i); 2) whether the taxicab should get charged in the region (denoted by y_i); and 3) what future time slots the taxicab will receive a recharge (denoted by z_k), which will indirectly influence y_i.

If $x_i = 1$, the taxicab is dispatched to g_i; if $x_i = 0$, the taxicab will not drive to

g_i. If $y_i = 1$, the taxicab will receive a recharge in g_i when it arrives at g_i; if $y_i = 0$, the taxicab will not receive a recharge in g_i. Since the taxicab can only drive to one region, we have the first constraint: $\sum_{g_i \in \widetilde{G}} x_i = 1$. Similarly, the taxicab can only charge in one region or not charge at all. Therefore, we have the second constraint: $\sum_{g_i \in \widetilde{G}} y_i \in \{0, 1\}$. If $z_k = 1$, the taxicab will need to charge in the k^{th} time slot, or otherwise if $z_k = 0$. Since we aim to avoid the taxicab from exhausting its SoC in each time slot, we have the third constraint: the taxicab's SoC in the j^{th} time slot must be higher than 0. Also, since the feasible range of a taxicab's SoC is within $[0, 1]$, we have the fourth constraint: the taxicab's SoC after the j^{th} time slot must be no higher than 1. Whenever a vacant taxicab (i.e., a taxicab without a passenger onboard) requires a dispatching guidance, the taxicab dispatching center executes the optimization of taxicab dispatching and charging to update the taxicab's driving route. Below, we introduce the details of the optimization problem.

Objective: minimizing the number of missed potential passengers due to charging. If the taxicab decides to receive a recharge during a certain time duration in n^{th} and $(n+1)^{th}$ time slot, the recharge will cause the taxicab to miss some passengers in the short term. In addition, charging or not in the short-term decision will also indirectly influence the exhaustion of the taxicab's SoC in the long-term future. Therefore, we need to consider the number of missed potential passengers due to both short-term (denoted by D_s^m) and long-term (denoted by D_l^m) dispatching and charging decisions.

We first explain how *CD-Guide* calculates the number of missed potential passengers due to short-term charging decision. Suppose the taxicab's charging time duration is $[t_0 + \tau_i^d, t_0 + \tau_i^d + \tau_i^c]$, where t_0 is current time, τ_i^d is the taxicab's driving time to g_i, and τ_i^c is the taxicab's full recharge time based on its current SoC in g_i. Based on Equation (5.7), its number of missed potential passengers due to charging is $\Phi_i(SoC|[t_0 + \tau_i^d, t_0 + \tau_i^d + \tau_i^c])(\widetilde{D}_i^c(n) + \widetilde{D}_i^c(n+1))$. This is because that the taxicab will miss the passengers that appear during the taxicab's charging in g_i (i.e., $[t_0+\tau_i^d, t_0+\tau_i^d+\tau_i^c]$). Then, we can calculate the taxicab's number of missed potential passengers due to charging in a candidate region of $\widetilde{G}$ during n^{th} or $(n+1)^{th}$ time slot (i.e., short-term dispatch decision) as:

$$D_s^m = \sum_{g_i \in \widetilde{G}} \Phi_i(SoC|[t_0+\tau_i^d, t_0+\tau_i^d+\tau_i^c])(\widetilde{D}_i^c(n) + \widetilde{D}_i^c(n+1))x_i y_i. \tag{5.9}$$

D_s^m consists of the number of passengers that the taxicab may miss due to charging in each of the candidate regions in $\widetilde{G}$. Since the taxicab can only choose one region ($\sum_{g_i \in \widetilde{G}} x_i = 1$) and choose whether to have a recharge in the region ($\sum_{g_i \in \widetilde{G}} y_i \in \{0,1\}$), the sum D_s^m is the taxicab's number of missed potential passengers due to charging at some time within n^{th} and $(n+1)^{th}$ time slots.

Next, we explain how *CD-Guide* calculates the number of missed potential passengers due to long-term charging decision. We use $z_k \in \{0,1\}$ to denote whether the taxicab will charge in the rest k time slots of the day (i.e., $k = n+2, \ldots, N_s-1$, where N_s is the total number of time slots in a day). It is impossible to know the taxicab's actual position in the future k time slots, we use the maximum observed passenger demand among all the regions in each time slot $D_k^{\max}, k = n+2, \ldots, N_s-1$ (which can be obtained from historical passenger demands) to estimate the taxicab's potential number of missed passengers in the future. The reason we use the maximum value is that we expect the estimation of the number of missed potential passengers in the rest k time slots to be conservative. Recall that if $z_k = 1$, it means that the taxicab will need to charge in k^{th} time slot, and this charge may cause the taxicab to miss $D_k^{\max}$ passengers. Thus, the estimation of the taxicab's number of missed passengers in the rest time slots of the day (i.e., long-term dispatch decision) can be calculated by:

$$D_l^m = \sum_{k=n+2}^{N_s-1} z_k \Phi_i(SoC_k|[t_0 + (k-1)T, t_0 + (k-1)T + \tau_c]) D_k^{\max}. \tag{5.10}$$

where $\Phi_i(SoC_k|[t_0 + (k-1)T, t_0 + (k-1)T + \tau_c])$ is the taxicab's service ability in the region with the passenger demand value $D_k^{\max}$ during the k^{th} time slot, which is determined by its SoC in the k^{th} time slot (i.e., SoC_k). The detailed estimation of SoC_k will be explained in Equation (5.14).

Since charging or not in the short-term decision will directly affect the exhaustion of the taxicab's SoC in the long-term future, we use D_l^m to estimate the impact of short-term dispatch decision (controlled by x_i and y_i) on the number of missed potential passengers in the long-term. By this way, we can obtain the global optimal short-term dispatch decision. In order to minimize the taxicab's number of missed passengers throughout a day, we need to minimize the sum of D_s^m and D_l^m.

Objective: maximizing the probability of picking up a passenger. We also need to dispatch the taxicab to a region (say g_i) with as many potential passengers as possible to increase its probability of picking up a passenger. Thus, the number of potential passenger that the taxicab can pick up can be calculated as:

$$D^p = \sum_{g_i \in \widetilde{G}} (\Phi_i(1|[t_0+\tau_i^d+\tau_i^c, t_0+2T])y_i + \Phi_i(SoC|[t_0+\tau_i^d, t_0+2T])(1-y_i))(\widetilde{D}_i^c(n)+\widetilde{D}_i^c(n+1))x_i, \tag{5.11}$$

where $\Phi_i(1|[t_0 + \tau_i^d + \tau_i^c, t_0 + 2T])$ is the probability that a passenger will appear in g_i after the taxicab reaches and finishes charging in g_i (i.e., the taxicab's service ability in g_i after charging). Note that if $y_i = 1$, the taxicab will firstly fully recharge its battery and then drive to pick up a passenger. Therefore, $SoC = 1$ in this case. $\Phi_i(SoC|[t_0+\tau_i^d, t_0+2T])$ is the probability that a passenger will appear in g_i after the taxicab reaches g_i but does not receive a recharge (i.e., the taxicab's service ability in g_i without charging). Both of these values are obtained from historical passenger demands. Recall that $\widetilde{D}_i^c(n) + \widetilde{D}_i^c(n+1)$ is the the taxicab's total number of potential passengers in g_i adjusted with the maximum predictability of passenger demand in g_i. The dispatching and charging approach needs to maximize D^p as much as possible.

Constraints. To achieve the above two objectives, the dispatching and charging approach needs to follow several constraints. First, recall that we can only choose one region to dispatch the taxicab:

$$\sum_{g_i \in \widetilde{G}} x_i = 1. \tag{5.12}$$

Similarly, the dispatched taxicab can only charge in one region or not charge at all:

$$\sum_{g_i \in \widetilde{G}} y_i \in \{0, 1\}. \tag{5.13}$$

Second, in the optimization of the taxicab's charging, we aim to avoid the taxicab from exhausting its SoC in the rest time slots of the day. That is, the taxicab's SoC in j^{th} time slot (denoted by $SoC_j, j = n+2, \ldots, N_s - 1$) must be higher than 0:

$$SoC_j = SoC + \sum_{g_i \in \widetilde{G}} r\tau_i^c x_i y_i + \sum_{k=n+2}^{j-1} rTz_k - \sum_{k=n+2}^{j-1} \tilde{c}_k^e T(1 - z_k) > 0, \tag{5.14}$$

recall that SoC is the taxicab's current SoC. r is the charging rate (i.e., the amount of SoC charged in unit time) of a charging infrastructure, τ_i^c is the taxicab's charging time in g_i. Thus, $\sum_{g_i \in \widetilde{G}} r\tau_i^c x_i y_i$ is the amount of charged SoC caused by the taxicab's short-term decision. T is the duration of a time slot, and $\tilde{c}_k^e$ is the taxicab's heuristic SoC exhaustion rate (i.e., the amount of SoC consumed in unit time) in k^{th} time slot, which can be estimated as the average value of the taxicab's historical SoC exhaustion rates in k^{th} time slot. Thus, $\sum_{k=n+2}^{j-1} rTz_k - \sum_{k=n+2}^{j-1} \tilde{c}_k^e T(1 - z_k)$ is the amount of charged and consumed SoC from $(n+2)^{th}$ time slot to j^{th} time slot. Finally, SoC_j is the taxicab's estimated SoC in j^{th} time slot.

Third, since the feasible range of SoC is within [0, 1], we also need to consider below constraint in the optimization:

$$SoC_j + rTz_j \leqslant 1, \tag{5.15}$$

where $SoC_j + rTz_j$ represents the taxicab's SoC after j^{th} time slot, which must be no larger than 1.

Problem statement. We combine Objectives (5.9), (5.10) and (5.11) together to model the problem of charging optimization. Finally, the optimization problem can be formulated as:

$$\begin{aligned} &\text{minimize} && D_s^m + D_l^m \\ &\text{maximize} && D^p \\ &\text{subject to} && x_i, y_i, z_k \in \{0,1\} \\ & && \text{Constraints}(5.12), (5.13), (5.14) \text{ and } (5.15) \end{aligned} \tag{5.16}$$

Problem solution. The optimization problem is a Multi-Objective Combinatorial Optimization (MOCO) problem which may have multiple Pareto optimal solutions (i.e., Pareto front) [103]. The outputs are: 1) which region the taxicab should drive to (denoted by x_i); 2) whether the taxicab should get charged in the region (denoted by y_i); and 3) what future time slots the taxicab will receive a recharge (denoted by z_k), which will indirectly influence y_i. Since finding the Pareto front is well-known to be very hard and traditional stochastic algorithms for approximating the Pareto front (e.g., genetic evolution algorithms) is time-consuming, we utilize a guided improvement algorithm [47], which can quickly converge to the Pareto front of

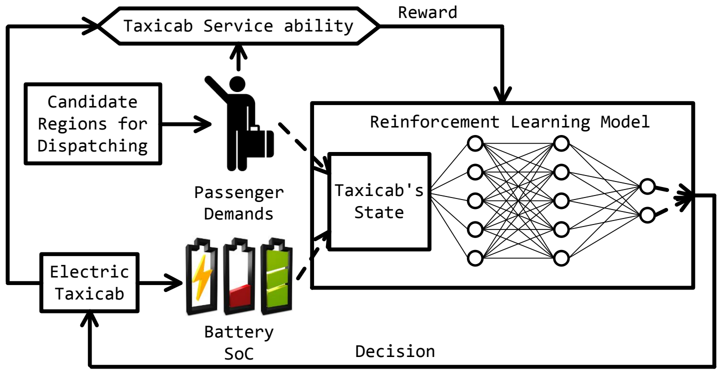

Figure 5.12: Training of reinforcement learning model.

this problem, to enable a real-time scheduling. Generally, it firstly finds a potential solution to meet all the constraints, and then continues to improve the solution by repeatedly meeting the constraints with better objective metrics. Finally, the output solution is guaranteed to be the Pareto front.

Reinforcement Learning Model: In the second taxicab dispatching and charging solution, we use the reinforcement learning (RL) model to generate the action. Specifically, the RL mode produces policy $\pi : s_n \mapsto a_n$, that is, given state s_n, it outputs a_n as the optimal action that maximize the reward. We define *reward* as the number of potential passengers that the taxicab can pick up. We utilize the taxicab's SoC and the predicted passenger demands of the candidate regions ($\widetilde{G}$) in the n^{th} and $(n+1)^{th}$ time slots (i.e., $\{\widetilde{D}_i^c(n) + \widetilde{D}_i^c(n+1) | g_i \in \widetilde{G}\}$) to describe the state s_n. That is, $s_n = (SoC, \{\widetilde{D}_i^c(n) + \widetilde{D}_i^c(n+1) | g_i \in \widetilde{G}\})$. As shown in Figure 5.12, the state is the input to the reinforcement learning model. The output of the model is an action (a_n), i.e., the decision for dispatching and charging in the n^{th} time slot including: 1) which region the taxicab should drive to (denoted by $x_i \in \{0, 1\}$); 2) whether the taxicab should get charged in the region (denoted by $y_i \in \{0, 1\}$). That is, $a_n = (x_i, y_i)$. Specifically, if $x_i = 1$, the taxicab is dispatched to g_i; if $x_i = 0$, the taxicab will not drive to g_i. If $y_i = 1$, the taxicab will receive a recharge in g_i when it arrives at g_i; if $y_i = 0$, the taxicab will not receive a recharge in g_i.

We use the number of potential passengers that the taxicab can pick up by taking an action as the reward for the Reinforcement Learning (RL) model. If $x_i = 1$ and $y_i = 1$ (i.e., the taxicab will drive to g_i and receive a recharge in g_i), the taxicab will spend τ_i^d on driving to g_i, and τ_i^c on receiving a full recharge in g_i based on its current SoC. Thus, starting from current time t_0, the time duration that the taxicab can pick up passengers in the n^{th} and $(n+1)^{th}$ time slots is $[t_0 + \tau_i^d + \tau_i^c, t_0 + 2T]$, where T is the duration of a time slot. $[t_0 + \tau_i^d + \tau_i^c, t_0 + 2T]$ is defined as the time duration from the taxicab's completion of charging in region g_i until the end of the n^{th} and $(n+1)^{th}$ time slots. Similarly, if $x_i = 1$ but $y_i = 0$ (i.e., the taxicab will drive to g_i but will not receive a recharge in g_i), the time duration that the taxicab can pick up passengers in the n^{th} and $(n+1)^{th}$ time slots is $[t_0 + \tau_i^d, t_0 + 2T]$. Note that the taxicab's service ability during a specific time duration can be calculated by Equation (5.7), the taxicab's reward function resulted by x_i and y_i can be represented as:

$$r(s_n, a_n, s_{n+1}) = (\Phi_i(1|[t_0+\tau_i^d+\tau_i^c, t_0+2T])y_i+\Phi_i(SoC|[t_0+\tau_i^d, t_0+2T])(1-y_i))(\widetilde{D}_i^c(n)+\widetilde{D}_i^c(n+1))x_i, \tag{5.17}$$

where $\Phi_i(1|[t_0 + \tau_i^d + \tau_i^c, t_0 + 2T])$ is the taxicab's service ability in g_i after charging. The reason $SoC = 1$ is that the taxicab will firstly fully recharge its battery and then drive to pick up a passenger. $\Phi_i(SoC|[t_0 + \tau_i^d, t_0 + 2T])$ is the taxicab's service ability in g_i without charging. Both $\Phi_i(1|[t_0 + \tau_i^d + \tau_i^c, t_0 + 2T])$ and $\Phi_i(SoC|[t_0 + \tau_i^d, t_0 + 2T])$ are obtained from historical passenger demands.

We use the Deep Neural Network (DNN) to obtain the optimal policy as in [74]. The optimal policy π^* is defined as one map $\pi^* : s_n \mapsto a_n$ that maximizes the reward received by taking the correspoinding action a_n given state s_n. It is the training result of the reinforcement learning model. The trained RL mode outputs the dispatching and charging action a_n when the input state is s_n. To discover the optimal dispatching and charging action strategy that maximizes the reward (i.e., number of potential passengers for the taxicab) under various states, we utilize the long-term historical passenger demands (e.g., passenger demands in previous 365 days) for offline training of the reinforcement learning model. Once the model training is complete, the taxicab can utilize the model to generate the dispatching and charging action in real time. During the training process, the inputs are the state, the different actions the taxicab takes (i.e., driving to each region and choose to get recharged or not) and the reward calculated by Equation (5.17), i.e., the number of potential passengers that the taxicab can pick up by taking an action. Specifically, we suppose that the taxicab's initial state starts from a randomly selected region with $SoC = 1$. Then, we simulate the movement of the taxicab from one region to another region. That is, the taxicab transfers from one state to another state by taking different actions. Thus, starting from the initial state, we can collect all possible series of successive actions. Finally, we utilize the historical passenger demand value information at each time when the taxicab takes an action in the simulation to calculate the reward. The RL model calculates the Q value of a series of successive actions as the sum of the rewards resulted from the actions. Reinforcement learning finds a policy that is optimal in the sense that it maximizes the expected value of the total reward over all the series of successive actions, starting from the initial state.

However, one major difficulty in finding the optimal dispatching and charging policy is: the total number of all possible states is too large. For the state $s = (SoC, \{\widetilde{D}_i^c(n) + \widetilde{D}_i^c(n+1) | g_i \in \widetilde{G}\})$, suppose that SoC changes between 0 and 1, and there are 10 candidate regions in $\widetilde{G}$, and each region's $\widetilde{D}_i^c(n) + \widetilde{D}_i^c(n+1)$ changes between 0 and 2000. If we set the change unit of SoC is 0.001, the change unit of $\widetilde{D}_i^c(n) + \widetilde{D}_i^c(n+1)$ is 200, the total number of possible states reaches at the 10^{13} level, which will result in the curse of dimensionality problem in practice [8]. Besides, these many state values can result in huge overload in computing Q-values. To solve this difficulty, we apply DNN into the reinforcement learning model to approximate the Q-values and help form the optimal policy π^*. More details of applying the DNN into the RL model can be found in [74].

5.4 Performance Evaluation

5.4.1 Comparison Methods

To evaluate *CD-Guide*'s performance, we compare its taxicab passenger demand inference performance with a representative method that utilizes Bilinear Poisson regression model to consider the effects of random factors on passenger demand values (*BilinearPoisson* in short) [99], and the method introduced in Section 5.2.1.1 (*Similar* in short). Specifically, throughout all the time slots in a day, *Similar* utilizes the historical demand value, of which histogram of passenger building tags has the smallest χ_j^2 to that of current passenger demand value, as the predicted passenger demand in the next time slot. *BilinearPoisson* develops a bilinear Poisson regression model, which takes all the historical demands as input training data without selection. It uses random factors including day of week, holidays and weather as inputs to the model and learn their effects on passenger demand based on the training data. Finally, the model outputs the passenger demand of each region in the next time slot considering the demand value and random factors in current time slot.

We divide *CD-Guide* into two forms: *CD-Guide_Opt* represents the form that uses optimization problem for taxicab dispatching; *CD-Guide_RL* represents the form that uses RL model for taxicab dispatching. We also compare the performance of *CD-Guide_Opt* and *CD-Guide_RL* in increasing the number of served passenger pick-up requests with a representative taxicab dispatching method (*PrivateHunt* in short)

[111], and a baseline method that randomly dispatches the taxicab to a nearby region (*Baseline* in short). In *PrivateHunt*, it utilizes the future passenger demand inferred from historical passenger demands to determine the cruising policy for each taxicab, in order to maximize the taxicab's likelihood of picking up passengers. For fairness, we use the passenger demand inference result output by *CD-Guide*. Then, it utilizes a Markov Decision Process to model the appearance of passengers and calculate the probability of picking up a passenger with the probability of passenger appearance in each region. in each region. Finally, it recommends the region that has the maximum probability of picking up a passenger to the taxicab. The distribution of chargers follow the existing charging stations in Shenzhen. Since *PrivateHunt* and *Baseline* do not have specific methods to optimize the charging of taxicabs, we set that the taxicabs in these two methods will drive to the nearest charger for charging whenever their SoC is below a threshold (20% in this experiment). The threshold is determined so that an EV is able to reach the nearest charger with its residual SoC.

5.4.2 Experiment Settings

We suppose that every electric taxicab starts driving with full energy in battery at the beginning of a day. The battery capacities of the taxicabs follow a uniform distribution from 65 kWh to 85 kWh, which is the common battery capacity of electric taxicabs in Shenzhen [62]. With the most recent research implementations (e.g., Oak Ridge National Laboratory [85]), it is expected that within a 10-year timeframe, it is possible to reach a charging rate over 100kW for EV wireless charging. Therefore, we use 150kW as the charging rate of a charging infrastructure. The energy consumption rate of a taxicab is a 0.425 kWh/km [62, 117]. The SoC lower bound $SoC_{\min}$ is set to 20%. We use the historical data from July, 2014 to June, 2015 as the training data for *CD-Guide*, *Similar* and *BilinearPoisson*. The random factors such as day of week and holidays are obtained from Shenzhen's calendar of 2015, and the weather data is obtained from the China Meteorological Data Service Center [21]. All 16 weather types (e.g., Sunny, Rainy) are denoted with one hot coding (i.e., if a day is sunny, its code is 1, or 0 otherwise). We aim to infer the passenger demand in each time slot of July 15, 2015 to compare the accuracy of different passenger demand inference methods. To validate our inference model in different situations, we also measured the inference accuracy of the methods in 7 different days, which are January 12 (Monday), March 10 (Tuesday), May 13 (Wednesday), July 16 (Thursday), September 18 (Friday), November 21 (Saturday) and December 13 (Sunday) in 2015. These days are representative because they are unrelated to each other, belong to 4 different seasons, and cover weekdays and weekends [121]. The values of parameters related to training (i.e., N^D, β) are $N^D = 365$ and $\beta = 10\%$. We also use the historical demand data to train the reinforcement learning model that determines the dispatching and charging policy with the maximum reward. Specifically, we utilize Flow [110], which is a vehicle traffic simulation framework with the integration of deep reinforcement learning, to implement the reinforcement learning based optimization of taxicab dispatching and charging. Flow utilizes SUMO [56] to simulate the states and actions of taxicabs and utilizes DNN to train the optimal dispatching and charging policy with the maximum reward. Based on the deployment of existing charging stations in Shenzhen, we use SUMO [56] to simulate the operation of 1,000 EVs on Shenzhen's road network for 24 hours in 7 different days (i.e., January 12, March 10, May 13, July 16, September 18, November 21 and December 13 in 2015). We converted OpenStreetMap road network of Shenzhen to a SUMO road network file. In SUMO, we let taxicabs drive by the dispatching strategy designed by each comparison methods. The parameters are listed in Table 5.1.

We use the movement records of the taxicabs mentioned in Section 2.2 for performance evaluation. Below, Figure 5.13 to Figure 5.17 demonstrate the metrics of the

Table 5.1: Table of parameters.

Parameters	Setting	Source
Battery capacity of an EV	65kWh – 85kWh	Li *et al.* [62]
Charging rate $\mathcal{C}$	150 kW	Chen *et al.* [20, 31, 113]
Energy consumption rate c_e	$500/m	Li *et al.* [62]
SoC lower bound $SoC_{\min}$	20%	Author's assumption
Total number of days of observed passenger demands N^D	365	Author's assumption
Ratio of extracted suitable historical passenger demands β	10%	Author's assumption

vehicles under different hours on July 15, 2015. Figure 5.18 to Figure 5.19 demonstrate the metrics of the vehicles in multiple days, which are January 12 (Monday), March 10 (Tuesday), May 13 (Wednesday), July 16 (Thursday), September 18 (Friday), November 21 (Saturday) and December 13 (Sunday) in 2015. These days are representative because they are unrelated to each other, belong to 4 different seasons, and cover weekdays and weekends [121]. Specifically, we measured the following metrics:

- *Passenger demand inference sMAPE*. For each region, we measure the sMAPE over all time slots throughout a day for each region, and collect the CDF of the sMAPEs of all the regions. We also collect the CDF of the Absolute Percentage Error (APE) [105, 132] (i.e., APE $= \frac{|\text{inferred demand}-\text{actual demand}|}{\text{inferred demand}+\text{actual demand}+1}$) of the inference result in each time slot of all the regions. The purpose of this metric is to compare the inference accuracy of different passenger demand inference methods.
- *The number of served passengers*. We measure the number of passengers served by all taxicabs in all time slots throughout a day. We also measure the number of passengers served by each taxicab, and collect the CDF of the served passengers of all the taxicabs. The purpose of this metric is to compare the performance of different taxicab dispatching methods in serving passengers.
- *Taxicab SoC*: For each taxicab, we measure its SoC in each time slot throughout a day. Then, we measure the medium, 5^{th} percentile and 95^{th} percentile values of all the taxicabs' SoC in each time slot. The purpose of this metric is to compare the performance of different taxicab dispatching methods in supporting the SoC of

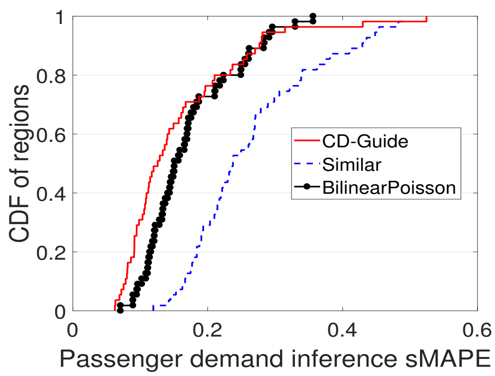

Figure 5.13: Distribution of passenger demand inference sMAPEs.

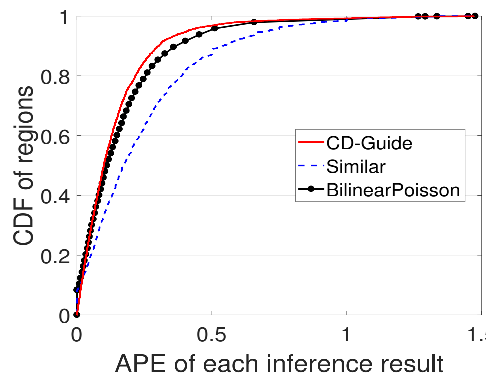

Figure 5.14: Distribution of the APEs of all inference results.

taxicabs.

5.4.3 Experimental Results

5.4.3.1 Passenger Demand Inference sMAPE

Figure 5.13 shows the distribution of the sMAPEs of taxicab passenger demand inference results in all regions. Figure 5.14 shows the distribution of the APEs of the inference results in each time slot of all regions. We can see that for most regions (>90%), the sMAPEs follow: *CD-Guide*<*BilinearPoisson*<*Similar*. While for the other regions (<10%), the sMAPEs follow: *CD-Guide*≈*BilinearPoisson*<*Similar*. The APEs of the inference results generally follow *CD-Guide*⩽*BilinearPoisson*<*Similar*.

Similar results in the highest average sMAPE over all regions. This is because that it uses only one suitable historical passenger demand value, of which histogram of passenger building tags has the smallest χ_j^2 to that of current passenger demand value, as the demand value in the next time slot. Although the historical data is a good indicator of the changing trend of passenger demand in the next time slot, simply using a historical passenger demand value as a future demand value will inevitably cause a high inference error, because one suitable historical data sometimes cannot catch the influence of all random factors.

In comparison, *BilinearPoisson* has a much lower sMAPE in all regions. This is because that *BilinearPoisson* regresses the change of passenger demand value by time via the bilinear Poisson regression model. After training the time-variant Poisson parameter with large-scale historical data, it has taken into account the long-term temporal change pattern of taxicab passengers. In addition, after adding the quantified effect of random factors to the bilinear Poisson regression model, *BilinearPoisson* can better adjust its inference result against unexpected cases (e.g., day of the week, weather) that are not reflected in historical data. However, its inference accuracy is constrained by the maximum predictability of future passenger demand in some regions. This is why the sMAPEs of *BilinearPoisson* in around 75% of the regions are similar or lower than those in *CD-Guide*.

Compared with *BilinearPoisson*, *CD-Guide* achieves a lower sMAPE in around 75% of the regions, a similar sMAPE in around 20% of the regions, and a slightly higher sMAPE in the rest 5% of the regions. This is because that in *CD-Guide*, the suitable historical data extraction process has ensured that the training data for inference have been limited to previous days that have similar histograms of passenger tags, which means that they are under the influence of similar random factors. For most regions (i.e., 95%) with a relatively higher passenger demand predictability, the extracted suitable historical data has covered sufficient random factors that may influence the region's future passenger demand. What's more, *CD-Guide* utilizes the linear regression to learn the weights of the random factors in generating the inference result. As a result, the inference accuracies of passenger demands in the 95% regions are sufficiently high. For the rest 5% regions, which have relatively lower predictability, their future passenger demand does not have much commonness with their historical demands (i.e., unpredictable), catching the overall random factors that affect the historical demands does not help improve the predictability of (i.e., unpredictable), catching the overall random factors that affect the historical demands does

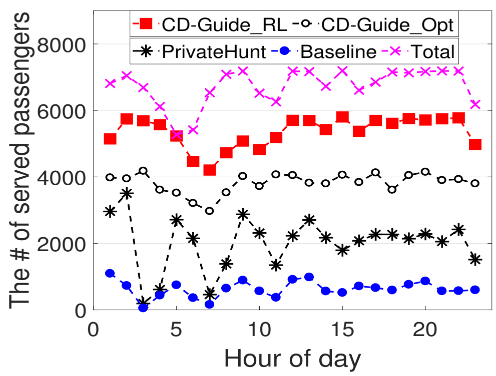

Figure 5.15: The number of served passengers of all taxicabs.

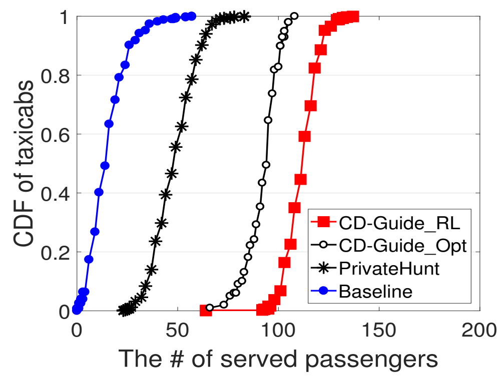

Figure 5.16: Distribution of the numbers of taxicabs' served passengers.

not help improve the predictability of passenger demand As a result, *BilinearPoisson* achieves a lower sMAPE due to its learned influence of several random factors. This experiment result demonstrates that *CD-Guide*'s passenger demand inference method is effective in approximating the actual passenger demand with a higher accuracy, and its effectiveness differs in the regions due to the different predictability of passenger demand in the regions.

The distribution of the APEs of each inference result is consistent with the distribution of passenger demand sMAPEs of all the regions. The APEs of about 90% of the inference results in *CD-Guide* are lower or approximate to that of *BilinearPoisson*. The APEs of almost all the inference results in *Similar* are higher than the other two methods. This result further confirms *CD-Guide*'s high accuracy in passenger demand inference for regions with various maximum predictability.

5.4.3.2 The Number of Served Passengers

Figure 5.15 shows the number of passengers served by all the taxicabs in each hour of a day under different taxicab dispatching methods. For reference convenience, we also drew the actual total number of passengers reflected by trace data in each hour throughout the day (denoted by *Total*). Figure 5.16 shows the CDF of the numbers of served passengers of all the taxicabs under different methods. We can see that in both figures, the results follow: *Total>CD-Guide_RL>CD-Guide_Opt>PrivateHunt>Baseline*.

In Figure 5.15, *Baseline* always achieves the minimum total number of served passengers during all hours in a day. This is because that it simply dispatches the taxicab to a nearby region without considering the passenger demand in the region. So the taxicab cannot efficiently discover passengers when driving. From Figure 5.16, we can see that almost all taxicabs cannot pick up more than 50 passengers in a day.

In comparison, the taxicabs of *PrivateHunt* picked up much more passengers than those in *Baseline*. This is primarily because that *PrivateHunt* employs a Markov Decision Process to determine the probability of picking up a passenger and the possible duration of cruising time without a passenger onboard for each nearby region. The dispatched taxicab is able to quickly discover a passenger by following the recommend driving route. However, we can also observe that there are several conspicuous drops of the number of served passengers at around 03:00, 07:00, 11:00 and 15:00. This generally matches the time of taxicabs' charging events, which is analyzed in Section 5.2.1.3. The reason is the same: some of the taxicabs exhausted SoC and have to recharge at around these time slots, so they missed many potential passengers during these time slots. By comparing the result curve of *PrivateHunt* with *Total*, we can see that the total number of passengers is actually increasing or remaining high at 03:00, 07:00 and 15:00. During their charging, they missed many passengers, which results in the conspicuous drops of the number of served passengers. From Figure 5.16, we can see that more than 50% of the taxicabs picked up more than 50 passengers in a day, which is much higher than that in *Random*. In Section 5.4.3.3, we will illustrate the change of the taxicabs' SoC to further explain the effect of charging on degrading the taxicabs' service.

The taxicabs of *CD-Guide_RL* and *CD-Guide_Opt* achieve the highest and the second highest total number of served passengers during all hours in a day, respectively. We can see that the curves of *CD-Guide_RL* and *CD-Guide_Opt* generally change accordingly with the change of the total number of passengers. This observation verifies that the service of the taxicabs of *CD-Guide_RL* and *CD-Guide_Opt* was not greatly effected by their charging time. This is because that the optimal taxicab dispatching and charging policies of these two methods take into account the effect of charging time on the number of potential passengers, and meanwhile ensure that the taxicab has sufficient SoC throughout a day. We can also observe that *CD-Guide_RL*'s curve is a bit higher than that of *CD-Guide_Opt*. This is because that *CD-Guide_RL*'s taxicab dispatching and charging model is trained after trying the optimal policy, which has considered the state change under various passenger demands and avoids the taxicab from charging at the state with many passengers appearance. In comparison, although *CD-Guide_Opt* tries to minimize the number of missed potential passengers in both short-term and long-term, its estimation of long-term missed potential passengers is inaccurate since it only uses the maximum observed passenger demand among all the regions for the estimation. Therefore, the dispatching and charging guidance provided by *CD-Guide_RL* is more effective in increasing the number of served passengers for the taxicabs. Since both *CD-Guide_RL* and *CD-Guide_Opt* try to dispatch each taxicab to the nearby region with the maximum number of potential passengers, all the taxicabs of *CD-Guide* and *CD-Guide_Opt* can serve more than 60 passengers during a day as illustrated in Figure 5.16.

5.4.3.3 Taxicab SoC

Figure 5.17 shows the medium, 5^{th} percentile and 95^{th} percentile values of all the taxicabs' SoC after every two hours in a day under different taxicab dispatching methods. We can see that the results of *CD-Guide* is much more stable than the other methods. The medium values generally follow: *CD-Guide_Opt*≈*CD-Guide_RL*>*PrivateHunt*≈*Baseline*.

In *PrivateHunt* and *Baseline*, after driving for around 4 hours from 00:00 to 04:00, the taxicabs began to run out of SoC (<20%) and drove to a charging infrastructure

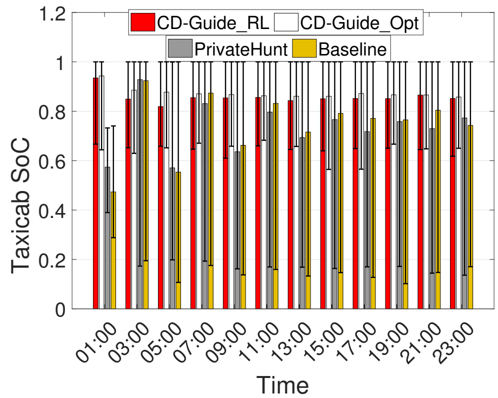

Figure 5.17: Taxicabs' SoC.

for a full recharge, which makes their medium SoCs return to around 0.9 at 04:00. But their recharge downtime caused them to miss a high volume of passengers that happened during this time interval, which is reflected as the conspicuous drops of the number of served passengers of *PrivateHunt* and *Baseline* in Figure 5.15. Similar cases also happened at around 07:00 and 15:00, when the passenger demand in many regions is still high, but many taxicabs drove to charging infrastructures to restore SoC. The reason behind this is that both *PrivateHunt* and *Baseline* do not consider the optimization of the taxicabs' charging in dispatching, so the taxicabs occasionally run out of SoC right during the time when passenger demand is still high.

In contrast, the medium taxicab SoCs of *CD-Guide_Opt* and *CD-Guide_RL* remain relatively more stable throughout the day. We can see that the taxicabs' medium SoC keeps dropping between 00:00 and 05:00, this is because that the dispatching and charging policies of *CD-Guide_RL* and *CD-Guide_Opt* take into account the change of passenger demand and do not let the taxicabs spend a long time for a full recharge between 00:00 and 05:00. Later, after the total number of passengers dropped to a valley point at around 05:00, the taxicabs of *CD-Guide_RL* and *CD-Guide_Opt* began to drive for a recharge and restored their medium SoC to around 0.85. Since for each taxicab's dispatching request, the dispatching and charging policies of *CD-Guide_RL* and *CD-Guide_Opt* determine the best charging time and position that affect the

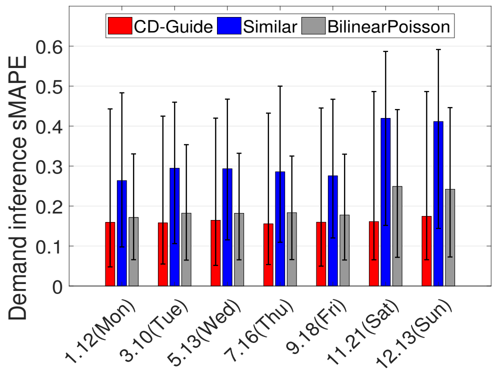

Figure 5.18: Passenger demand inference sMAPEs in different days.

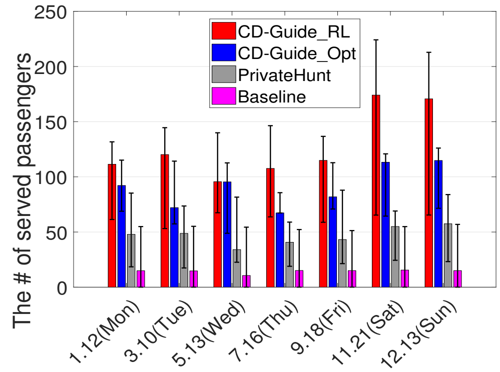

Figure 5.19: The number of served passengers in different days.

least on the taxicab's service, the medium SoCs of the taxicabs of *CD-Guide_RL* and *CD-Guide_Opt* remain above 0.8 with small fluctuations after 07:00.

5.4.3.4 Performance Evaluation on Multiple Days

To further validate the effectiveness of our passenger demand inference method and taxicab dispatching method under different scenarios, we measured the passenger demand inference sMAPE of all regions and the number of passengers served by all the taxicabs on different days. Figure 5.18 shows the median, 5^{th} and 95^{th} percentiles of the passenger demand inference sMAPE of all the regions on different days. Figure 5.19 shows the median, 5^{th} and 95^{th} percentiles of the number of passengers served by all the taxicabs on different days.

From Figure 5.18, we can see that the median values of the demand inference sMAPEs generally follow: *CD-Guide*≈*BilinearPoisson*<*Similar* on weekdays. However, the demand inference sMAPEs of *BilinearPoisson* and *Similar* significantly increase on weekends, while the median value of the passenger demand inference sMAPE of *CD-Guide* only slightly increases on weekends. This is primarily because that the passenger appearance on weekends has much more randomness compared with those on weekdays. Although *BilinearPoisson* takes into account the long-term temporal change pattern of passenger appearance (e.g., day of the week, weather), its inference accuracy in the regions with low predictability is further reduced due to the higher random factors on weekends. While *Similar* uses only one suitable historical passenger demand that has the most similar histogram of passenger building tags as current passenger demand, the single data is not sufficient to capture the randomness that affects the real-time passenger demand. By selecting multiple suitable historical data, *CD-Guide* has maximally considered the random factors reflected in historical data in generating the inference result. As a result, except for the regions with low predictability (the 95^{th} percentile of the passenger demand inference sMAPE on weekends is higher than that on weekdays), the median values of the passenger demand inference sMAPE remains approximate to those on weekdays.

From Figure 5.19, we can see that the median values of the number of passengers served by the taxicabs generally follow: *CD-Guide_RL*>*CD-Guide_Opt*>*PrivateHunt*>*Baseline* on different days. On weekends, the taxicabs under all methods picked up more passengers than weekdays. However, the taxicabs in *CD-Guide_RL* and *CD-Guide_Opt* picked up much more passengers than those in *PrivateHunt* and *Baseline*. This is primarily because that there are much more passenger appearances on weekends. The optimal taxicab dispatching and charging policies of *CD-Guide_RL* and *CD-Guide_Opt* take into account the effect of charging time on the number of potential passengers, and meanwhile ensure that the taxicab has sufficient SoC throughout a day. Moreover, the RL based dispatching method of *CD-Guide_RL* can more adaptively adjust the driving route of taxicabs according to the real-time change of passenger demand, which further increases the number of passengers picked up by taxicabs on weekends.

5.5 Summary

Accurate inference of future passenger demand and avoidance of missing too many passengers caused by battery charging is essential for efficient dispatching of electric taxicabs. Our proposed *CD-Guide* is the first electric taxicab *C*harging and *D*ispatching approach that *Guide*s electric taxicabs to minimize their number of missed passengers due to charging. Our analytical results on a metropolitan-scale electric taxicab passenger demand dataset provide insights for the design of *CD-Guide*. We utilize the histogram of passengers' building tags to extract suitable historical passenger demands for training a linear regression based passenger demand inference model, and adjust the inference result considering the maximum predictability of taxicab passenger demand in each region. We design a reinforcement learning based model that guides a taxicab to receive charging with minimized number of missed passengers, maximized probability of picking up a passenger and sufficient SoC during the rest time slots of a day. We conducted trace-driven experiments on SUMO to verify the performance of *CD-Guide*. Compared with previous methods, *CD-Guide* increases the number of served passengers by 100% on average, and maintains the average SoC of all taxicabs above 80% during all time slots.

Chapter 6

Related Work

Over the past decades, with ever increasing concerns on wide adoption of EVs, wireless power transfer for EVs have attracted more and more efforts to support EVs' applications under various Intelligent Transportation Systems scenarios. In this chapter, we discuss existing efforts in improving the performance of WPT charging systems for EVs.

The remainder of this chapter is organized as follows. Section 6.1 introduces the state-of-the-art in WPT techniques for EVs. Section 6.2 discusses the existing works for optimizing the deployment of chargers for EVs. Section 6.4 presents the works about the inference methods of taxicab passenger demand. Section 6.6 discusses the efforts in utilizing the passenger demand inference results to guide the driving of taxicabs.

6.1 Wireless Power Transfer for EVs

In 2006, Karalis *et al.* [53] from MIT introduced a resonant coupler that wirelessly transmits a large amount of power to EVs at low frequencies. Jang *et al.* [48] formulated an optimization problem, which considers battery capacity and charging lane length as constraints, to deploy wireless charging lanes to maintain the SoC of buses on a single determined route with the minimum cost. Sarker *et al.* [94] developed a wireless power transfer system for balancing the SoC of EVs in a charging lane in the urban scenario. However, the problem of deploying wireless charging lanes in a metropolitan road network considering different sources of traffic and many roads has not been studied.

6.2 Deployment of Plug-in Chargers

Driven by the traffic flow and city-wide travel patterns of people reflected in the ubiquitous taxicab movement data, several recent works studied the problem of minimizing average seeking time for the nearest charging station of EVs from the perspective of urban facility planning. Qin *et al.* [89] scheduled the plug-in charging stations to minimize the time on seeking and waiting in charging stations based on the estimated time and location that each EV needs to be charged. Zhang *et al.* [130] further considered the uncertainty of the EVs' arrival times at the charging stations to shorten the time on seeking chargers and charging. Li *et al.* [62] determined the locations for deploying plug-in charging stations that minimize the time on seeking chargers. Bae *et al.* [5] proposed to deploy charging stations through analyzing the spatial and temporal dynamics of charging demand profiles at potential positions using the fluid dynamic model. Zheng *et al.* [137] formulated an optimization problem trying to maximize the number of EVs charged while minimizing the life cycle cost of all the stations. Eisel *et al.* [26] aimed at dealing with drivers' range anxiety (i.e., fear of being unable to reach destination due to insufficient charging opportunities) by transforming the drivers' preference in charging into planning of stations.

Further, several traffic flow based charging station deployment algorithms have been proposed Lam *et al.* [58] formulated the station placement as a vertex cover problem, proved its NP-hardness and proposed four solutions. Wang *et al.* [108] determined constraints (e.g., driving range, traffic volume) from EV traffic statistics, and formulated and solved a multi-objective location optimization problem to maximize the coverage of EV traffic. Sánchez-Martín *et al.* [93] proposed to deploy charging stations at the positions with many parking events and suitable parking time length with the minimum deployment cost to offer EVs enough charging opportunities. Yao *et al.* [119] formulated a problem trying to minimize deployment cost to maximize the covered EV traffic flow. Li *et al.* [62] proposed the first work (Optimal Charging Station Deployment (OCSD)) for deploying plug-in charging stations that minimize the time on seeking chargers through analyzing a large-scale electric taxi trajectory data. Yang *et al.* [118] applied a large-scale GPS trajectory data collected from the taxi fleet to allocate chargers for battery EV taxis, and investigated the tradeoff between installing more chargers versus providing more waiting spaces. Cai *et al.* [14] demonstrated the potential public charging stations by extracting public parking "hotspots" from taxi trajectory data in Beijing, China. Shahraki *et al.* [97] developed an optimization model to determine optimal charger allocation, with the objective of maximizing electrified fleet vehicle miles traveled (VMT) of plug-in hybrid electric vehicles (PHEVs). Based on an event-based simulation, Sellmair *et al.* [96] proposed an algorithm to optimize the number of charging stations per taxi stand based on real world driving patterns of conventional taxis in Munich, Germany. The objective was to maximize economic benefit of the entire system including BEV taxi drivers and charging station investors. Jung *et al.* [52] proposed a bi-level simulation-optimization model to allocate chargers for a fleet of 600 shared-taxis in Seoul, Korea, with an objective of minimizing the queue delay. Ahn *et al.* [1] proposed an Estimating the Required Density of EV Charging (ERDEC) stations model to estimate the optimal density of charging stations aiming at minimizing the range anxiety based on taxi trajectories in Daejeon City, Korea, which was a pioneering work considering charging queuing. Although these works can support the continuous operability of the taxicabs by adapting the deployment of chargers to cover the actual traffic, the taxicabs still have to spend extra idle time on seeking chargers and charging upon the exhaustion of the battery.

6.3 Optimal Deployment of Wireless Chargers for EVs.

He *et al.* [39] proposed two pricing models and formulated a mathematical program to optimize the deployment of wireless charging tolls. Ko *et al.* [54] designed a mathematical optimization model to allocate the in-motion wireless chargers and determine buses battery size given specific bus driving routes. Riemann *et al.* [91] proposed a mixed-integer nonlinear program model to maximize the captured traffic flow of deployed in-motion wireless chargers through applying the stochastic user equilibrium to describe EVs' route choice. Fuller *et al.* [31] considered various combinations of charging power and EV driving range, and formulated and solved a flow-based set covering problem to determine the number of wireless charging infrastructures required in California. Chen *et al.* [19] developed a user equilibrium model for describing the equilibrium flow distribution across a road network, and formulated a mathematical program to optimize the charging lane deployment. Hwang *et al.* [45] proposed a Particle Swarm Optimization (PSO) method to solve a mathematical model that optimizes the economical allocation of charging lanes, given the battery size and multi-route environment. Chen *et al.* [20] further studied the deployment problem of both stationary and in-motion wireless chargers through considering different scenario requirements. Liu *et al.* [66] proposed a deterministic model and a robust model to address the problem of optimizing the charging lane locations for a real-world bus system that consists of 8 bus lines. Bi *et al.* [9] proposed a novel multi-objective optimization model framework based on life cycle assessment (LCA) to solve the deployment problem of in-motion wireless chargers in a multi-route electric bus system. Manshadi *et al.* [73] proposed a decentralized optimization framework to address the impact of wireless charging on electricity and transportation networks. Li *et al.* [59] designed a bi-objective model considering both traffic delay and charger utilization rate to optimize the deployment of wireless chargers on urban road networks with traffic signals. However, these works are designed and evaluated for small-scale road networks (mostly no more than 20 road segments) with synthetic traffic. Therefore, they cannot solve the challenge of deploying wireless charging lanes in a metropolitan road network with different sources of traffic, which however is much more formidable.

6.4 Taxicab Passenger Demand Inference

Multiple urban passenger demand inference methods have been proposed. Fan *et al.* [29] proposed to decompose passenger demand into several patterns representing the influence of different random factors, and use the patterns to infer the number of population at specific times in each region. Shimosaka *et al.* [99] proposed to utilize a bilinear Poisson regression model, which considers random factors including day of week, holidays, etc., to predict passenger demand in a metropolitan scale. Zhang *et al.* [126] developed a customized online training model with both historical and real-time GPS position data of taxicabs to infer taxicab passenger demand. Zhang *et al.* [128] proposed a residual Convolutional Neural Network (CNN) based model to learn the influence of several random factors (e.g., weather, period and trend of passenger demand), and achieved a higher inference accuracy than previous methods.

However, these methods have insufficient accuracy because they fail to catch the influence of all random factors.

6.5 Prediction of Traffic Demand

As an essential component for efficient traffic management, the short-term prediction models of traffic demand have been extensively studied. Smith *et al.* [100] proposed to use seasonal Autoregressive Integrated Moving Average (ARIMA) model to forecast the traffic demand value in the near future. Stathopoulos *et al.* [102] developed a multivariate time-series state space model to increase the prediction accuracy. Ghosh *et al.* [32] further developed a multivariate structural time series model to consider multiple factors that may affect real-time traffic demand, such as trend, seasonal, cyclical, and calendar variations. Hinsbergen *et al.* [41] applied extended Kalman filter techniques, which assume the traffic network has nonlinear state space, for traffic demand prediction. Carrese *et al.* [16] utilized Local Ensemble Transformed Kalman Filter (LETKF) to consider increasingly abundant heterogeneous traffic data for online traffic demand prediction. In recent years, machine learning techniques have been widely used for traffic demand prediction. Zhang *et al.* [131] proposed a v-Support Vector Machine (v-SVM) model, which overcomes local minima and overfitting in training process, for short-term traffic demand prediction. Wei *et al.* [109] proposed an approach which combines Empirical Mode Decomposition (EMD) and Back-Propagation Neural networks (BPN) to predict short-term traffic demand in metro systems. Ma *et al.* [70] utilized Long Short-Term Neural Network (LSTM NN) to capture nonlinear traffic dynamic of vehicle driving speed and the prediction of traffic demand. Lin *et al.* [64] proposed to utilize Graph Convolutional Neural Network with data-driven graph filter for the prediction of hourly traffic demand. Lv *et al.* [69] proposed a deep-learning-based traffic flow prediction method, which considers the spatial and temporal correlations of traffic features (e.g., driving speed, weather), for traffic demand prediction. These works are similar to taxicab passenger demand inference methods (Section 6.4) since they all rely on historical demand data for prediction and need to consider multiple random factors that may affect the prediction result. However, these works cannot quantify the maximum predictability of the traffic demand value (i.e., reliability of the prediction result) as in Section 5.3.3.3 and proper use of the predictability for improving the service efficiency of taxicab dispatching as in Section 5.3.4.2.

6.6 Taxicab Dispatching

In recent years, thanks to the ubiquitous mobile sensing data harvested from GPS-equipped taxicabs in metropolitan cities, many taxicab dispatching methods have been proposed to guide taxicabs to efficiently pick up passengers with reduced cruising miles [122, 123, 125, 134]. Yuan *et al.* [122] introduced a method that schedules the pick-up locations with the shortest routes for taxi drivers and the waiting locations for passengers to reduce the cruising time. Zheng *et al.* [134] modeled the behavior of vacant taxicabs with a non-homogeneous Poisson process to find the optimal waiting positions for passengers. Zhang *et al.* [123] proposed a method to estimate the revenue of each route, and guide the taxicab to the route with the maximum estimated revenue. Zhang *et al.* [125] proposed *pCruise*, in which each taxicab collects the passenger requests from nearby taxicabs and accordingly cruises on the routes with the maximum probability of finding a passenger. Although these works aim to guide taxicabs to pick up the expected passengers with the shortest route, the taxicabs still need to spend much time on driving to the suggested locations without passengers on board. Moreover, the time wasted on seeking chargers and charging is not considered in these works.

Chapter 7

Conclusions

7.1 Summary of Dissertation

To fulfill metropolitan transit demands, public transportation EVs are expected to be continuously operable without recharging downtime. Although there have been many previous mature works on plug-in cable charging systems, EVs must stop and get plugged in the charging points of the charging stations to get recharged, which wastes time and becomes an obstacle for the continuous operability of public transportation EVs. Recently, WPT techniques for EV charging are emerging as a solution to keeping the EVs continuously operable. The WPT techniques are expected to be a complementary charging approach to the stationary wireless chargers; forming a hybrid WPT charging system composed of stationary and dynamic wireless chargers. In this dissertation, we mainly investigated the thesis statement:

- By exploiting our generic traffic model and methodologies based on spatial and temporal analysis of passenger appearance, entropy-based categorization and clustering of flow attributes, and customized selection and training of suitable historical taxicab passenger demand data, we can develop a hybrid WPT charging system that can better serve public transportation EVs in terms of continuous operability, electricity utilization efficiency, and charging service efficiency compared to the state of the art.

Based on the results presented in the preceding chapters, we believe the work in this dissertation supports this thesis statement. We claim the following contributions in this dissertation:

- In Chapter 3, we presented a stationary wireless charger deployment approach, named *PickaChu*. *PickaChu* utilizes spatial and temporal analysis of passenger appearance and a generic traffic model to both maximize the taxicabs' opportunity of picking up passengers at the chargers and support the taxicabs' continuous operability on roads with the minimal deployment cost We implemented *PickaChu* on SUMO. Through large-scale trace-driven simulation based on the metropolitan-scale mobility dataset of taxicabs, we showed that *PickaChu* has superior performance over other representative methods in terms of reducing idle time and supporting the operability of the taxicabs.

- In Chapter 4, we presented a dynamic wireless charger deployment approach, named *CatCharger*. *CatCharger* utilizes categorization and clustering of traffic flow attributes and a generic traffic model to support the continuous operability of electric vehicles on roads with the minimal deployment cost. We implemented *CatCharger* on SUMO and used the Shenzhen datasets to drive the experiment. Through large-scale trace-driven simulation based on the metropolitan-scale mobility dataset of buses, we showed that *CatCharger* has superior performance over other representative methods in maintaining the SoC and operability of the buses.

- In Chapter 5, we presented a taxicab dispatching and charging approach, named *CD-Guide*. *CD-Guide* utilizes customized selection and training of suitable historical passenger demand data and charging optimization to minimize the taxicab's number of missed potential passengers due to charging. We implemented *CD-Guide* on SUMO. The evaluation results demonstrate that compared with previous methods, *CD-Guide* increases the total number of served passengers and the SoC of all taxicabs during all time slots.

7.2 Future Work

This dissertation represents some of the first steps to design a hybrid WPT charging system composed of stationary and dynamic wireless chargers to support the charging demands of a metropolitan-scale group of public transportation EVs. The work can be improved, enhanced or extended in many ways. We anticipate that, in the near future, more and more autonomous EVs will be put in use, and we will apply our proposed algorithms to more other cities to verify their effectiveness and locate emerging research problems. Future work might focus more on optimizing the EV traffic flow using the shared mobility information of the autonomous EVs while protecting the privacy of the EVs' mobility information. Specifically, we list a number of potential future work here.

- To maximize the service efficiency of deployed dynamic wireless chargers without suffering from traffic congestion, we must properly manage the traffic of the EVs and coordinate their arrivals at the charger lanes to avoid the generation of traffic congestion at the charger lanes and on the road segments to them. We will extend our traffic model in this dissertation to consider the real-time change of EV traffic to maximally avoid the generation of congestion.

- With the rapid development of wireless charging, we anticipate that vehicle-to-vehicle dynamic wireless charging will prevail to save the EVs' cost on finding charging infrastructures. We will further identify the challenges for the routing of vehicle-to-vehicle dynamic wireless chargers, and provide solutions to utilizing the wireless chargers for maintaining the continuous operability of EVs.

- With more and more applications using vehicle mobility information for service, we anticipate that the privacy of vehicle mobility information will be increasingly more important. We plan to further explore context-aware protection of vehicle mobility information.

Bibliography

[1] Y. Ahn and H. Yeo. “An Analytical Planning Model to Estimate the Optimal Density of Charging Stations for Electric Vehicles”. In: *PloS one* 10.11 (2015).

[2] M. J. Alves and J. Clímaco. “A review of interactive methods for multiobjective integer and mixed-integer programming”. In: *European Journal of Operational Research* 180.1 (2007).

[3] *Apache Hadoop 2.7.3*. `http://hadoop.apache.org/`. Accessed in August, 2017. 2017.

[4] *Apache Spark 1.5.2*. `http://spark.apache.org/`. Accessed July 24, 2016.

[5] S. Bae and A. Kwasinski. “Spatial and temporal model of electric vehicle charging demand”. In: *TSG* (2012).

[6] F. Bai and B. Krishnamachari. “Spatio-temporal variations of vehicle traffic in VANETs: facts and implications”. In: *Proc. of VANET*. 2009.

[7] D. Barbará, Y. Li, and J. Couto. “COOLCAT: an entropy-based algorithm for categorical clustering”. In: *Proc. of CIKM*. 2002.

[8] R. Bellman, R. Corporation, and K. M. R. Collection. *Dynamic Programming*. Princeton University Press, 1957.

[9] Z. Bi, G. A. Keoleian, and T. Ersal. “Wireless Charger Deployment for an Electric Bus Network: A Multi-Objective Life Cycle Optimization”. In: *Applied energy* 225 (2018).

[10] Z. Bi, G. A. Keoleian, Z. Lin, M. R. Moore, K. Chen, L. Song, and Z. Zhao. “Life Cycle Assessment and Tempo-Spatial Optimization of Deploying Dynamic Wireless Charging Technology for Electric Cars”. In: *TRC: Emerging Technologies* 100 (2019).

[11] *BMW Stationary Wireless Charger*. https://www.theverge.com/2017/9/25/16363038/bmw-wireless-charging-pad-for-cars-530e.

[12] *Bombardier Primove e-bus*. `http://primove.bombardier.com/fileadmin/primove/content/GENERAL/PUBLICATIONS/English/PT_PRIMOVE_Datasheet_2015_Braunschweig_EN_print_110dpi.pdf`. Accessed July, 2019. 2019.

[13] N. Caceres, L. M. Romero, F. G. Benitez, and J. M. del Castillo. “Traffic flow estimation models using cellular phone data”. In: *IEEE TITS* 13.3 (2012).

[14] H. Cai, X. Jia, A. S. Chiu, X. Hu, and M. Xu. “Siting Public Electric Vehicle Charging Stations in Beijing Using Big-Data Informed Travel Patterns of the Taxi Fleet”. In: *TRD: Transport and Environment* 33 (2014).

[15] J. Candia, M. C. González, P. Wang, T. Schoenharl, G. Madey, and A.-L. Barabási. “Uncovering Individual and Collective Human Dynamics From Mobile Phone Records”. In: *Journal of physics A: mathematical and theoretical* 41.22 (2008).

[16] S. Carrese, E. Cipriani, L. Mannini, and M. Nigro. “Dynamic Demand Estimation and Prediction for Traffic Urban Networks Adopting New Data Sources”. In: *TRC: Emerging Technologies* 81 (2017).

[17] A. Charnes, E. L. Frome, and P.-L. Yu. "The Equivalence of Generalized Least Squares and Maximum Likelihood Estimates in the Exponential Family". In: *Journal of the American Statistical Association* 71.353 (1976).

[18] K. Chen and L. Liu. "The 'Best K' for entropy-based categorical data clustering". In: *Proc. of SSDBM*. 2005.

[19] Z. Chen, F. He, and Y. Yin. "Optimal Deployment of Charging Lanes for Electric Vehicles in Transportation Networks". In: *TRB: Methodological* 91 (2016).

[20] Z. Chen, W. Liu, and Y. Yin. "Deployment of Stationary and Dynamic Charging Infrastructure for Electric Vehicles Along Traffic Corridors". In: *TRC: Emerging Technologies* 77 (2017).

[21] *China Meteorological Data Service Center*. `http://data.cma.cn/`. Accessed in October, 2018. 2018.

[22] W. G. Cochran. "The $\chi 2$ Test of Goodness of Fit". In: *The Annals of Mathematical Statistics* 23.3 (1952).

[23] K. C. Dey, L. Yan, X. Wang, Y. Wang, H. Shen, M. Chowdhury, L. Yu, C. Qiu, and V. Soundararaj. "A review of communication, driver characteristics, and controls aspects of cooperative adaptive cruise control (CACC)". In: *IEEE TITS* 17.2 (2016).

[24] P. Dutta. "Coordinating Rendezvous Points for Inductive Power Transfer Between Electric Vehicles to Increase Effective Driving Distance". In: *Proc. of ICCVE*. 2013.

[25] *Dynamic Wireless Charging: What's Feasible?* https://chargedevs.com/features/dynamic-wireless-charging-whats-feasible-qa-with-qualcomms-graeme-davison/.

[26] M. Eisel, J. Schmidt, and L. Kolbe. "Finding suitable locations for charging stations". In: *Proc. of IEVC*. 2014.

[27] *ElectReon inductively charges a Renault Zoe in transit.* https://www.electrive.com/2019/09/23/electreon-enables-renault-zoe-to-charge-inductively-while-driving. Accessed Oct 27, 2019.

[28] *Electric Vehicles, Towards Dynamic Wireless Charging?* https://group.renault.com/en/news/blo renault/electric-vehicles-towards-dynamic-wireless-charging/.

[29] Z. Fan, X. Song, and R. Shibasaki. "CitySpectrum: A Non-Negative Tensor Factorization Approach". In: *Proc. UbiComp*. 2014.

[30] T. M. Fisher, K. B. Farley, Y. Gao, H. Bai, and Z. T. H. Tse. "Electric Vehicle Wireless Charging Technology: A State-of-the-Art Review of Magnetic Coupling Systems". In: *Wireless Power Transfer* 1.2 (2014).

[31] M. Fuller. "Wireless Charging in California: Range, Recharge, and Vehicle Electrification". In: *TRC: Emerging Technologies* 67 (2016).

[32] B. Ghosh, B. Basu, and M. O'Mahony. "Multivariate Short-Term Traffic Flow Forecasting Using Time-Series Analysis". In: *IEEE TITS* 10.2 (2009).

[33] A Gil and J Taiber. "A Literature Review in Dynamic Wireless Power Transfer for Electric Vehicles: Technology and Infrastructure Integration Challenges". In: *Sustainable Automotive Technologies 2013*. 2014.

[34] S. A. Glantz et al. "Primer of Biostatistics". In: (2002).

[35] N. Groot, B. De Schutter, and H. Hellendoorn. "Toward system-optimal routing in traffic networks: a reverse Stackelberg game approach". In: *IEEE TITS* 16.1 (2015).

[36] D. Gross. *Fundamentals of Queueing Theory*. John Wiley & Sons, 2008.

[37] J. Habbema, J Hermans, and K Van Der Broek. "A Stepwise Discrimination Program Using Density Estimation". In: *Compstat*. Vol. 1974. 1974.

[38] H. Hanabusa and R. Horiguchi. "A Study of the Analytical Method for the Location Planning of Charging Stations for Electric Vehicles". In: *Proc. of KES*. 2011.

[39] F. He, Y. Yin, and J. Zhou. "Integrated Pricing of Roads and Electricity Enabled by Wireless Power Transfer". In: *TRC: Emerging Technologies* 34 (2013).

[40] *HEVO Stationary Wireless Charger*. https://www.hevopower.com/.

[41] C. P. van Hinsbergen, T. Schreiter, F. S. Zuurbier, J. Van Lint, and H. J. Van Zuylen. "Localized Extended Kalman Filter for Scalable Real-Time Traffic State Estimation". In: *IEEE TITS* 13.1 (2011).

[42] Y. Hou, W. Zhong, L. Su, K. Hulme, A. W. Sadek, and C. Qiao. "TASeT: Improving the Efficiency of Electric Taxis With Transfer-Allowed Rideshare". In: *IEEE TVT* 65.12 (2016).

[43] D. Hristova, M. J. Williams, M. Musolesi, P. Panzarasa, and C. Mascolo. "Measuring Urban Social Diversity Using Interconnected Geo-Social Networks". In: *Proc. WWW*. 2016.

[44] D. Hristova, M. J. Williams, M. Musolesi, P. Panzarasa, and C. Mascolo. "Measuring Urban Social Diversity Using Interconnected Geo-Social Networks". In: *Proc. of WWW*. 2016.

[45] I. Hwang, Y. J. Jang, Y. D. Ko, and M. S. Lee. "System Optimization for Dynamic Wireless Charging Electric Vehicles Operating in a Multiple-Route Environment". In: *IEEE TITS* 19.6 (2017).

[46] *Israeli technology charges your car while you drive.* `https://beholdisrael.org/israeli-technology-charges-your-car-while-you-drive`. Accessed Oct 27, 2019.

[47] D. Jackson, H Estler, D. Rayside, et al. "The Guided Improvement Algorithm for Exact, General-Purpose, Many-Objective Combinatorial Optimization". In: 2009.

[48] Y. J. Jang, E. S. Suh, and J. W. Kim. "System Architecture and Mathematical Models of Electric Transit Bus System Utilizing Wireless Power Transfer Technology". In: *Systems Journal* (2015).

[49] Y. J. Jang. "Survey of the Operation and System Study on Wireless Charging Electric Vehicle Systems". In: *TRC: Emerging Technologies* 95 (2018).

[50] S. Jeong, Y. J. Jang, and D. Kum. "Economic Analysis of the Dynamic Charging Electric Vehicle". In: *TPE* (2015).

[51] N. Jiang, C. Xie, J. C. Duthie, and S. T. Waller. "A Network Equilibrium Analysis on Destination, Route and Parking Choices With Mixed Gasoline and Electric Vehicular Flows". In: *EURO Journal on Transportation and Logistics* 3.1 ().

[52] J. Jung, J. Y. Chow, R Jayakrishnan, and J. Y. Park. "Stochastic Dynamic Itinerary Interception Refueling Location Problem With Queue Delay for Electric Taxi Charging Stations". In: *TRC: Emerging Technologies* 40 (2014).

[53] A. Karalis, J. D. Joannopoulos, and M. Soljačić. "Efficient wireless non-radiative mid-range energy transfer". In: *Annals of Physics* (2008).

[54] Y. D. Ko and Y. J. Jang. "The optimal system design of the online electric vehicle utilizing wireless power transmission technology". In: *IEEE TITS* 14.3 (2013).

[55] D. Kosmanos, L. A. Maglaras, M. Mavrovouniotis, S. Moschoyiannis, A. Argyriou, A. Maglaras, and H. Janicke. “Route Optimization of Electric Vehicles Based on Dynamic Wireless Charging”. In: *IEEE Access* 6 (2018).

[56] D. Krajzewicz, J. Erdmann, M. Behrisch, and L. Bieker. “Recent Development and Applications of SUMO - Simulation of Urban MObility”. In: *International Journal On Advances in Systems and Measurements* 5.3&4 (2012).

[57] T. Kurczveil, P. Á. López, and E. Schnieder. “Implementation of an Energy Model and a Charging Infrastructure in SUMO”. In: *Proc. of SUMO User Conference*. 2013.

[58] A. Lam, Y.-W. Leung, and X. Chu. “Electric vehicle charging station placement: Formulation, complexity, and solutions”. In: *TSG* (2014).

[59] M. Li, X. Wu, Z. Zhang, G. Yu, Y. Wang, and W. Ma. “A Wireless Charging Facilities Deployment Problem Considering Optimal Traffic Delay and Energy Consumption on Signalized Arterial”. In: *IEEE TITS* (2019).

[60] R. Li, H. Chai, and J. Tang. “Empirical Study of Travel Time Estimation and Reliability”. In: *Mathematical Problems in Engineering* 2013 (2013).

[61] R. Li, G. Rose, and M. Sarvi. “Using automatic vehicle identification data to gain insight into travel time variability and its causes”. In: *JTRB* 1945 (2006).

[62] Y. Li, J. Luo, C.-Y. Chow, K.-L. Chan, Y. Ding, and F. Zhang. “Growing the charging station network for electric vehicles with trajectory data analytics”. In: *Proc. of ICDE*. 2015.

[63] Z. Li, B. Ding, J. Han, R. Kays, and P. Nye. “Mining periodic behaviors for moving objects”. In: *Proc. of SIGKDD*. 2010.

[64] L. Lin, Z. He, and S. Peeta. "Predicting Station-Level Hourly Demand in a Large-Scale Bike-Sharing Network: A Graph Convolutional Neural Network Approach". In: *TRC: Emerging Technologies* 97 (2018).

[65] Y. Liu, C. Kang, S. Gao, Y. Xiao, and Y. Tian. "Understanding Intra-Urban Trip Patterns From Taxi Trajectory Data". In: *Journal of geographical systems* 14.4 (2012).

[66] Z. Liu and Z. Song. "Robust Planning of Dynamic Wireless Charging Infrastructure for Battery Electric Buses". In: *TRC: Emerging Technologies* 83 (2017).

[67] J.-L. Lu, M.-Y. Yeh, Y.-C. Hsu, S.-N. Yang, C.-H. Gan, and M.-S. Chen. "Operating Electric Taxi Fleets: A New Dispatching Strategy With Charging Plans". In: *Proc. of IEVC*. 2012.

[68] M. Lubin and I. Dunning. "Computing in Operations Research Using Julia". In: *INFORMS Journal on Computing* 27.2 (2015).

[69] Y. Lv, Y. Duan, W. Kang, Z. Li, and F.-Y. Wang. "Traffic Flow Prediction With Big Data: A Deep Learning Approach". In: *IEEE TITS* 16.2 (2014).

[70] X. Ma, Z. Tao, Y. Wang, H. Yu, and Y. Wang. "Long Short-Term Memory Neural Network for Traffic Speed Prediction Using Remote Microwave Sensor Data". In: *TRC: Emerging Technologies* 54 (2015).

[71] L. A. Maglaras, F. V. Topalis, and A. L. Maglaras. "Cooperative Approaches for Dymanic Wireless Charging of Electric Vehicles in a Smart City". In: *Proc. of ENERGYCON*. 2014.

[72] F. Malandrino, C. Casetti, and C.-F. Chiasserini. "A Holistic View of Its-Enhanced Charging Markets". In: *IEEE TITS* 16.4 (2015).

[73] S. D. Manshadi, M. E. Khodayar, K. Abdelghany, and H. Üster. "Wireless Charging of Electric Vehicles in Electricity and Transportation Networks". In: *IEEE TSG* 9.5 (2017).

[74] H. Mao, R. Netravali, and M. Alizadeh. "Neural Adaptive Video Streaming With Pensieve". In: *Proc. Sigcomm*. 2017.

[75] F. J. Massey Jr. "The Kolmogorov-Smirnov test for goodness of fit". In: *Journal of the American statistical Association* 46.253 (1951).

[76] F. Miao, S. Han, A. M. Hendawi, M. E. Khalefa, J. A. Stankovic, and G. J. Pappas. "Data-driven distributionally robust vehicle balancing using dynamic region partitions". In: *Proc. of ICCPS*. 2017.

[77] R. G. Michael and S. J. David. "Computers and intractability: a guide to the theory of NP-completeness". In: *W. H. Freeman* (1979).

[78] S Moschoyiannis, L Maglaras, J Jiang, F Topalis, and A Maglaras. "Dynamic Wireless Charging of Electric Vehicles on the Move With Mobile Energy Disseminators". In: *IJACSA* 6.6 (2015).

[79] *MultiJuMP multiobjective optimisation package*. `https://github.com/anriseth/MultiJuMP.jl`. Accessed in August, 2017. 2017.

[80] *National Household Travel Survey*. `http://nhts.ornl.gov/briefs/EVFeasibility20160701.pdf`. Accessed in July, 2016.

[81] *National Household Travel Survey*. `nhts.ornl.gov/2009/pub/Compendium_2016.pdf`. Accessed in August, 2018. 2018.

[82] *NYTimes Web Site*. http://www.nytimes.com.

[83] O. C. Onar, J. M. Miller, S. L. Campbell, C. Coomer, C. White, L. E. Seiber, et al. "A novel wireless power transfer for in-motion EV/PHEV charging". In: *Proc. of APEC*. 2013.

[84] *OpenStreetMap*. http://www.openstreetmap.org/. Accessed July, 2016.

[85] *ORNL demonstrates 120-kilowatt wireless charging for vehicles*. https://www.ornl.gov/news/ornl-demonstrates-120-kilowatt-wireless-charging-vehicles?page=1. Accessed Oct 27, 2019.

[86] E. Ozatay, S. Onori, J. Wollaeger, U. Ozguner, G. Rizzoni, D. Filev, J. Michelini, and S. Di Cairano. "Cloud-Based Velocity Profile Optimization for Everyday Driving: A Dynamic-Programming-Based Solution". In: *IEEE TITS* 15.6 (2014).

[87] K. Pearson. "Note on regression and inheritance in the case of two parents". In: *Proc. of the Royal Society of London*. 1895.

[88] *Plugless Stationary Wireless Charger*. https://www.pluglesspower.com/.

[89] H. Qin and W. Zhang. "Charging Scheduling With Minimal Waiting in a Network of Electric Vehicles and Charging Stations". In: *Proc. of VANET*. 2011.

[90] *Qualcomm Wireless Charging System*. https://www.qualcomm.com/solutions/automotive/wevc.

[91] R. Riemann, D. Z. Wang, and F. Busch. "Optimal Location of Wireless Charging Facilities for Electric Vehicles: Flow-Capturing Location Model With Stochastic User Equilibrium". In: *TRC: Emerging Technologies* 58 (2015).

[92] M. A. Ruiz, F. A. Abdallah, M. Gagnaire, and Y. Lascaux. "Telewatt: An Innovative Electric Vehicle Charging Infrastructure Over Public Lighting Systems". In: *Proc. of ICCVE*. 2013.

[93] P. Sanchez-Martin, G. Sanchez, and G. Morales-Espana. "Direct load control decision model for aggregated EV charging points". In: *TPS* (2012).

[94] A. Sarker, C. Qiu, H. Shen, A. Gil, J. Taiber, M. Chowdhury, J. Martin, M. Devine, and A. Rindos. “An Efficient Wireless Power Transfer System To Balance the State of Charge of Electric Vehicles”. In: *Proc. of ICPP*. 2016.

[95] J. Schneider. “SAE J2954 Overview and Path Forward”. In: *SAE International: Warrendale, PA, USA* (2013).

[96] R. Sellmair and T. Hamacher. “Optimization of Charging Infrastructure for Electric Taxis”. In: *Transportation Research Record* 2416.1 (2014).

[97] N. Shahraki, H. Cai, M. Turkay, and M. Xu. “Optimal Locations of Electric Public Charging Stations Using Real World Vehicle Travel Patterns”. In: *TRD: Transport and Environment* 41 (2015).

[98] *Shenzhen Wiki*. `https://en.wikipedia.org/wiki/Shenzhen`. Accessed July 24, 2016.

[99] M. Shimosaka, K. Maeda, T. Tsukiji, and K. Tsubouchi. “Forecasting Urban Dynamics With Mobility Logs by Bilinear Poisson Regression”. In: *Proc. of UbiComp*. 2015.

[100] B. L. Smith, B. M. Williams, and R. K. Oswald. “Comparison of Parametric and Nonparametric Models for Traffic Flow Forecasting”. In: *TRC: Emerging Technologies* 10.4 (2002).

[101] C. Song, Z. Qu, N. Blumm, and A.-L. Barabási. “Limits of Predictability in Human Mobility”. In: *Science* 327.5968 (2010).

[102] A. Stathopoulos and M. G. Karlaftis. “A Multivariate State Space Approach for Urban Traffic Flow Modeling and Prediction”. In: *TRC: Emerging Technologies* 11.2 (2003).

[103] M. Terra-Neves, I. Lynce, and V. Manquinho. “Enhancing Constraint-Based Multi-Objective Combinatorial Optimization”. In: *Proc. of AAAI*. 2018.

[104] Z. Tian, T. Jung, Y. Wang, F. Zhang, L. Tu, C. Xu, C. Tian, and X.-Y. Li. "Real-Time Charging Station Recommendation System for Electric-Vehicle Taxis". In: *IEEE TITS* 17.11 (2016).

[105] Y. Tong, Y. Chen, Z. Zhou, L. Chen, J. Wang, Q. Yang, J. Ye, and W. Lv. "The Simpler the Better: A Unified Approach to Predicting Original Taxi Demands Based on Large-Scale Online Platforms". In: *Proc. SIGKDD*. 2017.

[106] M. Vlachos, S. Y. Philip, and V. Castelli. "On Periodicity Detection and Structural Periodic Similarity." In: *Proc. of SIAM*. 2005.

[107] M. P. Wand and M. C. Jones. *Kernel smoothing*. CRC Press, 1994.

[108] G. Wang, Z. Xu, F. Wen, and K. P. Wong. "Traffic-constrained multiobjective planning of electric-vehicle charging stations". In: *TPD* (2013).

[109] Y. Wei and M.-C. Chen. "Forecasting the Short-Term Metro Passenger Flow With Empirical Mode Decomposition and Neural Networks". In: *TRC: Emerging Technologies* 21.1 (2012).

[110] C. Wu, A. Kreidieh, K. Parvate, E. Vinitsky, and A. M. Bayen. "Flow: Architecture and Benchmarking for Reinforcement Learning in Traffic Control". In: *arXiv* (2017).

[111] X. Xie, F. Zhang, and D. Zhang. "PrivateHunt: Multi-Source Data-Driven Dispatching in For-Hire Vehicle Systems". In: *ACM IMWUT* 2.1 (2018).

[112] M. Xu, D. Wang, and J. Li. "DESTPRE: A Data-Driven Approach to Destination Prediction for Taxi Rides". In: *Proc. UbiComp*. 2016.

[113] M. Xylia, S. Leduc, P. Patrizio, F. Kraxner, and S. Silveira. "Locating Charging Infrastructure for Electric Buses in Stockholm". In: *TRC: Emerging Technologies* 78 (2017).

[114] L. Yan and H. Shen. "TOP: Vehicle Trajectory based Driving Speed Optimization Strategy for Travel Time Minimization and Road Congestion Avoidance". In: *Proc. of MASS*. 2016.

[115] L. Yan, H. Shen, J. Zhao, C. Xu, F. Luo, and C. Qiu. "CatCharger: Deploying Wireless Charging Lanes in a Metropolitan Road Network through Categorization and Clustering of Vehicle Traffic". In: *Proc. of INFOCOM*. 2017.

[116] L. Yan, H. Shen, S. Li, and Y. Huang. "Electrical Vehicle Charging Station Placement Determination based on Real World Vehicle Trace". In: *Proc. of IOV*. 2016.

[117] L. Yan, H. Shen, Z. Li, A. Sarker, J. A. Stankovic, C. Qiu, J. Zhao, and C. Xu. "Employing Opportunistic Charging for Electric Taxicabs to Reduce Idle Time". In: *ACM IMWUT* 2.1 (2018).

[118] J. Yang, J. Dong, and L. Hu. "A data-driven optimization-based approach for siting and sizing of electric taxi charging stations". In: *TRC: Emerging Technologies* 77 (2017).

[119] W. Yao, J. Zhao, F. Wen, Z. Dong, Y. Xue, Y. Xu, and K. Meng. "A multi-objective collaborative planning strategy for integrated power distribution and electric vehicle charging systems". In: *TPS* (2014).

[120] J. Yuan, Y. Zheng, and X. Xie. "Discovering regions of different functions in a city using human mobility and POIs". In: *Proc. of SIGKDD*. 2012.

[121] J. Yuan, Y. Zheng, C. Zhang, W. Xie, X. Xie, G. Sun, and Y. Huang. "T-drive: driving directions based on taxi trajectories". In: *Proc. of GIS*. 2010.

[122] J. Yuan, Y. Zheng, L. Zhang, X. Xie, and G. Sun. "Where to Find My Next Passenger?" In: *Proc. of UbiComp*. 2011.

[123] D. Zhang, L. Sun, B. Li, C. Chen, G. Pan, S. Li, and Z. Wu. "Understanding Taxi Service Strategies From Taxi GPS Traces". In: *IEEE TITS* 16.1 (2015).

[124] D. Zhang, J. Huang, Y. Li, F. Zhang, C. Xu, and T. He. "Exploring human mobility with multi-source data at extremely large metropolitan scales". In: *Proc. of MobiCom*. 2014.

[125] D. Zhang, T. He, S. Lin, S. Munir, and J. A. Stankovic. "Online Cruising Mile Reduction in Large-Scale Taxicab Networks". In: *IEEE TPDS* 26.11 (2015).

[126] D. Zhang, T. He, S. Lin, S. Munir, and J. A. Stankovic. "Taxi-Passenger-Demand Modeling Based on Big Data From a Roving Sensor Network". In: *IEEE TBD* 3.3 (2017).

[127] D. Zhang, J. Zhao, F. Zhang, and T. He. "UrbanCPS: A Cyber-Physical System Based on Multi-Source Big Infrastructure Data for Heterogeneous Model Integration". In: *Proc. ICCPS*. 2015.

[128] J. Zhang, Y. Zheng, and D. Qi. "Deep Spatio-Temporal Residual Networks for Citywide Crowd Flows Prediction". In: *Proc. of AAAI*. 2017.

[129] Q. Zhang and H. Li. "MOEA/D: A Multiobjective Evolutionary Algorithm Based on Decomposition". In: *IEEE TEC* 11.6 (2007).

[130] T. Zhang, W. Chen, Z. Han, and Z. Cao. "Charging Scheduling of Electric Vehicles With Local Renewable Energy Under Uncertain Electric Vehicle Arrival and Grid Power Price". In: *IEEE TVT* 63.6 (2014).

[131] Y. Zhang and Y. Xie. "Forecasting of Short-Term Freeway Volume With V-Support Vector Machines". In: *Transportation Research Record* 2024.1 (2007).

[132] K. Zhao, D. Khryashchev, J. Freire, C. Silva, and H. Vo. "Predicting Taxi Demand at High Spatial Resolution: Approaching the Limit of Predictability". In: *Proc. of ICBD*. 2016.

[133] K. Zheng, Y. Zheng, N. J. Yuan, S. Shang, and X. Zhou. “Online Discovery of Gathering Patterns Over Trajectories”. In: *IEEE TKDE* 26.8 (2014).

[134] X. Zheng, X. Liang, and K. Xu. “Where to Wait for a Taxi?” In: *Proc. of SIGKDD*. 2012.

[135] Y. Zheng. “Trajectory data mining: an overview”. In: *TIST* (2015).

[136] Y. Zheng, T. Liu, Y. Wang, Y. Zhu, Y. Liu, and E. Chang. “Diagnosing New York City’s Noises With Ubiquitous Data”. In: *Proc. UbiComp*. 2014.

[137] Y. Zheng, Z. Y. Dong, Y. Xu, K. Meng, J. H. Zhao, and J. Qiu. “Electric vehicle battery charging/swap stations in distribution systems: comparison study and optimal planning”. In: *TPS* (2014).

[138] Y. Zheng, L. Capra, O. Wolfson, and H. Yang. “Urban Computing: Concepts, Methodologies, and Applications”. In: *ACM TIST* 5.3 (2014).

[139] Y. Zheng, Y. Liu, J. Yuan, and X. Xie. “Urban Computing With Taxicabs”. In: *Proc. UbiComp*. 2011.